

NUCLEAR MAGNETIC RESONANCE APPLIED TO  
PROBLEMS OF MOLECULAR MOTION IN SOLIDS

F. A. Rushworth

A Thesis Submitted for the Degree of PhD  
at the  
University of St Andrews



1953

Full metadata for this item is available in  
St Andrews Research Repository  
at:  
<http://research-repository.st-andrews.ac.uk/>

Please use this identifier to cite or link to this item:  
<http://hdl.handle.net/10023/14694>

This item is protected by original copyright

**NUCLEAR MAGNETIC RESONANCE**  
**APPLIED TO**  
**PROBLEMS OF MOLECULAR MOTION IN SOLIDS**

**A Thesis**  
**presented by**  
**F. A. Rushworth, B.Sc., A.R.C.S.**  
**to the**  
**University of St. Andrews**  
**in application for the Degree**  
**of Doctor of Philosophy.**



ProQuest Number: 10171258

All rights reserved

INFORMATION TO ALL USERS

The quality of this reproduction is dependent upon the quality of the copy submitted.

In the unlikely event that the author did not send a complete manuscript and there are missing pages, these will be noted. Also, if material had to be removed, a note will indicate the deletion.



ProQuest 10171258

Published by ProQuest LLC (2017). Copyright of the Dissertation is held by the Author.

All rights reserved.

This work is protected against unauthorized copying under Title 17, United States Code  
Microform Edition © ProQuest LLC.

ProQuest LLC.  
789 East Eisenhower Parkway  
P.O. Box 1346  
Ann Arbor, MI 48106 – 1346

COMPTON

ms  
1,460

LONDON

**DECLARATION**

I hereby declare that this thesis  
has been composed by me, is a record of work  
carried out by me and has not previously  
been presented for a higher degree.



LONDON

CERTIFICATE

I certify that Francis Alwyn Rushworth, B.Sc., A.R.C.S., has spent the equivalent of nine terms as a research student in the Physical Laboratory of the United College of the University of St. Andrews, that he has fulfilled the conditions of Ordinance No. 16 of the University Court of St. Andrews and that he is qualified to submit the accompanying thesis in application for the degree of Doctor of Philosophy.

LONDON

Research Supervisor



## STATEMENT OF RESEARCH TRAINING

After graduating at the University of London (Imperial College of Science and Technology) in 1941 I spent six years as an Experimental Officer in H.M. Anti-Submarine Experimental Establishment. I joined the staff of the Department of Natural Philosophy in the United College of the University of St. Andrews in 1947. In January 1948 I was admitted by the Senatus Academicus as a research student and commenced the work which is the subject of this thesis.

I should like to express my sincere thanks to Professor J.F. Allen, F.R.S., for suggesting the topic of nuclear resonance and for his encouragement throughout, to Dr. E.R. Andrew for much helpful advice and many clarifying discussions and to Mr. J. Gerrard for his help with the photography.

## CONTENTS

<u>Section</u>		<u>Page</u>
	<u>Introduction</u>	1
1	<u>General Theory</u>	
1.1	The Nuclear Magnetic Absorption Process	2
1.2	Spin-Lattice Interaction	6
1.3	Spin-Spin Interaction	8
2	<u>Experimental Methods and Apparatus</u>	
2.1	Principles of Absorption Methods	13
2.2	Regenerative Method	13
2.3	Bridge Method	18
2.4	Measurement of Line-shape and Second Moment	19
2.5	Measurement of Spin-Lattice Relaxation Times	23
2.6	Comparison of Regenerative and Bridge Methods	27
2.7	Temperature Control Apparatus	30
3	<u>The Permanent Magnet</u>	
3.1	Requirements of Magnetic Field	32
3.2	General Design of Permanent Magnet	34
3.3	Ring Shims for Coned Magnet Polecaps	40
3.4	Performance of Magnet	48



## CONTENTS

<u>Section</u>	<u>Page</u>
4	<u>Experimental Results</u>
4.1	Introduction 56
4.2	Anthracene and Ethylene Glycol 58
4.3	Cyclopentane 65
4.4	n-Pentane and n-Hexane 80
4.5	Early Qualitative Investigations 98
	<u>Appendix I</u> 102
	<u>Appendix II</u> 105
	<u>References</u> 108

## INTRODUCTION

The discovery of nuclear magnetic resonance in bulk matter in 1945 has led to advances in several branches of physics. One of the most interesting applications of these new techniques has been to problems of the solid state, where information about molecular motion and thermal relaxation effects can be obtained. It is with this field of research that the nuclear magnetic resonance absorption experiments reported in this thesis are concerned.

The general theory of nuclear magnetic absorption is developed first and the relevant apparatus and experimental methods are then described. The design and performance of a large permanent magnet made specially for nuclear resonance work is considered and experiments on suitable solids are reported and discussed in the final section.

## 1. GENERAL THEORY

### 1.1 The Nuclear Magnetic Absorption Process

Nuclear magnetism was first postulated to account for the hyperfine structure of certain spectral lines. The interaction between this nuclear magnetism and the orbital electrons splits the electron energy levels by small amounts and enables the observed transitions to be explained. A nucleus is considered to have a quantised angular momentum and an associated magnetic moment, both related to a nuclear spin quantum number  $I$ . The unit of nuclear magnetism is the nuclear magneton,  $e\hbar/2Mc$ , where  $e$  is the electronic charge,  $\hbar$  is Planck's constant divided by  $2\pi$ ,  $M$  the mass of the proton and  $c$  the velocity of light. This unit is defined by analogy with the magnetic moment of an electron. The proton and the electron each have a spin quantum number of  $\frac{1}{2}$  and the electron has a magnetic moment of 1 Bohr magneton,  $e\hbar/2mc$ , where  $m$  is the electron mass. Unlike the electron, however, the proton does not have an intrinsic magnetic moment of 1 nuclear magneton. Its magnetic moment is found to be 2.7925 nuclear magnetons. The magnetic moment of any nucleus is usually related to its spin quantum number  $I$  by the equation  $\mu = g\beta I$ , where  $\beta$  is the nuclear magneton and  $g$  a dimensionless constant. For the proton, therefore,  $g$  has the value 5.585. This  $g$ -factor is analogous

to the Landé splitting factor in electronic systems. Many nuclei have zero spin and hence zero angular momentum. These are also found to have zero magnetic moment.

The picture has been rather simplified, since the true angular momentum of a nucleus is  $\sqrt{I(I+1)}\hbar$  and the spin vector is always at an angle with the chosen direction (usually the direction of an applied external magnetic field). The maximum value of the projection of this space-quantised spin along the chosen direction is  $I$ , and it is this quantity which is measured experimentally. As the nuclear magnetic moment  $\mu$  is always measured along this direction it is normally associated with  $I$  rather than  $\sqrt{I(I+1)}$ .

In bulk matter, neglecting the effect of the earth's magnetic field, the spin directions are randomly oriented and only become space-quantised on the application of a magnetic field  $H$ . The degeneracy is then removed and there are  $(2I+1)$  levels with projected spin vectors along the field direction of  $I, (I-1), \dots, -(I-1), -I$ . In the case of the proton there are only two levels with energy spacing  $(\mu H/I)$  of  $2\mu H$ . The relative population of these levels is of great importance, but for the present we will assume that an equilibrium state is soon reached after the field has been applied.

Taking this case of spin  $\frac{1}{2}$  as the simplest, the state

anti-parallel to the direction of the applied field has the greater energy. We will call this the - state and the lower energy state the + state. If a typical proton in the lower + state were given an energy  $2\mu H$  it might be excited into the upper - state. The necessary quantum of energy to do this would be  $h\nu = 2\mu H$ , or  $\nu = \mu H/h$ , with an associated angular frequency  $\omega = \gamma H$ .  $\gamma$  is the ratio between the magnetic moment  $\mu$  and the angular momentum  $Ih$  and is sometimes called the gyromagnetic ratio (although the term magnetogyric ratio is more appropriate). Knowing approximate values for the magnetic moment of the proton, we find that if  $H = 5500$  gauss the necessary frequency to cause a transition is about 23 megacycles per second, a convenient radiofrequency. This frequency is identical with the Larmor frequency of precession which relates, in a classical manner, the motion of a vector round a polarising direction. This semi-classical picture of a spinning nucleus precessing round a magnetic field vector is useful in several topics connected with nuclear magnetic effects, but we shall mainly be concerned with the purely quantum description of the process.

The idea of changing the orientation of a nuclear spin vector by a radiofrequency field was applied to molecular beams by Rabi and his collaborators in the late thirties. Attempts were made by Gorter (1936) and by Gorter and Broer (1942) to detect the resonance absorption by matter

in bulk rather than by producing molecular and atomic beams. Gorter's methods were based (a) on the expected heating effect of energy absorbed when inducing transitions and (b) on the change in the effective magnetic susceptibility, but both attempts were unsuccessful. The first successful detection of nuclear magnetic resonance in bulk matter came simultaneously and independently in late 1945 from Purcell, Torrey and Pound (1946) and from Bloch, Hansen and Packard (1946). Both these experiments used protons, but whereas the Purcell group based their theory on a quantum approach, the experiments of the Bloch group could more clearly be explained using the semi-classical picture of precessing vectors. In fact the Bloch method was called "nuclear induction" because the changed directions of precession of the nuclear spin vectors at resonance were used to produce an induced e.m.f. in a suitably placed radiofrequency coil.

These new methods enable the values of nuclear magnetic moments to be determined with much greater precision than either hyperfine structure or molecular beam experiments. In addition, these experiments can give a surprising amount of information about the solid state of matter, and it is with part of this latter application that we shall be concerned.

## 1.2 Spin-lattice Interaction

In the preceding section we treated an isolated system of spins - in this case protons. In general this system will not be isolated, but will interact with the rest of the crystal lattice. When the spin system is in thermal equilibrium with the lattice system at a temperature  $T^\circ \text{K}$ , the population of the two levels will follow a Boltzmann distribution, with more protons in the lower + state than in the upper - state. If the number in the lower state is  $N_+$  and in the upper state  $N_-$ , then the ratio between these numbers is

$$\frac{N_+}{N_-} = e^{h\nu/kT} = e^{2\mu H/kT} = 1 + \frac{2\mu H}{kT} + \dots \quad (1)$$

where  $k$  is Boltzmann's constant. For  $H = 6000\text{gauss}$  and  $T = 300^\circ \text{K}$ , this factor  $2\mu H/kT$  is  $\sim 4 \times 10^{-6}$ . Thus for every million protons in the upper energy state there are one million and four in the lower state. It is this small excess which makes the whole process possible.

The quantum-mechanical transition probabilities for absorption and emission of energy are the same for the two states, and so for a net absorption to occur there must be more protons in the lower energy state than in the upper energy state. But when energy is absorbed and protons move up into the higher level, the population is disturbed and the spin temperature  $T$  (defined from equation 1) will therefore rise. When the population ratio of the levels approaches

unity, so must  $T$  approach infinity and the energy absorption will decrease to zero. To counteract this rise in spin-temperature, the interaction between spins and lattice distributes the spin-heat throughout the whole system. If this interaction is small, when the spin-temperature is increased by the application of a radiofrequency field and this field is then removed, the spins will take a long time to come into thermal equilibrium with the lattice reservoir. The effective heat capacity of the spin-system is small compared with that of the lattice, so it is the lattice temperature which is the dominant factor and which is effectively constant. We can ascribe a spin-lattice relaxation time to the process, and on the basis of an exponential decay can write for the relation between the excess number  $n$  in the lower state at time  $t$  and the equilibrium excess  $n_0$

$$n = n_0(1 - e^{-t/T_1}) \quad (2)$$

where  $T_1$  is the spin-lattice relaxation time.  $T_1$  can vary within wide limits, and in experiments to be described later it has been measured as long as 100 seconds and as short as 0.01 second. This relaxation time can be related to the quantum-mechanical transition probability  $P$  for the transition referred to above, and Bloembergen, Purcell and Pound (1948) have shown that  $T_1 = 1/2P$ . This pioneer paper by Bloembergen, Purcell and Pound will be referred to several times as the



theory is developed and will be denoted by BPP, an abbreviation which has become quite common in the literature.

### 1.3 Spin-Spin Interaction

In addition to the interaction between spins and lattice, there will be interaction between the nuclear spins themselves. The total magnetic field at any one nucleus consists not only of the constant external field  $H_0$ , but must also include local crystalline magnetic fields produced by neighbouring spins. These spins act like magnetic dipoles of moment  $\mu$ , and this local field depends on the relative orientation and separation of the nuclei. Taking a nucleus of magnetic moment 1 nuclear magneton, at a distance of 1 angstrom,  $H_{loc} \sim \mu/r^3 \sim 5$  gauss. Different nuclei will therefore experience slightly differing total fields and have slightly differing values of  $\nu$ . The effect is to broaden the energy levels and introduce a finite line-width to the absorption process. The importance of this line-width is its dependence on the inter-nuclear distances in the crystal, and it can thus be applied to confirm or deny particular dipole configurations. The detailed calculation for two-spin and equilateral three-spin configurations have been made, but any other configuration leads to complications. A further form of line-broadening, which is an undesirable one, is caused by the external magnetic field not being homogeneous

over the volume of the sample. This is under a certain amount of control, and will be referred to in more detail later. There are other sources of line broadening, but in general the spin-spin effects are dominant in controlling the line-width.

In order to put the spin-spin interaction on a more quantitative basis, a spin-spin relaxation time  $T_2$  is introduced which is related to the normalised line shape. If we describe the shape of the resonance absorption line as a function  $g$  of the frequency  $\nu$  in a constant field and normalise  $g$  such that

$$\int_0^{\infty} g(\nu) d\nu = 1 \quad (3)$$

then  $T_2$  is defined by BPP as

$$T_2 = \frac{1}{2} g(\nu)_{\max} \quad (4)$$

This definition of  $T_2$  will be used in the discussion of saturation in section 2.5. It also relates the BPP theory with the complementary theory developed by Bloch (1946).

We shall define the width of a simple absorption line as the separation between the points of maximum and minimum slope, measured on either a frequency or field scale. The precise relation between  $T_2$  and this line-width ( $\Delta\nu$  or  $\Delta H$ ) depends on the idealised mathematical shape of the curve assumed. For a Lorentz shape function, traditional in the theory of spectral line broadening,  $T_2 = 1/\sqrt{3}\pi\Delta\nu$ ; for a Gaussian function,  $T_2 = 1/2\sqrt{2}\pi\Delta\nu$ . The frequency width

$\Delta\nu$  is related to  $\Delta H$  (expressed in gauss) by the equation  
 $2\pi\Delta\nu = \gamma\Delta H$ .

Although the general problem involving more than two or three interacting spins has not been fully worked out, a theory due to Van Vleck (1948) can be used. For any postulated spin configuration, this theory enables a value for the second moment of the expected line shape to be calculated. The second moment (analogous to the square of radius of gyration in mechanics) is defined as

$$\langle (\Delta\nu)^2 \rangle_{av} = \int_0^{\infty} (\nu - \nu_0)^2 g(\nu) d\nu \quad (5)$$

where  $g(\nu)$  is the normalised value of the line function at a frequency  $\nu$  and  $\nu_0$  is the central resonant frequency. This second moment is usually converted to units of gauss<sup>2</sup>, since the line-shape is experimentally plotted on the basis of a field variation rather than a frequency variation. For interaction between like spins (and we shall only be concerned with protons) Van Vleck's formula can be expressed as

$$S = \langle (\Delta H)^2 \rangle_{av} = \frac{3}{2} \frac{I(I+1)}{N_s} N_s^{-1} g^2 \beta^2 \sum_{j>k} (3\cos^2\theta_{jk} - 1) r_{jk}^{-6} \quad (6)$$

where  $r_{jk}$  is the internuclear distance between protons  $j$  and  $k$ ,  $\theta_{jk}$  the angle between the internuclear vector  $r_{jk}$  and the direction of the external field  $H_0$  and  $N_s$  is the number of resonating nuclei in the nuclear group considered when evaluating  $\sum r_{jk}^{-6}$ . For a powder sample the values of

$(3\cos^2\theta_{ik}-1)^2$  are averaged over a sphere, with the result that

$$S = \frac{6}{5} I(I+1)N g^2 \beta^2 \sum_{i>k} r_{ik}^{-6} \quad (7)$$

For protons, using the values of  $g$  and  $\beta$  given by Bearden and Watts (1951), the expression reduces to

$$S = \frac{715.9}{N} \sum_{i>k} r_{ik}^{-6} \quad (8)$$

where  $r_{ik}$  is expressed in angstroms.

In a solid, the normal behaviour might be that as the temperature is raised the line-width and second moments are more or less constant, apart from normal thermal lattice expansion effects. At the melting point the lattice is no longer rigid and so all these local fields will average out in the disturbed liquid state, with the result that the line-width and second moment should decrease abruptly. It is usually found that the line-width decreases to a value less than the value of the field inhomogeneity over the volume of the sample.

However, in a number of substances changes are found in the line-width and second moment values at temperatures below the melting point. The change is usually a decrease with increasing temperature. This suggests that there is some sort of motion in the solid and that certain of the local fields are being averaged out by this motion. It is this application of nuclear resonance technique with which we

shall mostly be concerned. By evaluating the theoretical second moment for a particular rigid nuclear configuration, and comparing it with the experimental value, the accuracy of the assumed configuration can be checked. If the experimental second moment is smaller than the theoretical rigid lattice value, then the theoretical value can sometimes be recalculated on the basis of various possible types of molecular motion. Equivalence between the two values would be evidence strongly in favour of that particular type of molecular motion.

The experimental method of measuring the second moment is discussed in section 2.4.

## 2. EXPERIMENTAL METHODS AND APPARATUS

### 2.1 Principles of Detection of Nuclear Resonance

The absorption of energy by the nuclear spin system can be measured by noting the effect of this absorption on a tuned radiofrequency coil containing the specimen. This coil is placed in a magnetic field such that the radiofrequency field is at right angles to the external field, and when the resonance condition  $h\nu = \mu H/I$  is obeyed, the absorption shows up as a change in the amplification factor  $Q$  of the coil. The nuclear magnetic resonance absorption methods measure this change of  $Q$ , whereas the nuclear induction method has another radiofrequency coil at right angles to the first coil to measure the e.m.f. induced by the precessing nuclei. The nuclear induction method was not used in any of the experiments described here, and will not be referred to in detail. Two methods have been used for the measurement of the change in  $Q$ . One is based on a controlled regenerative principle first suggested by Roberts (1947) and the other is the more standard bridge technique of BPP.

### 2.2 Regenerative Methods

In any single-valve oscillator there must be a feedback system between anode circuit and grid circuit which

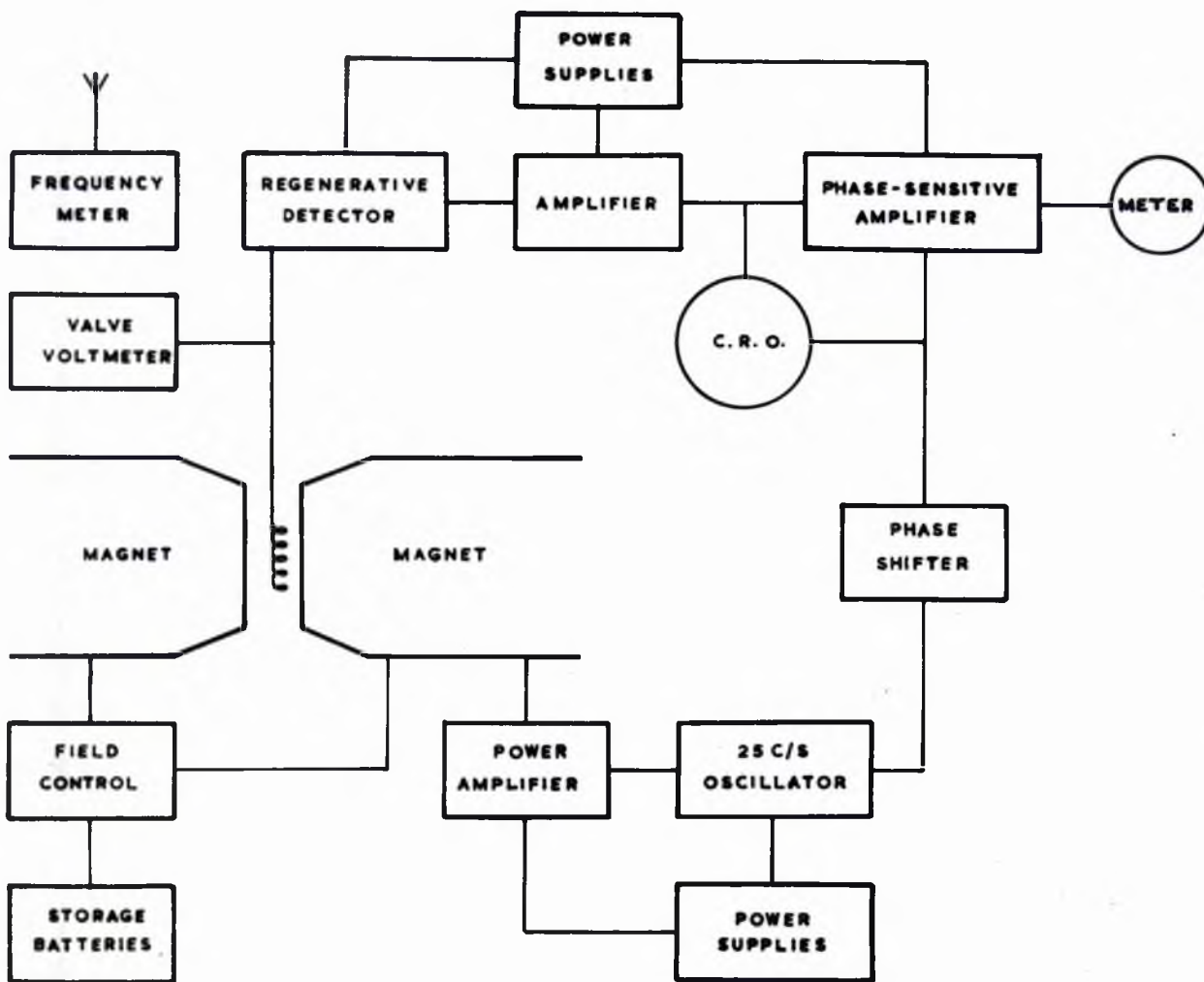


Figure 1

Block diagram of apparatus

(a) introduces a phase shift of  $180^\circ$  to counteract the inherent phase shift of the valve, and (b) allows a sufficient amount of feedback to sustain oscillation. Normally connected, a standard valve oscillator allows a much greater amount of feedback than the necessary minimum. The oscillations build up until a natural limit is reached, usually due to the curvature of the valve characteristic. If some method can be found of controlling either the gain of the valve or the amount of feedback, then a very low level of oscillation can be maintained. This means that the total effective negative resistance of the oscillating circuit is very small.

Applied to the detection of nuclear magnetic resonance absorption, the coil containing the sample is made part of this feedback network and is tuned to the required oscillatory frequency governed by the relation  $\nu = \mu H / I h$ . Any small change in the effective coil resistance due to resonance absorption within the coil appears as a large relative change of total circuit resistance and shows up as a change of the level of oscillation. If the magnetic field is being changed sinusoidally about a mean value  $H_0$  with a frequency of 25 cycles per second and a few gauss amplitude, then the absorption shows up as an amplitude modulation of the oscillatory frequency. This can be detected by conventional methods or alternatively the actual oscillating valve itself



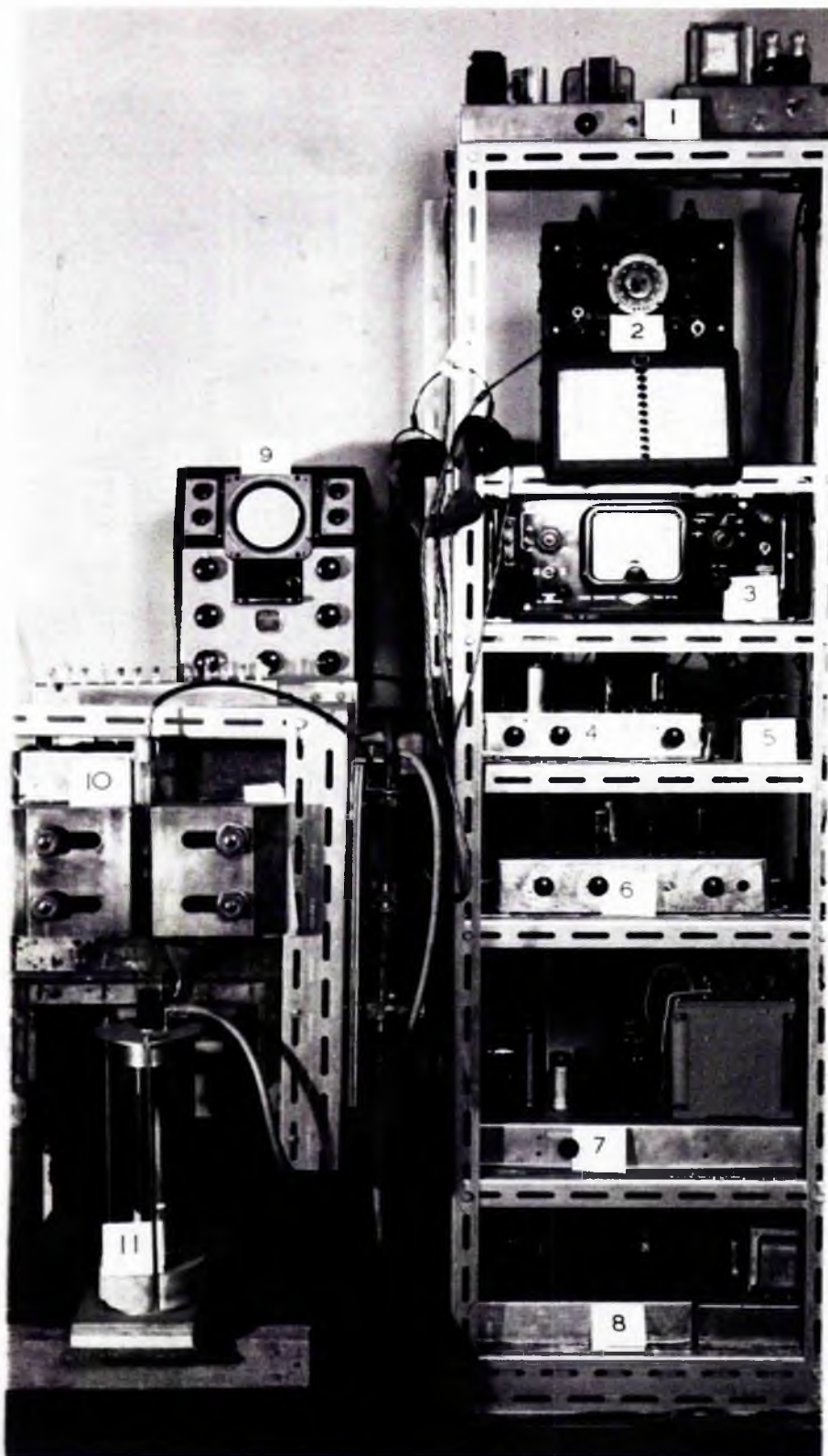


Figure 2      Photograph of Apparatus

can be used as an autodyne detector.

It is obviously desirable to keep the level of oscillation small and near the threshold, firstly to have high sensitivity and secondly to work on an effectively linear part of the valve characteristic. Several regenerative systems were built, the main object in the various circuits being to improve the signal-to-noise ratio. It is important to ensure that the onset of oscillation is smooth and gradual as the regeneration control is increased, and to have as little "backlash" as possible in this control. Figure 1 shows a block diagram of the general apparatus and a photograph is in figure 2. The important parts of the electronic system will now be considered in more detail, the numbers referring to the various units in figure 2.

The regenerative circuit (4) consisted of an EF54 valve maintained at a low level of oscillation. Both the gain of the valve and the amount of regeneration were under direct control. A coaxial cable connected this valve circuit to the coil in the magnet gap, and the working frequency was about 8 Mc/s with this particular magnet. The coil was 1.8 cm long and 1 cm diameter, with 24 turns of copper wire wound on a Teflon former. The radiofrequency voltage across the coil could be continuously varied from about 0.08 volts to 1.5 volts. Below 0.08 volt the system became unreliable as the working point was too near the threshold limiting

value and minor fluctuations were often sufficient to stop the valve oscillating. For practical purposes the figure 0.08 volt was the useful lower limit. This is important, and will be discussed later in section 2.6. The modulated radiofrequency was amplified and detected by conventional methods and the resulting audiofrequency signal further amplified. It was then fed through suitable low-pass filters either to a cathode-ray oscillograph (9) for visual observation or to a phase-sensitive detector (6) of the type described by Bloembergen (1948). For strong, narrow lines the C.R.O. was used; for weak, broad lines the phase-sensitive detector was employed.

The phase-sensitive detector (6) was essentially a very narrow band amplifier. The input signal was passed through a band pass feed-back filter and was then mixed with a pure 25 c.p.s. voltage. The resulting output was fed through a resistance-capacity network of long time-constant to a direct current push-pull amplifier and the meter M recorded any 25 c.p.s. component in the original input. In later work with a bridge system this output meter was replaced by a recording meter, which was arranged to give a continuous plot of the line-shape derivative.

The field modulating equipment is shown in the unit (7). A 25 c.p.s. resistance-capacity oscillator fed a power amplifier of the type described by Williamson (1949).

The massive output transformer seen on the right of the chassis was of large inductance ( $\sim 200$  henries) to load the output valves correctly at this low frequency of 25 c.p.s.. The amplifier could give about 15 watts into the field modulating coil. This coil was specially wound on one of the arms of the electromagnet and contained 1000 turns of 28 gauge copper wire. Part of the 25 cps. oscillator voltage was taken and fed through a phase-shifting device (5) to the X-plates of the C.R.O. (via a further amplifier) and to the phase-sensitive detector (6) where it acted as the mixer voltage. The phase-shifter was necessary to make the sinusoidal sweep of the X-plates in phase with the modulation of the magnetic field, as relative phase shifts were inherent in the electronic system and from the magnet coil inductance.

The frequency of oscillation was determined by a BC221 frequency meter (2). This was checked against the B.B.C. 200 kc/s transmission from Droitwich, which is maintained at this frequency to 5 parts in 10 million.

The remainder of the electronic equipment consisted of suitable power supplies (1),(8). The regenerative unit valve-heaters were fed from accumulators, but the remainder of the valves were quite satisfactorily heated by normal a.c. methods.

The magnet (10) was a small electromagnet whose tapered pole-pieces were reversed to give a larger gap

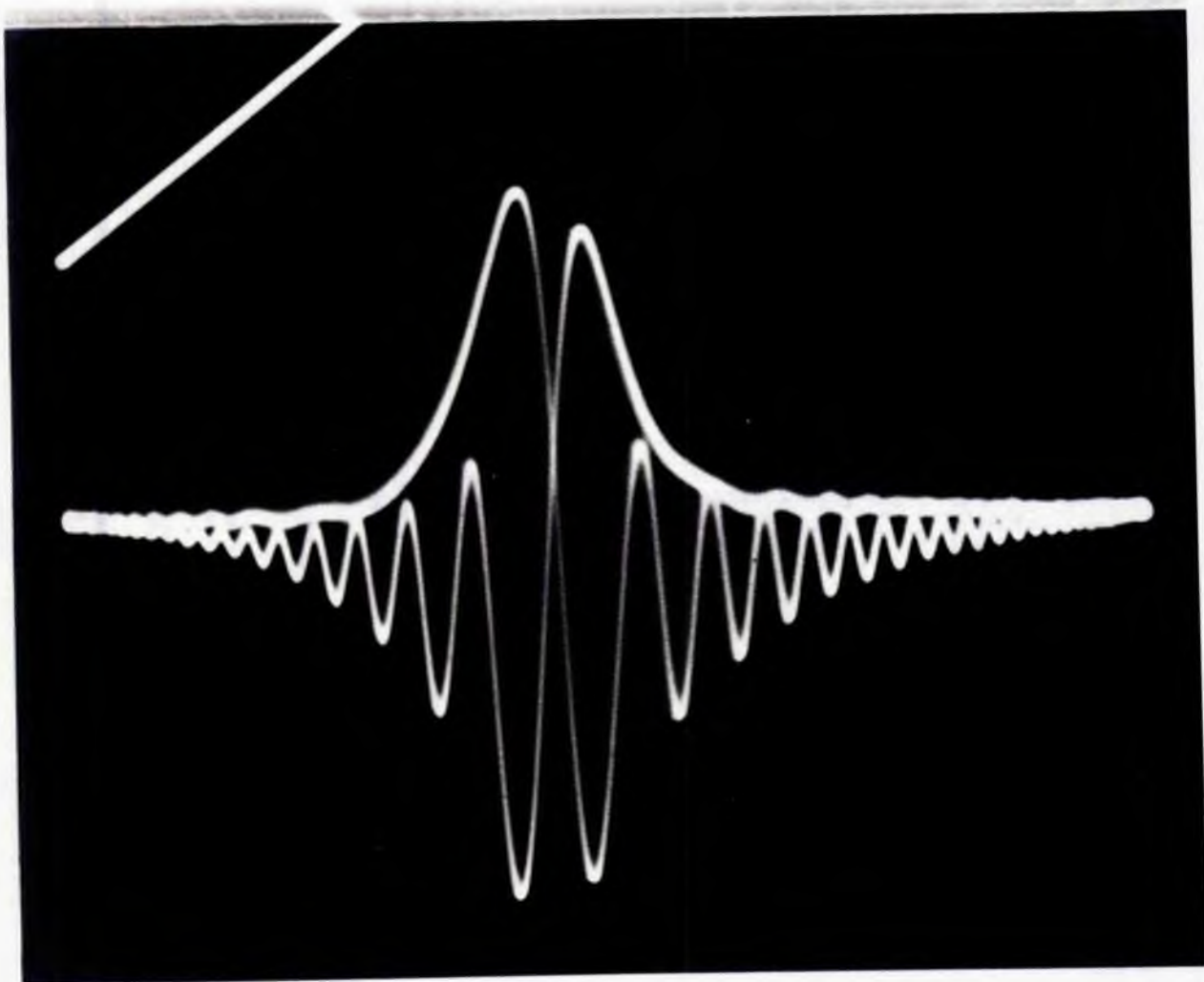


Figure 3

Resonance absorption signal in paraffin oil showing "wiggles"

cross-section in an attempt to produce a more uniform field over the volume of the sample. This magnet is referred to in more detail in section 3.1.

A typical strong signal from protons in paraffin is shown in figure 3. The peak to peak modulation was  $\sim 1.5$  gauss. The so-called "wiggles" are a well-known effect caused by the precessing frequency of the nuclei following the changing modulation field and beating with the fixed radiofrequency applied to the coil. The wiggles only occur after the modulating field has passed through the critical value for resonance, and the decay of the beats can be related to the spin-spin relaxation time  $T_2$ .

The normal methods of measuring line-shapes and relaxation times are described in sections 2.4 and 2.5, where the function of the various parts of the apparatus will become more apparent.

### 2.3 Bridge Method

This is the most widely used method and was originally developed by BPP. A radiofrequency voltage of variable level is fed into two identical tuned circuits connected in parallel. The coil of one circuit is filled with the material under investigation and placed in the field  $H_0$ . The outputs from the two circuits are fed out of phase into a high gain communications receiver and any variation of the effective

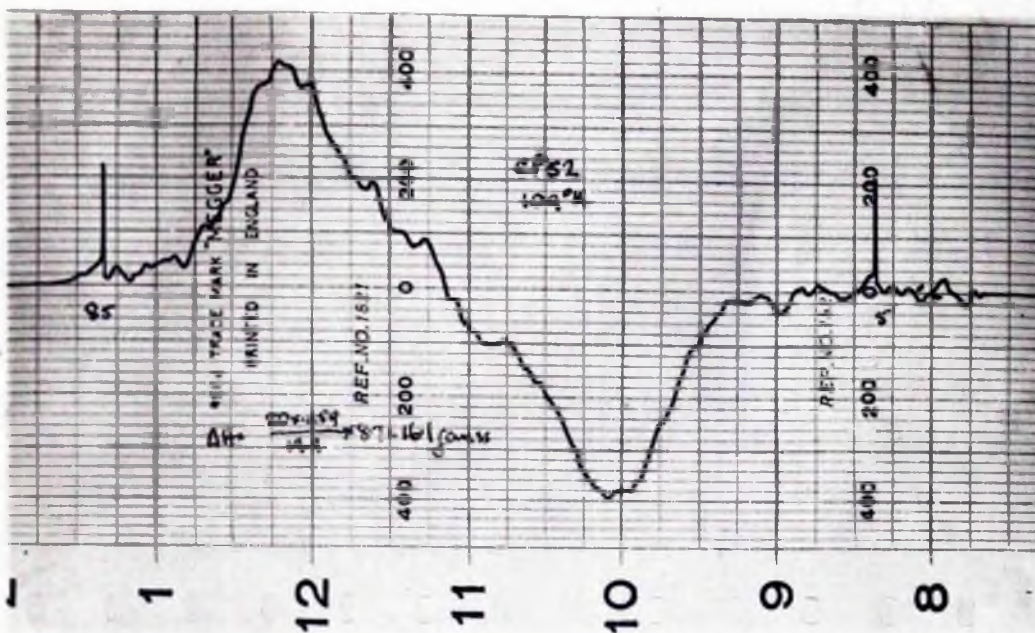
Q of the first coil due to absorption of energy by the spin system shows up as a change in the r.f. level at the input to the receiver. If the main field is changed sinusoidally at 25 c.p.s. about the mean value  $H_0$ , then the input level to the receiver is modulated and the Q variation appears after detection as a small audiofrequency signal.

A bridge system was built for use with the electro-magnet shown in figure 2, but was abandoned owing to lack of constancy of this magnetic field. A completely new bridge system was built by Dr. R. G. Eades for use with the permanent magnet and has been fully described elsewhere (Eades 1952). Much of the modulation and detection equipment is similar to that described for use with the regenerative method in the previous section.

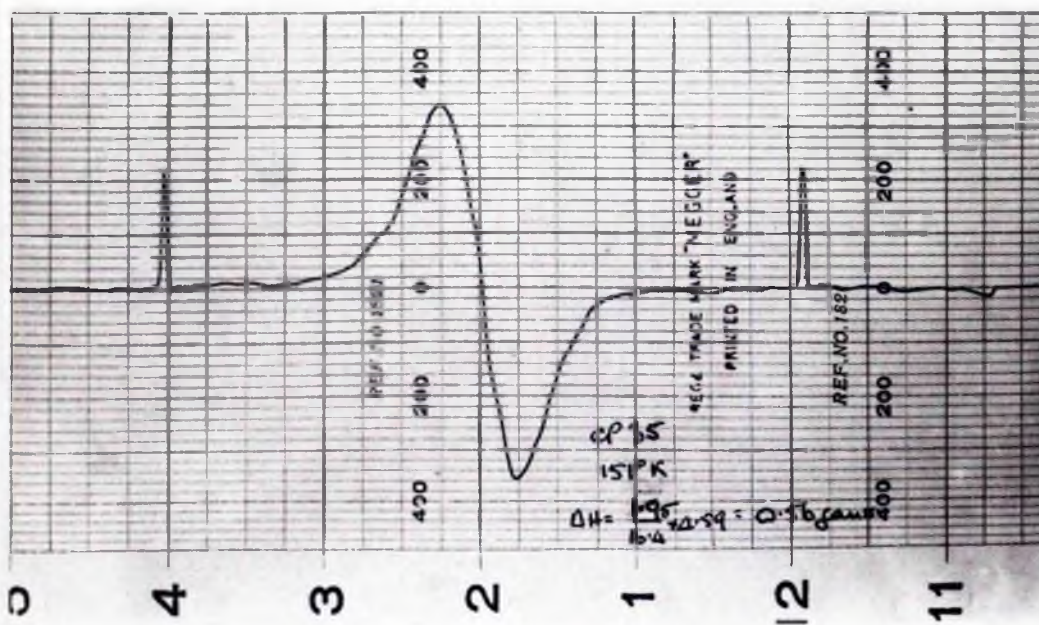
The relative merits of the two methods will be discussed after the particular types of experiment performed have been described.

#### 2.4 Measurement of Line-shape and Second Moment

For detailed line-shape plotting, the peak-to-peak value of the field modulation was reduced to a fraction of the line-width (usually  $< \frac{1}{3}$ ) and the steady magnetic field was slowly changed by a suitable biasing coil from several gauss below the central resonant field value to several gauss above this value. The resulting output from the phase-sensitive amplifier



(a) cyclopentane at 109° K



(b) cyclopentane at 151° K

Figure 4 Recorder plots of line-shape derivative



gave the variation of the slope of the absorption curve at the various field values taken. The peaks on this curve therefore represented the points of maximum and minimum slope, and a normal absorption curve has a derivative curve with one maximum and one minimum value. Any fine structure of the absorption line showed up very well on this derivative plot, provided the field modulation was not so large as to smooth out this fine structure. The recording meter was invaluable for producing permanent records of these derivative plots, and two of these are shown in figure 4. The upper curve has a large line-width and a poor signal-to-noise ratio, while the lower curve is of a narrow line (greater than the field inhomogeneity) with a good signal-to-noise ratio. If we define line-width as the separation on a gauss scale between the points of maximum and minimum slope of the absorption curve, then the derivative curve gives this value directly. The recorder time-scale was accurately calibrated in terms of the known field bias from the calibration marks shown on each side of the derivative curve and the biasing field current was automatically varied by a motor-driven potentiometer system.

The second moment can be obtained from this derivative curve without the need for replotting an integrated curve. Re-writing equation 5 in terms of a field variable,

$$S = \left\langle (\Delta H)^2 \right\rangle_{av} = \frac{\int_0^{\infty} (H - H_0)^2 g(H) dH}{\int_0^{\infty} g(H) dH} \quad (9)$$

where  $g(H)$  is the measured height of the absorption curve at field value  $H$ ,  $H_0$  being the field at the centre of the resonance curve. The denominator is introduced because  $g(H)$  is not necessarily normalised when experimental values are taken. The integration limits of 0 to  $\infty$  can be taken as  $-\infty$  to  $+\infty$  in practice, as  $g(H)$  is always zero as far remote from the resonance centre as  $H_0$  gauss. Changing the variable from  $H$  to  $h = H - H_0$ , the new variable  $h$  represents the field deviation from the resonance centre, and we have

$$S = \frac{\int_{-\infty}^{+\infty} h^2 g_1(h) dh}{\int_{-\infty}^{+\infty} g_1(h) dh} \quad (10)$$

where  $g_1(h) = g(H)$ . This can be written

$$S = \frac{\int_{-\infty}^{+\infty} g_1(h) \frac{1}{3} d(h^3)}{\int_{-\infty}^{+\infty} g_1(h) dh} = \frac{\left[ \frac{1}{3} g_1(h) h^3 \right]_{-\infty}^{+\infty} - \frac{1}{3} \int_{-\infty}^{+\infty} h^3 f(h) dh}{\left[ g_1(h) h \right]_{-\infty}^{+\infty} - \int_{-\infty}^{+\infty} h f(h) dh}$$

where  $f(h) = \frac{dg_1(h)}{dh}$ , the line-shape derivative. Provided that  $g_1(h)h^3 \rightarrow 0$  as  $h \rightarrow \infty$ , and  $g_1(h)$  is usually zero only a few gauss away from the resonance centre, then both integrated terms are zero, and

$$S = \frac{1}{3} \frac{\int_{-\infty}^{+\infty} h^3 f(h) dh}{\int_{-\infty}^{+\infty} h f(h) dh} \quad (11)$$

This can be found from the derivative curve, and the trapezium rule is used to evaluate the two integrals.

To obtain a value for the second moment according to Van Vleck's theory necessitates a knowledge of both crystal and molecular structure, among other factors. The theoretical value is usually split into two parts. One part is the contribution from the interactions between protons in the same molecule, known as the intramolecular contribution; the other part is due to the interactions between protons of different molecules, and is known as the intermolecular contribution. The first depends on molecular structure and the second on crystal structure. The second moment is a function of the inverse sixth power of the interproton distances and so is very sensitive to the actual values of these distances. Changes in crystal structure will show up as changes in second moment values, and if there is any molecular motion in the crystal lattice, then provided the orientation frequency is high enough the second moments will be reduced by factors which may be calculable. Examples of this motion will be considered when the experimental results are discussed.

## 2.5 Measurement of Spin-Lattice Relaxation Times

The spin-lattice relaxation time  $T_1$ , is a measure of the interaction between the nuclear spins and the lattice, the larger  $T_1$ , the smaller the interaction. This relaxation mechanism is of interest, and it appears that the dominant factors are not thermal lattice vibrations as originally conceived but internal molecular or ionic reorientations together with impurity effects. We shall mostly be concerned with the manner in which  $T_1$  varies with temperature and shall be relating this temperature dependence with molecular reorientation in some of the experiments.

The interpretation of relaxation time data is complicated by the many variables which are involved, but has been fully analysed by BPP. We shall extract the necessary theory relevant to our particular cases.

From the definition of  $T_1$ , in equation 2, it follows that if the spin temperature is disturbed and then allowed to come back to equilibrium,

$$dn/dt = (n_0 - n)/T_1$$

where  $n$  is the surplus population of the lower level at any time  $t$  and  $n_0$  the value of  $n$  corresponding to thermal equilibrium with the lattice. If a radiofrequency field is also applied, then the rate of return will be reduced because nuclei from the lower level are now being raised to the higher level by this field.

Therefore

$$\frac{dn}{dt} = \frac{n_0 - n}{T_1} - 2nW_{+ \rightarrow -} \quad (12)$$

where  $W_{+ \rightarrow -}$  is the total transition probability. The factor 2 enters because if one proton changes levels, the population difference changes by two. A steady state is reached when  $dn/dt = 0$ , and the spin-temperature reducing effect of the spin-lattice interaction is compensated by the spin-temperature increasing effect of the radiation field and

$$\frac{n_0 - n}{T_1} = 2nW_{+ \rightarrow -}$$

The value of the transition probability follows from magnetic dipole transition theory and is  $\frac{1}{2} \gamma^2 H_1^2 g(\nu)$ , where  $\gamma$  is the gyromagnetic ratio of the proton,  $H_1$  is the amplitude of the radiofrequency field and  $g(\nu)$  the normalised line function.

Hence

$$\frac{n}{n_0} = \frac{1}{1 + \frac{1}{2} \gamma^2 H_1^2 T_1 g(\nu)} \quad (13)$$

At the resonance centre we can make use of the spin-spin relaxation time  $T_2$ , defined in equation 4, and

$$\frac{n}{n_0} = \frac{1}{1 + \gamma^2 H_1^2 T_1 T_2} \quad (14)$$

This relation is an important one, and we see that if  $n$  has not to be much less than  $n_0$ , then  $\gamma^2 H_1^2 T_1 T_2 < 1$ .

The methods of measuring  $T_1$  fall into two main groups, one where the direct recovery from saturation can be

measured and the other where the direct recovery from saturation is too rapid for measurement. We see from equation (14) that if  $H_1$  is large, then  $n < n_0$  and the absorption signal strength will be small. The direct recovery from saturation can be measured by using a suitable modulation amplitude and arranging the output meter to read either the maximum or minimum slope by correct adjustment of the biasing field. The spin-temperature is then increased and the sample "saturated" by increasing the r.f. level 30 to 40 db for a few seconds. The r.f. level is then reduced to its normal value and the rate of recovery of the meter needle noted. The lower r.f. level is arranged to be small enough for the equilibrium spin-temperature at that level to be almost the same as the temperature of the lattice. The recovery is exponential and a value for  $T_1$  can be found. This method is suitable when  $T_1$  is greater than about 30 seconds. Below this value the recovery is too rapid for accurate measurement. If, however, the line is strong and narrow and can be displayed on the C.R.O., then this recovery can be photographed by a cine-camera and a similar analysis made.

When the value of  $T_1$  is small, the progressive saturation method is used. This is based on equation 14 where  $n = \frac{1}{2}n_0$  when  $\gamma^2 H_1^2 T_1 T_2 = 1$ . If the readings of the output meter (assumed proportional to  $n$ ) are plotted against

increasing  $H_1$  (taken to be proportional to the radio-frequency voltage across the coil) then the half-value point at two temperatures  $T_A$  and  $T_B$  is such that

$$(H_1^2 T_1 T_2)_A = (H_1^2 T_1 T_2)_B$$

or

$$\frac{(T_1)_B}{(T_1)_A} = \frac{(H_1^2 T_2)_A}{(H_1^2 T_2)_B} = \left(\frac{V_A}{V_B}\right)^2 \left(\frac{\Delta H_B}{\Delta H_A}\right) \quad (15)$$

The spin-spin relaxation time  $T_2$  is taken to be inversely proportional to the line-width  $\Delta H$ , which is true for constant line-shape, and  $V_A, V_B$  are the r.f. voltages corresponding to r.f. fields  $(H_1)_A, (H_1)_B$ . Hence values of  $T_1$  throughout a given temperature range can be found in proportion to one standard time  $(T_1)_A$ , and if this is at a temperature where  $T_1$  is long enough to be measured by a direct recovery method, then absolute values of  $T_1$  throughout the temperature range can be deduced. The theory has been simplified a little from that given by BPP as there are further conditions which must be obeyed for this interpretation to be wholly correct. However, if these conditions are not quite fulfilled errors introduced are relatively small and they will be mentioned in the relevant sections where the experimental results are discussed.

All these methods have been used in the experiments reported in this thesis.

## 2.6 Comparison of Regenerative and Bridge Methods

We are now in a position to discuss the relative merits of the regenerative and bridge methods of detection of nuclear magnetic absorption in the light of the experiments undertaken.

The regenerative method has the advantages that:

- (a) it is not frequency dependent in that no frequency-sensitive balancing is necessary.
- (b) it only responds to the absorption part of the resonance and not the dispersion part.

The bridge method has the advantages that:

- (a) the radiofrequency field  $H_1$  can be varied over a wider range.
- (b) the frequency stability is better.

From these points it can be seen that the regenerative method should be useful where the frequency has to be varied, as for example in plotting out a magnetic field, or in a search for a new resonance by a frequency sweep rather than a field sweep. The bridge method should be more useful when frequency and field are fixed and it is the detailed line-shape which is desired. The main disadvantage of the bridge is that balance has to be made for both amplitude and phase. Usually the phase is accurately balanced and a small amount of amplitude unbalance allowed, so that this unbalance portion acts as a carrier wave for the resonance modulation.



If the amplitude is correctly balanced and a small amount of phase unbalance allowed, then the resulting curve would be a dispersion curve and not an absorption curve. Any departure from correct phase balance when the absorption curve is required results in an admixture of the two curves with consequent distortion. Variation of the temperature of the sample coil affects its characteristics, and constant attention must be paid to ensure correct phase balance throughout.

However it is in the value of the radiofrequency field that the bridge has the advantage when detailed line-shapes are plotted. The automatic sweep through a broad line takes about 15 minutes, during which time the spin system is being heated by the applied r.f. field. If this field is too high, then saturation will set in as described in the previous section, and the two halves of the derivative curve may not be equal. The factor  $\gamma^2 H_1^2 T_1 T_2$  must be less than 1 if serious saturation is to be avoided. If we take a typical case reported later, namely n-pentane, the measured  $T$  values range from 70 seconds at  $73^\circ\text{K}$  to 0.01 second at  $140^\circ\text{K}$ . The relation between  $H_1$  and the r.m.s. voltage  $V$  across the coil is calculable and using the known line-widths at these temperatures to calculate a value for  $T_1$ , we find that to avoid saturation

(a) at  $73^\circ\text{K}$   $V < \sim 0.07$  volt

(b) at  $140^\circ\text{K}$   $V < \sim 6$  volts.

These are only order of magnitude calculations and vary slightly with the nature of the coil and the working frequency. The important point, however, is that to avoid saturation when  $T_1$  is long the r.f. voltage across the coil must be of the same order as, or less than, the lowest stable voltage available from the regenerative circuit. At temperatures where  $T_1$  is short (provided  $T_2$  is approximately constant) this method will be satisfactory. If the line-width also changes by large factors (as for example in cyclopentane) then the variation of  $T_2$  must be taken into account and the product  $T_1 T_2$  considered.

As the substances used in the experiments were of high purity,  $T_1$  was not reduced by impurity effects and in practice it was found that in many cases the regenerative method did give unsymmetrical lines. It was mainly for this reason that the accurate determinations of line-widths and second moments were made with the bridge. In some cases the voltage across the coil had to be as low as 0.003 volt to avoid saturation, and in these cases the signal-to-noise ratio of the output from the phase-sensitive detector was low. The regenerative system was used for the early qualitative investigation of a number of substances, reported in section 4.6, and for the detailed plotting of the central field of the permanent magnet, reported in section 3.4.

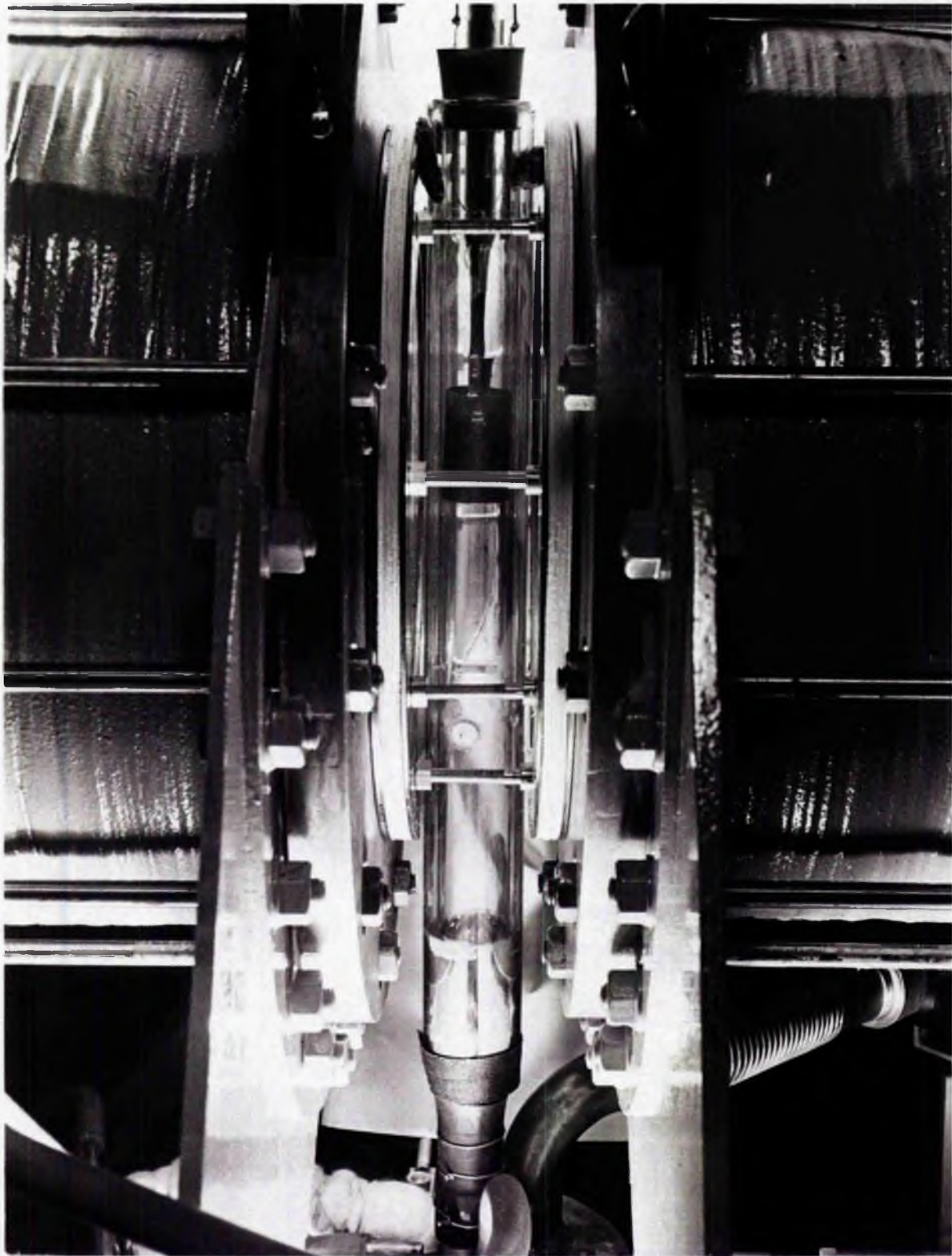
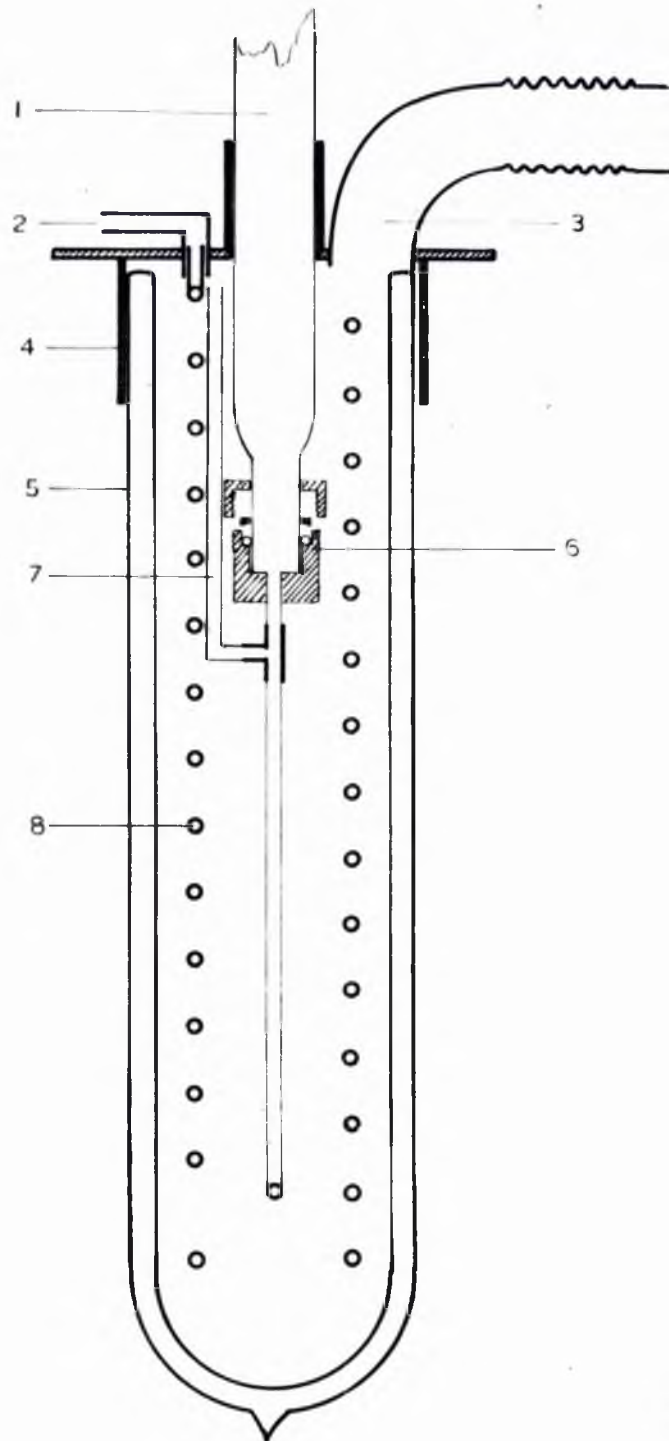


Figure 5 Magnet gap with Dewar tube in position



GAS CRYOSTAT.

Figure 6

## 2.7 Temperature Control Apparatus

### 2.7.1 Below room temperature

The temperature of the sample could be varied from room temperature down to  $70^{\circ}\text{K}$  by means of a cold gas flow method. The r.f. coil and sample were contained in a long Dewar tube between the poles of the magnet. This Dewar tube assembly is shown in figure 5 mounted between the poles of the permanent magnet to be described in section 3. The temperature of the flow gas is controlled by varying the rate of flow of the gas through a spiral immersed in liquid oxygen or liquid nitrogen. The compressed gas, which may be air, nitrogen or hydrogen depending on the temperature required, is dried and passed through a Rotameter flow gauge to a gas cryostat, a sectional drawing of which is in figure 6. The incoming gas enters at 2 and flows down the german silver spiral 8 immersed in the liquid coolant. This liquid is contained in the Dewar vessel 5. The cold gas then passes up the long Dewar tube 1, which is fixed to the spiral by a Gaco ring seal 6. The sample coil is in the upper part of this Dewar tube. With liquid oxygen as coolant and nitrogen or air as flow gas, the sample could be cooled to about  $98^{\circ}\text{K}$ . Temperatures down to  $70^{\circ}\text{K}$  could be reached using liquid nitrogen boiling under reduced pressure, the pumping line 3 being shown. For this lower temperature region the flow gas was hydrogen, and this was precooled by an auxiliary spiral

immersed in a separate Dewar flask in order to prevent excessive boiling away of the nitrogen in the main Dewar flask.

This cooling system has been found quite satisfactory in practice and temperatures can be maintained constant to about  $1^{\circ}\text{C}$ , a change to a new steady temperature being achieved in about 15 minutes. The temperatures were measured with a copper-constantan thermocouple. The absolute accuracy depended on the actual temperature but was  $\sim 1^{\circ}\text{C}$  except possibly in the region below about  $100^{\circ}\text{K}$  where the thermo-electric voltage developed by the thermocouple varied less rapidly with temperature.

### 2.7.2 Above room temperature

In the earlier experiments with the small electromagnet, substances which were solid at room temperatures were heated to their melting points in a small cylindrical furnace placed in the magnet gap. The furnace consisted of a pyrex tube of 15 mm inside diameter round which a length of nichrome strip of resistance 25 ohms was wound in the form of a spiral. The assembly was insulated against heat losses by a length of asbestos rope wound over the heating spiral. This simple furnace was quite efficient and temperatures up to  $700^{\circ}\text{K}$  could be reached with a current of 1.5 amps. The temperatures were measured by a copper-constantan thermocouple which was calibrated.

### 3. THE PERMANENT MAGNET

#### 3.1 Requirements of Magnetic Field

Theoretical considerations show that, with certain approximations, the signal-to-noise ratio for any given substance is almost proportional to the square of the magnetic field. It is therefore desirable to have a high field strength in order to be able to detect weak signals and to improve the signal strength all round. The actual value of the field will be limited by several factors, such as size and weight of the magnet, as well as by the magnetic characteristics of the material used. The ideal magnet would give a field which was both constant and homogeneous as well as high. Constant, because drift of field strength during the plotting of a detailed broad line-shape must be avoided; homogeneous, to allow very narrow lines to be measured without being masked by the variation of field strength over the volume of the sample. Fine structure in organic liquids recently reported by Arnold, Dharmatti and Packard (1951) showed that a resolution of  $\sim 1$  in  $10^7$  is required for the true line-widths of these liquids to be the dominant factor in determining the observed line-shape. The sample volume can be reduced to decrease the inhomogeneity, but this volume cannot be reduced too far as serious loss of signal strength would

result due to the smaller number of resonating nuclei present. Geometrical inhomogeneities will increase with increasing field strength, and so a compromise may have to be found between these conflicting requirements. This inhomogeneity effect is only troublesome for very narrow lines, and in most of the work reported here the line-widths are relatively broad (up to 16 gauss) and an inhomogeneity of  $\sim 0.3$  gauss is not too serious. Moreover when second moments are considered the inhomogeneity of the magnet means a correction of  $\sim 0.03$  gauss<sup>2</sup> to the second moment. This is usually small compared with the experimental accuracy, and the second moments of some lines can be  $\sim 25$  gauss<sup>2</sup>. It will have an appreciable effect on narrow lines, however, and must be allowed for.

The magnetic field can be produced either by an electromagnet driven from storage batteries or by a permanent magnet. An electromagnet has the advantage of flexibility in that the field strength can readily be changed if needed but, to offset this, it is usually larger and heavier than a corresponding permanent magnet. The electromagnet consumes power, and in order to achieve the constancy of field necessary for the experiments some form of electronic stabilisation is highly desirable. A small electromagnet was used for preliminary experiments with the regenerative system of detection. The magnet is shown on the left of figure 2. The pole-pieces were reversed in order to try and improve the geometric



homogeneity by increasing the area to length ratio of the gap, and the size of the gap was 4" x 6" x 1 $\frac{1}{8}$ ". The batteries used to energise this magnet were not stable enough to produce a constant field, and difficulty was always experienced from this inconstancy. An electronic stabiliser was not constructed in view of the imminence of a permanent magnet. In this small magnet a current of 2 amps gave a field of  $\sim$  2000 gauss and the inhomogeneity was  $\sim$  0.1 gauss over the volume of the sample ( $\sim$  0.5 cm ). At higher fields, although the inhomogeneity was not serious, the drain on the storage batteries proved too much for their capabilities.

Accordingly it was decided that for the particular work envisaged, in which protons would be the resonating nuclei, a permanent magnet giving a field of  $\sim$  6700 gauss was desirable. This corresponds to a working frequency of 28.5 Mc/s. The design of this magnet will be described and its actual performance examined. It has been in use since July 1951 and has proved an extremely useful and necessary part of the apparatus.

### 3.2 General Design of Permanent Magnet

The design of large individual magnets is a mixture of fundamental magnetic equations, practical engineering considerations and some rather vague empirical factors.

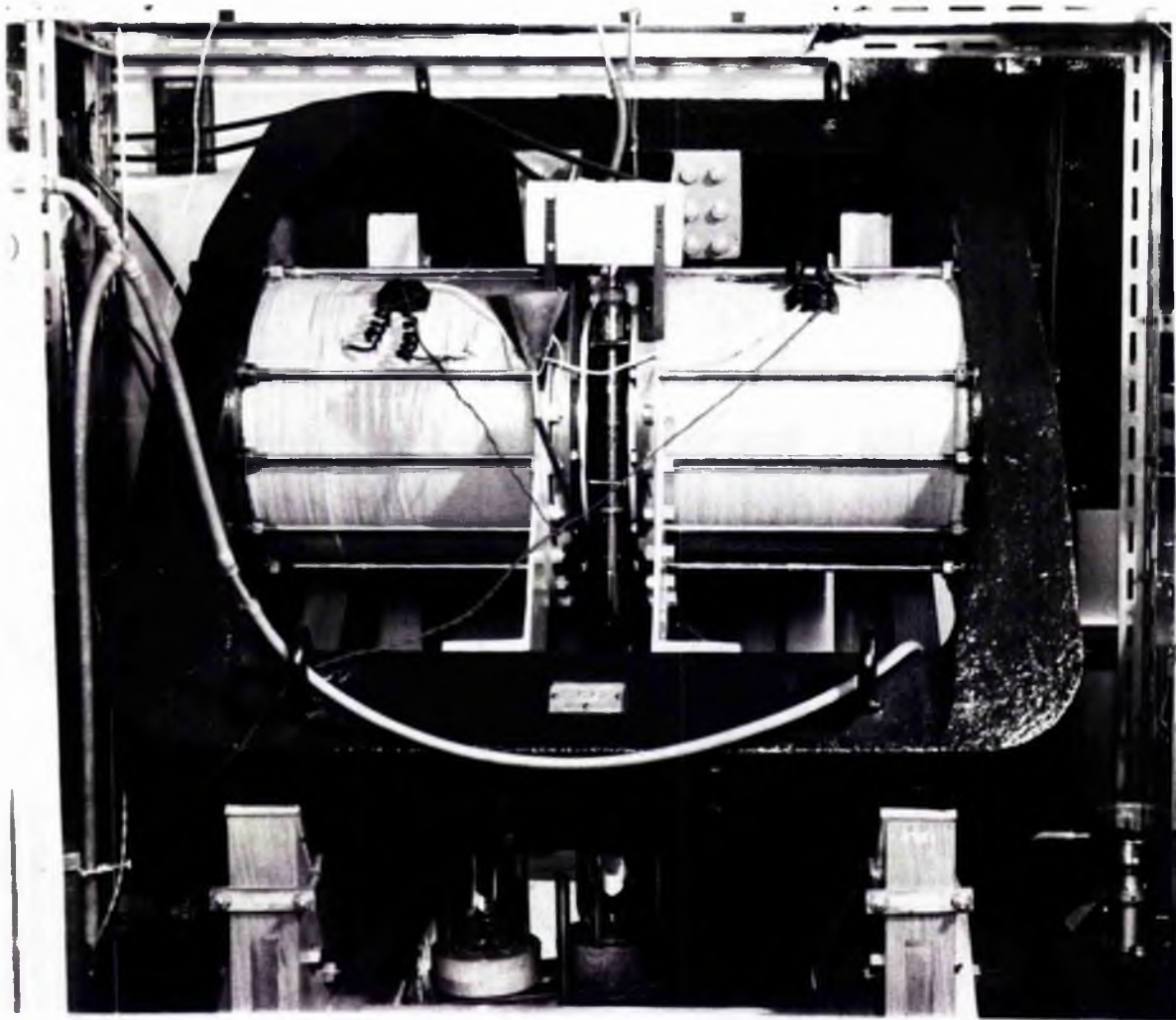


Figure 7      Photograph of Permanent Magnet

The fundamental equations governing design are well-known and are discussed in appendix 1. The main points are:

- (a) the length of magnetic material must be enough to produce sufficient magneto-motive force to overcome the reluctance of the magnetic circuit,
- (b) the cross-section of the magnetic material must be large enough to produce the necessary flux in the air gap.

From these considerations it follows that the magnetic material is used most economically when the working point on the magnetisation curve is such that the BH product of the material has a maximum value, where B is the induction corresponding to a coercive field H. If this is arranged, then the minimum volume of magnetic material will be required. The newer magnetic alloys show considerable improvement in their  $(BH)_{\max}$  values compared with cobalt-steel. For the present magnet the alloy Alcomax III was used. This alloy is anisotropic in its magnetic properties due to the heat treatment it receives during manufacture, when it is annealed in the presence of a magnetic field. The value of  $(BH)_{\max}$  for this alloy is about 4.75 mega-gauss-oersted, compared with a  $(BH)_{\max}$  of 0.96 mega-gauss-oersted for 35% cobalt-steel. This means a saving of a factor 5 in the amount of material needed for a given requirement.

The magnet was designed in collaboration with

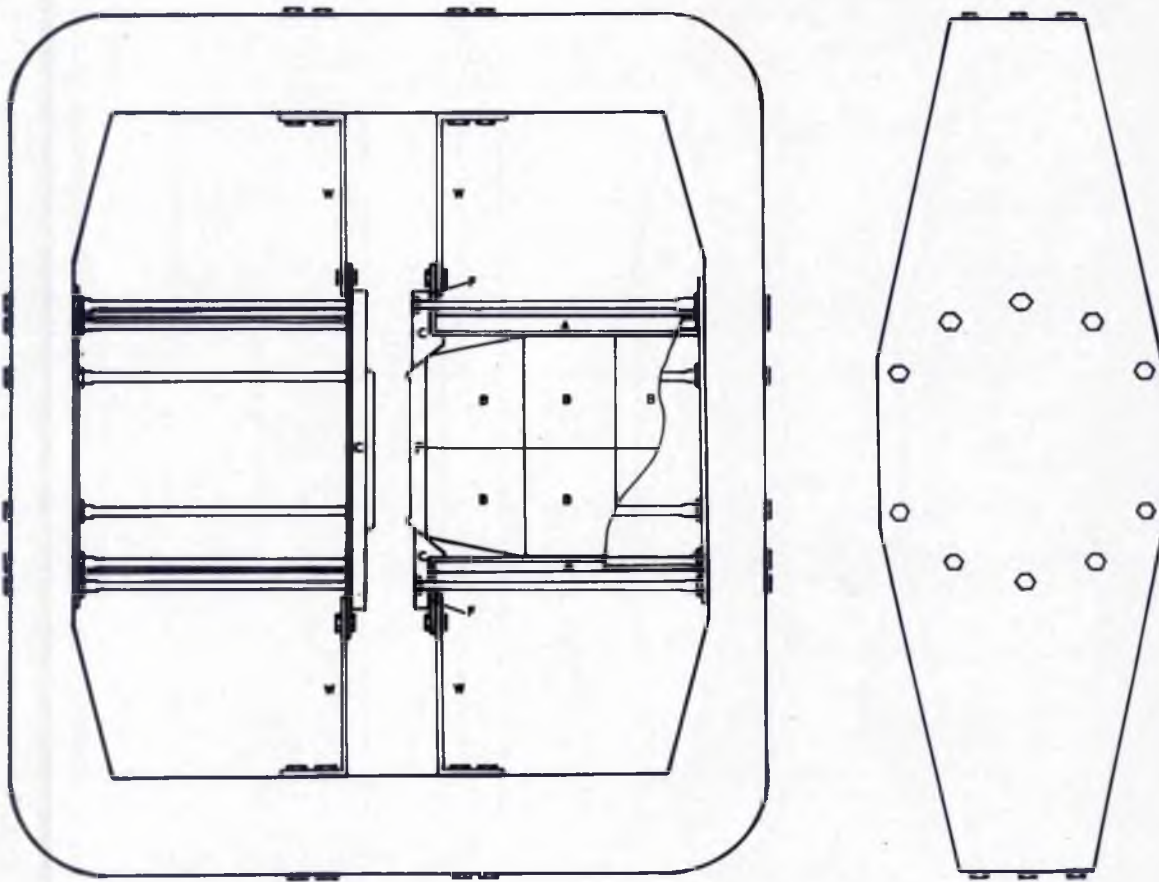


Figure 8

Permanent Magnet Assembly

Dr. E. R. Andrew, and technical details were supplied by Messrs. W. Jessop & Sons, Ltd., who were responsible for the construction of the magnet.

The specification was for a field of 6700 oersted in a gap 5.4 cm long of circular cross-section 20 cm diameter. A raised rim 0.2 cm was to be provided round the periphery of each pole-face; this was intended to remove the first order geometric inhomogeneity inherently present with plane circular pole-faces. The design of this rim is discussed in section 3.3. The final design of the magnet followed a double-yoke principle (Plesset, Harnwell & Seidl, 1942); figure 7 is a photograph of the magnet and figure 8 is a drawing showing the construction. The soft iron polecaps P abut on to blocks B of magnetic material, the whole assembly being held firmly to the yoke by a series of long stainless steel bolts acting through phosphor-bronze clamping plates C to the polecaps P. The magnetic blocks B are contained in a cylindrical brass coil formers F on to which are wound the magnetising coils A. Most of the weight of the polepieces is taken by the brass wings W attached to the upper and lower arms of the yoke. The yoke and polecaps of the magnet are of Armeo iron. Great attention was paid to the polecaps as previous experience with similar magnets in nuclear resonance work suggested that local variations in the quality of the iron of the polecaps contributed greatly

to the field inhomogeneities. The polecaps were to be forged, rough machined, carefully annealed in a neutral atmosphere and finally machined and ground to accurate size. Without careful annealing local patches may only have a permeability of  $\sim 500$ , compared with the normal value for this high quality soft iron of  $\sim 2500$  (Hoselitz, 1950). This would have serious effects on the homogeneity of the field in the gap. Careful tolerances were placed on the drawings and special attention was paid to the accuracy of parallelism of the polecaps. The magnetic material is in the form of segmental blocks with interior angle  $90^\circ$ , twelve of these blocks being placed each side. Each pole-piece could not be made from one large block due to technical difficulties, as the heat and magnetic treatments are unreliable for large blocks.

Alcomax III has a nominal  $(BH)_{\max}$  value of 4.75 mega-gauss-oersted, but for large specimens this value is rather lower. At this  $(BH)_{\max}$  value,  $H = 500$  oersted and so, neglecting the reluctance of the yoke and polecaps, the theory of appendix 1 gives the required length of material for a final gap field of 6700 oersted

$$L = \frac{6700 \times 5.4}{500} = 72.4 \text{ cm}$$

This was made 74 cm to allow for the small iron reluctance, giving two polepieces each 37 cm long.

The calculation of the cross-sectional area of the magnetic material presents more difficulty. The nominal value of  $B$  at the  $(BH)_{\max}$  point is 9500 gauss, but this will have to be modified because

- (a) about 10% is the proportion supposedly lost because of the large blocks of material,
- (b) about 5-10% is lost due to the artificial ageing process, normally carried out to accelerate the usual slow decrease of field experienced during the first months after magnetisation.

The effective  $B_m$  is therefore 7800 gauss. If this is the induction where the polecaps abut on to the magnetic material, then the area reduction due to the tapered polecaps, together with the leakage factor  $K$ , of 1.6 (see appendix 1) gives a gap field of 7000 oersted, a little in hand over the 6700 oersted specified.

The leakage from the surface of the magnetic material of one polepiece will be (a) to the yoke and (b) to the other magnetic polepiece across the median plane of the gap. This latter leakage will be the greater, and will increase towards the gap as the magnetic potential difference from one point to an equivalent point on the other pole is greater and the path difference smaller. To keep the induction in the material constant, the ideal shape of the pole-pieces would therefore be a gradually increasing taper from yoke to gap.

For practical purposes the taper was confined to the third set of blocks, where the leakage will be greatest. The construction can be seen from the cut-away right hand polepiece of figure 8. Eight of the Alcomax III blocks were fitted together giving a cylinder of magnetic material 30 cm diameter and 24 cm long. The third section was made from four blocks, each 13 cm long, tapering the total cross-section down from 30 cm to 24 cm. This allows for the calculated leakage factor  $K_2$  of 1.65 (see appendix 1). The total weight of the Alcomax III is about 800 lb.

The dimensions of the yoke were arranged to reduce the leakage from polepieces to yoke and to ensure that the cross-section of the yoke was large enough to carry the field without the iron becoming saturated. The main outside dimensions of the yoke are 100 cm by 118 cm.

The magnetising coils were arranged

- (a) to suit the magnetising voltage said to be available at the manufacturers, so that the material would be fully magnetised,
- (b) to enable these coils to be used for biasing the field about  $\pm 30$  oersted during the detailed plotting of a line-shape.

Each coil contains 1000 turns of 14 S.W.G. copper wire. The estimated magnetising current of 63 amps. would be in overload for this wire, but would only be flowing for a short time.



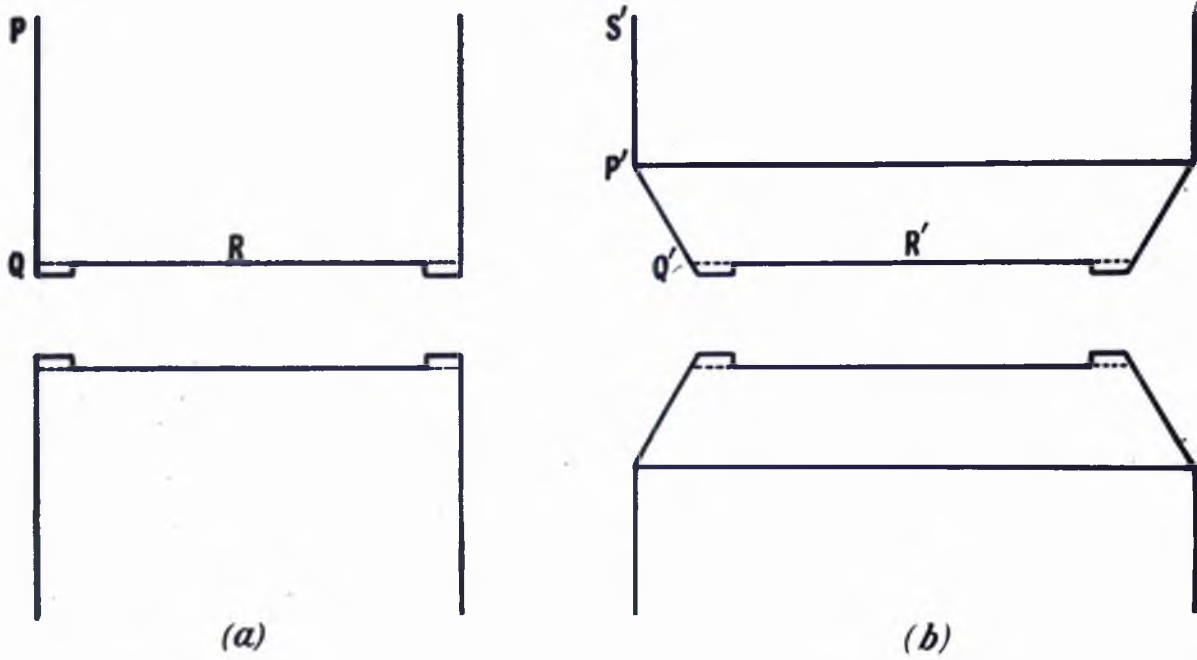


Figure 9

Diametrical sections of typical magnet polecaps

### 3.3 Ring Shims for Coned Magnet Polecaps

In any magnet fitted with plane parallel polecaps there is inevitably a smaller field near the edges of the gap as compared with the field in the centre. Rose (1938) showed how this decrease could be counteracted to a large extent by the use of a small raised rim round the periphery of each pole-face. His analysis envisages polecaps having axial symmetry, a diametrical section being shown in figure 9(a). The first order inhomogeneity can be removed by suitable choice of shim dimensions and Rose gives in graphical form the height of the necessary raised rim in terms of its width. His data only apply to the case shown in figure 9(a), namely that for which the angle PQR is  $90^\circ$ .

When a permanent magnet is employed, the efficient use of the permanent magnet material frequently requires the diameter of the poles to be greater than the diameter of the gap. The polecaps must then be in the form of truncated cones (figure 9(b)). The angle P'Q'R' is greater than  $90^\circ$ , so that Rose's data are not strictly applicable. The theory given by Rose was adapted by Dr.E.R.Andrew to cover the case of the permanent magnet discussed in the previous section. This theory has been extended to apply to the more general case, and calculations have been made to give the ring shim dimensions for all reasonable angles of coning (Andrew and Rushworth,1952).

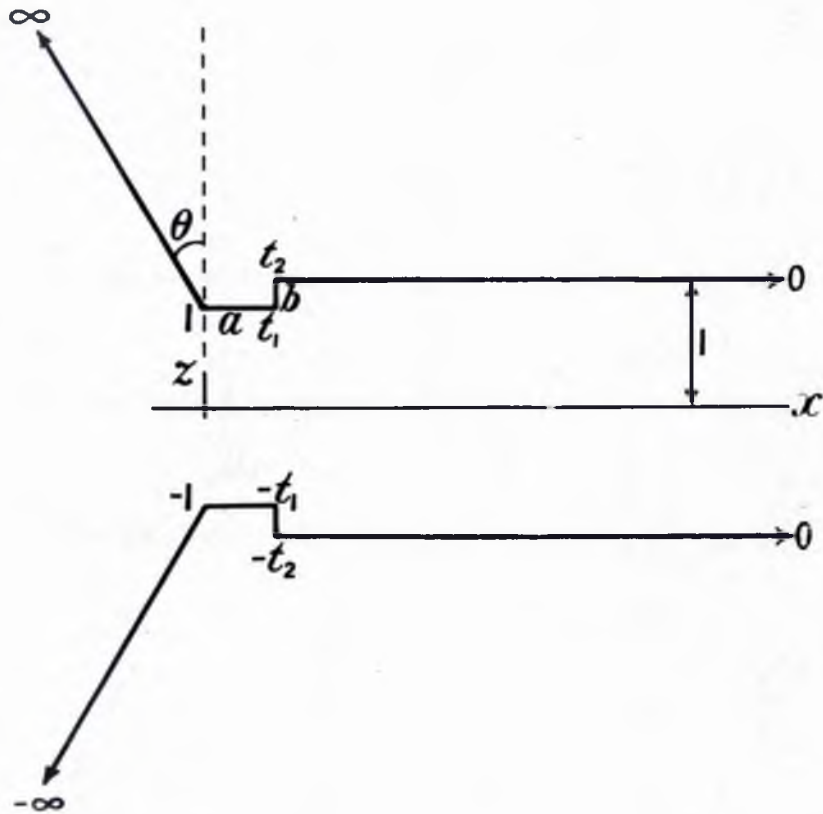


Figure 10

Conformal mapping of the  $t$ -plane on the  $\zeta$ -plane

Rose's analysis will not be repeated in detail, but the outline of his method will be given. He makes two main assumptions:

- (a) That the reluctance of the soft iron of which the polecaps are made is negligible; the surface of the polecaps may then be treated as equipotential surfaces.
- (b) That the diameter of the polecap is large compared with the width of the gap; the potential problem then approximates to one in two dimensions, and may be solved by conformal mapping using the Schwarz transformation method. (See for example Green, 1948).

Cartesian coordinates are chosen with the origin at the edge of the magnet and in the median plane. The z-axis is normal to the median plane through the edges of the gap. The unit of length throughout is half the width of the gap. The magnetic potential obeys Laplace's equation

$$\frac{\partial^2 V}{\partial x^2} + \frac{\partial^2 V}{\partial z^2} = 0$$

if assumption (b) is reasonably fulfilled. A variable  $\zeta = x + iz$  is introduced together with a potential U conjugate to V. The relation between U and V is given by the Cauchy-Riemann equations. In quoting these equations Rose makes an error in sign, but this error disappears later

and does not affect the result. The general solution of Laplace's equation gives the imaginary part of the complex function  $W = U + iV$  where  $U$  and  $V$  are functions of  $x$  and  $z$ . The procedure Rose adopts is to establish a connection by conformal mapping between  $W$  and an auxiliary variable  $t$  on one hand, and between  $\xi$  and  $t$  on the other hand. By eliminating  $t$  the relation between  $W$  (the potential) and  $\xi$  (the coordinates) can be found. The variable  $t$  assumes real values on equipotential surfaces and particular values are assigned to the corners of the poles (i.e. at the singularities). The connection between  $\xi$  and  $t$  is shown by Rose to be

$$\frac{d\xi}{dt} = -\frac{2}{\pi t} \prod_n \left(1 - \frac{t^2}{t_n^2}\right)^{\frac{\alpha_n}{\pi} - 1} \quad (16)$$

where the  $t_n$  are the values of  $t$  (all real) at the corners of the polygon formed by the air gap, the  $\alpha_n$  are the internal angles of the polygon, and the product is taken over the corners for which  $t_n > 0$ . For coned polecaps, figure 10 applies. Three values of  $t$  may be disposed arbitrarily (say  $0, 1, \infty$ ). The values  $-1$  and  $-\infty$  follow from the symmetry of the system about the median plane of the gap. Values of  $\pm t_1$  and  $\pm t_2$  are assigned to the remaining corners as shown. The diagram of figure 10 omits the corner  $P'$  of figure 9(b). The neglect of this corner is justified provided that  $P'Q'$  is greater than about half the width of

the gap, a condition which is usually met in practice. We shall return to this point later.

Rose shows that the necessary condition for obtaining a first order correction for the inhomogeneity of the field due to the edge of the gap is that the coefficient of  $t$  shall be zero in the expression

$$\prod_n \left( 1 - \frac{t^2}{t_n^2} \right)^{1 - \frac{\alpha_n}{\pi}}$$

in which, as before, the product is taken for values of  $t_n > 0$ . This requires that

$$\sum_n \left( 1 - \frac{\alpha_n}{\pi} \right) t_n^{-2} = 0 \quad (17)$$

This requirement will now be applied to the case shown in figure 10. The angle  $\Theta$  is the semi-angle of the truncated cones, which form the polecaps, and will be expressed as  $\eta\pi$ . The width and thickness of the rim are  $a$  and  $b$  respectively. The parameters of the corners are therefore:

$\zeta$	$t_n$	
$1(1-b)$	1	$\pi(3/2 - \eta)$
$a + 1(1-b)$	$t_1$	$3\pi/2$
$a + 1$	$t_2$	$\pi/2$

Substituting these values of  $t_n$  in (17) we find

$$t_2^2 = t_1^2 / [1 + (1 - 2\eta)t_1^2] \quad (18)$$

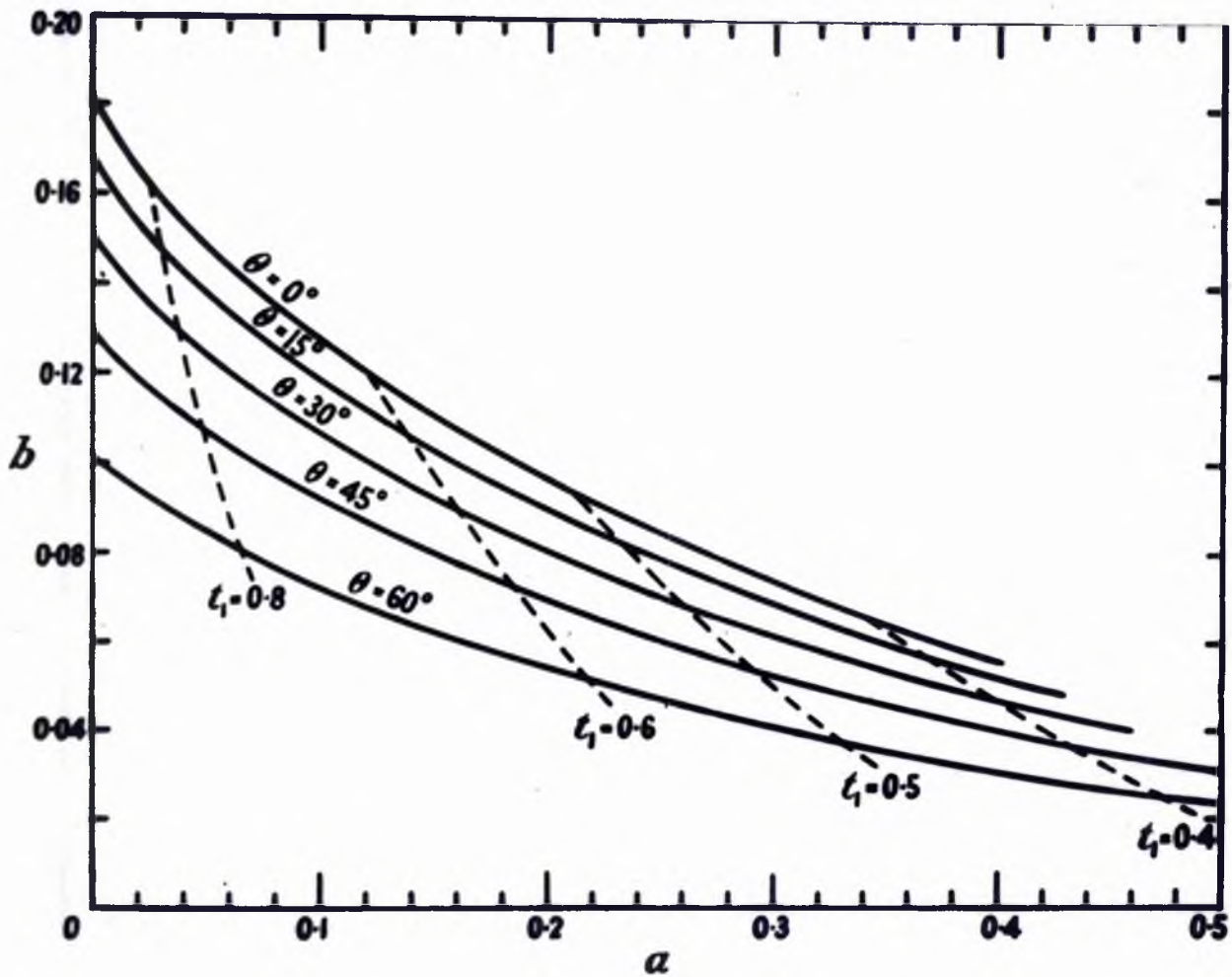


Figure 11

Dimensions of ring shim. The width of the ring  $a$  is plotted against its thickness  $b$  for various semi-angles  $\theta$

The value of  $a$  is obtained by integrating (16) from 1 to  $t_1$ .

This gives

$$a = \frac{2}{\pi} \int_{t_1}^1 t^{-1} (1-t^2)^{\frac{1}{2}-\eta} \left( \frac{t^2}{t_1^2} - 1 \right)^{\frac{1}{2}} \left( \frac{t^2}{t_1^2} - 1 \right)^{-\frac{1}{2}} dt \quad (19)$$

The value of  $b$  is obtained by integrating (16) from  $t_1$  to  $t_2$ .

This gives

$$b = \frac{2}{\pi} \int_{t_2}^{t_1} t^{-1} (1-t^2)^{\frac{1}{2}-\eta} \left( 1 - \frac{t^2}{t_1^2} \right)^{\frac{1}{2}} \left( \frac{t^2}{t_2^2} - 1 \right)^{-\frac{1}{2}} dt \quad (20)$$

For a given  $\eta$  and for each value of  $t_1$  between 0 and 1, values of  $a$  and  $b$  are obtainable from (18), (19) and (20). Eliminating the auxiliary variable  $t$ , the thickness of the rim  $b$  is found in terms of its width  $a$ .

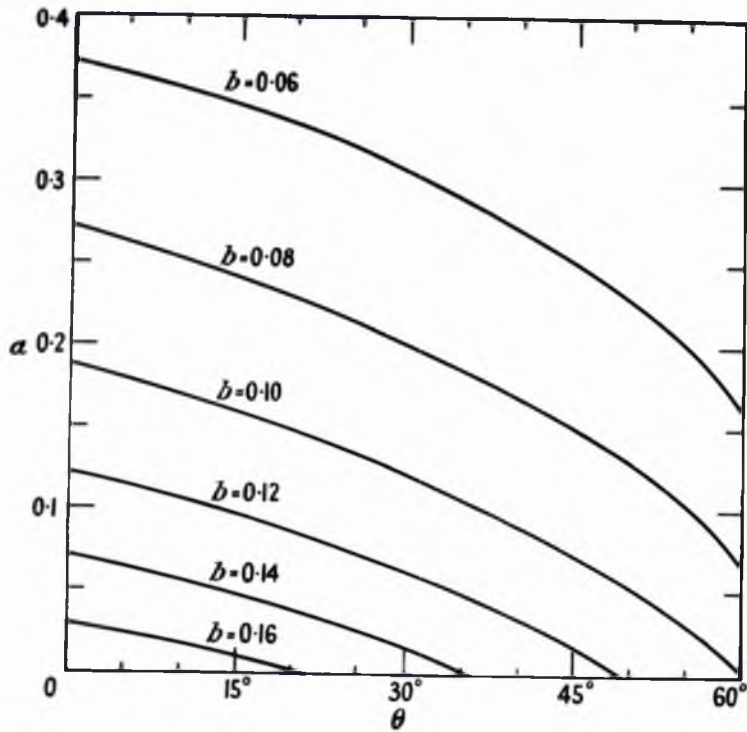
The integrals in (19) and (20) have been computed for semi-angles  $\theta$  equal to  $0^\circ$ ,  $15^\circ$ ,  $30^\circ$ ,  $45^\circ$  and  $60^\circ$ , ( $\eta$  equal to 0,  $1/12$ ,  $1/6$ ,  $1/4$ ,  $1/3$ ). For each  $\theta$ , values of  $a$  and  $b$  were obtained for  $t_1$  equal to 0.4, 0.5, 0.6, 0.8 and 1.0. In figure 11 the thickness of the rim  $b$  is plotted as a function of its width  $a$  for the five values of  $\theta$ . Figure 12 shows curves of  $a$  against  $\theta$  for constant  $b$  and of  $b$  against  $\theta$  for constant  $a$ , the values being obtained from figure 11 by interpolation.

The integrals were evaluated using Simpson's rule. The integrand in (19) is finite throughout the range of integration. In (20) however the integrand becomes infinite at the lower limit  $t_2$ . Simpson's rule was therefore

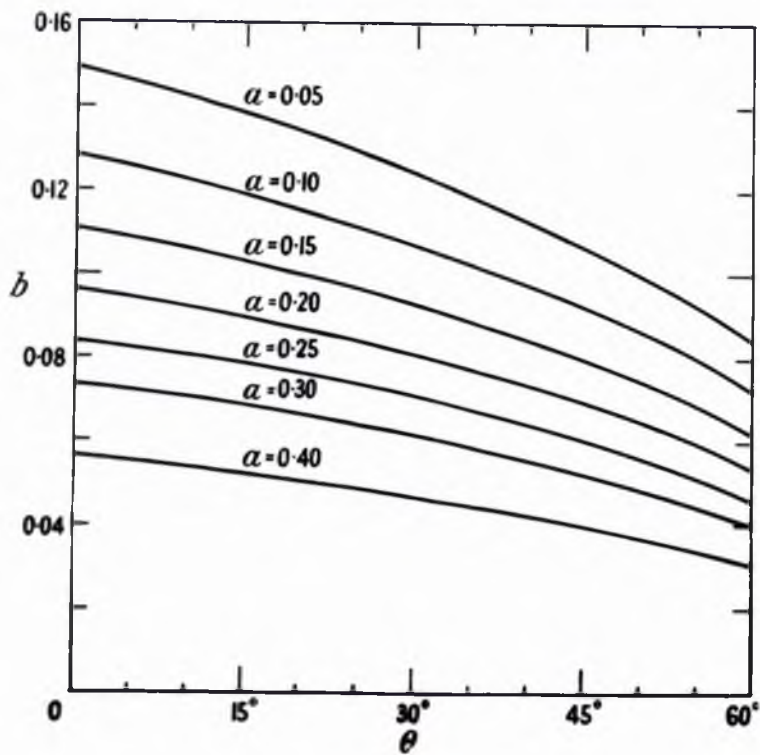


Figure 12

(i)



(ii)



(i) Variation of width  $a$  with  $\theta$  for various thicknesses  $b$

(ii) Variation of thickness  $b$  with  $\theta$  for various widths  $a$

applied from  $t_1$ , down to  $t_0$ , a value slightly greater than  $t_2$ . For the remaining range of integration from  $t_0$  to  $t_2$  all the factors in the integrand except the last were treated as constant,  $t$  taking the value  $t_m$  appropriate to the midpoint of this short range. The integral could then be evaluated in this range giving the following contribution to  $b$ :

$$\left(2t_2/\pi t_m\right)\left(1-t_m^2\right)^{\frac{1}{2}-\eta}\left(1-t_m^2/t_1^2\right)^{\frac{1}{2}}\ln\left[t_0/t_2+\left(t_0^2/t_1^2-1\right)^{\frac{1}{2}}\right] \quad (21)$$

When a magnet is designed, the value of  $b$  is often determined by consideration of the clearance required in the gap. If the designer wishes to calculate his own shim dimensions using (19) and (20) rather than by interpolating from figure 11, it is necessary for him to find by trial the value of  $t$ , which gives the desired value of  $b$ , and then to use this value of  $t$ , to find the value of  $a$ . In order to facilitate the finding of the value of  $t$ , in such cases, lines of constant  $t$ , have been drawn in figure 11 (broken lines).

We must now return to a consideration of the effect of neglecting the corner  $P'$  of figure 9(b). The surface  $P'S'$  beyond the corner may not be the surface of soft iron of low reluctance, but may for instance be permanent magnet material instead. Nevertheless, it should be a satisfactory approximation to consider that  $P'S'$  has the same magnetic

potential as the polecap. A value  $t_3$  is assigned to this corner. Reference to (16) shows that an extra factor  $(1 - t^2/t_3^2)^\eta$  now appears in the integrand of (19) and (20). An additional term also appears in (17), so that (18) must be replaced by:

$$t_2^{-2} = t_1^{-2} + 1 - 2\eta(1 - t_3^{-2}) \quad (22)$$

The use of equations (18), (19) and (20) is equivalent to the assumption that  $t_3^{-2} \ll 1$ . The value of  $t_3$  is found by integrating (16) from 1 to  $t_3$  to give the value of the length  $r$  of the conical surface P'Q':

$$r = \frac{2}{\pi} \int_1^{t_3} t^{-1} (t^2 - 1)^{\frac{1}{2} - \eta} \left( \frac{t^2}{t_1^2} - 1 \right)^{\frac{1}{2}} \left( \frac{t^2}{t_2^2} - 1 \right)^{-\frac{1}{2}} \left( 1 - \frac{t^2}{t_3^2} \right)^\eta dt \quad (23)$$

Approximate evaluation of (23) for various  $\eta$  shows that for  $r$  equal to 1.5 gap units  $t_3 \sim 7$ , the actual value depending somewhat on  $\eta$  and  $t_1$ . The effect of the terms in  $t_3^{-2}$  is in fact negligible for  $r \geq 1.5$ . For  $r = 1$  it is found that  $t_3 \sim 4$ , and the terms in  $t_3^{-2}$  become appreciable. For a fixed value of  $a$ , the correction to be applied to  $b$  increases with the angle  $\theta$ ; at  $\theta = 0$  the correction is of course zero, while at  $\theta = 60^\circ$   $b$  should be about 5% larger than given by figure 11, an increase of the order of 0.003 half-gap unit. The error caused by treating the problem as two-dimensional may often be of this order.

Thus, as stated earlier, provided  $r$  exceeds about

one half-gap unit the data given in figures 11 and 12 should be satisfactory. If  $r$  should be less than this, the problem must be worked out specially. The value of  $t_3$  which gives the correct value of  $r$  for the particular  $\theta$  must be found by trial from (22) and (23). The values of  $a$  and  $b$  may then be found from (19) and (20) after inclusion of the additional factor  $(1 - t^2/t_3^2)^\pi$  in both integrals, using the new value of  $t_2$  from (22).

A ring shim of this type was incorporated in the design of the permanent magnet described in section 3.2. The soft iron polecaps are in the form of truncated cones of semi-angle  $38^\circ 40'$ . The magnet was designed to have a gap of 5.40 cm and a pole-face diameter of 20 cm. The thickness of the rim was chosen to be 2 mm, and for this thickness the appropriate width was calculated to be 5.43 mm. After construction, the magnet was found to have a gap of 5.54 cm instead of the specified value of 5.40 cm. The dimensions of the shim should therefore have been 2.6% larger. The effect of this shim on the value of the field is discussed in the following section, when the performance of the magnet as a whole is considered. A comparison is made of the actual field measured near the edge of the gap and the theoretical value of the field without shims.

### 3.4 Performance of Magnet

When the magnet was assembled, although the parallelism between the pole-faces was within the limits of  $\pm 0.001$  inch, the actual gap length was 5.54 cm instead of the specified 5.40 cm. This increase was exactly twice the sum of the relevant tolerances, even taking them all in the same direction, and could only be ascribed to mechanical errors during manufacture.

On magnetisation at the works, the maximum voltage available was found to be only 260 volts instead of the stated 350 volts. This gave a peak magnetising field of only 1250 ampere-turns per cm, compared with the required 1700 ampere-turns per cm. There is thus a certain amount of doubt as to whether the material has been fully magnetised.

These errors must inevitably affect the performance of the magnet, and when the field was measured it was found to be 5520 oersted and has decreased in 18 months to about 5460 oersted. Detailed analysis of the magnet performance has been made with a view to

- (a) measuring the homogeneity over the median plane in the gap,
- (b) measuring the field variation in the median plane near the edge of the gap,
- (c) measuring the leakage flux over the whole surface area.

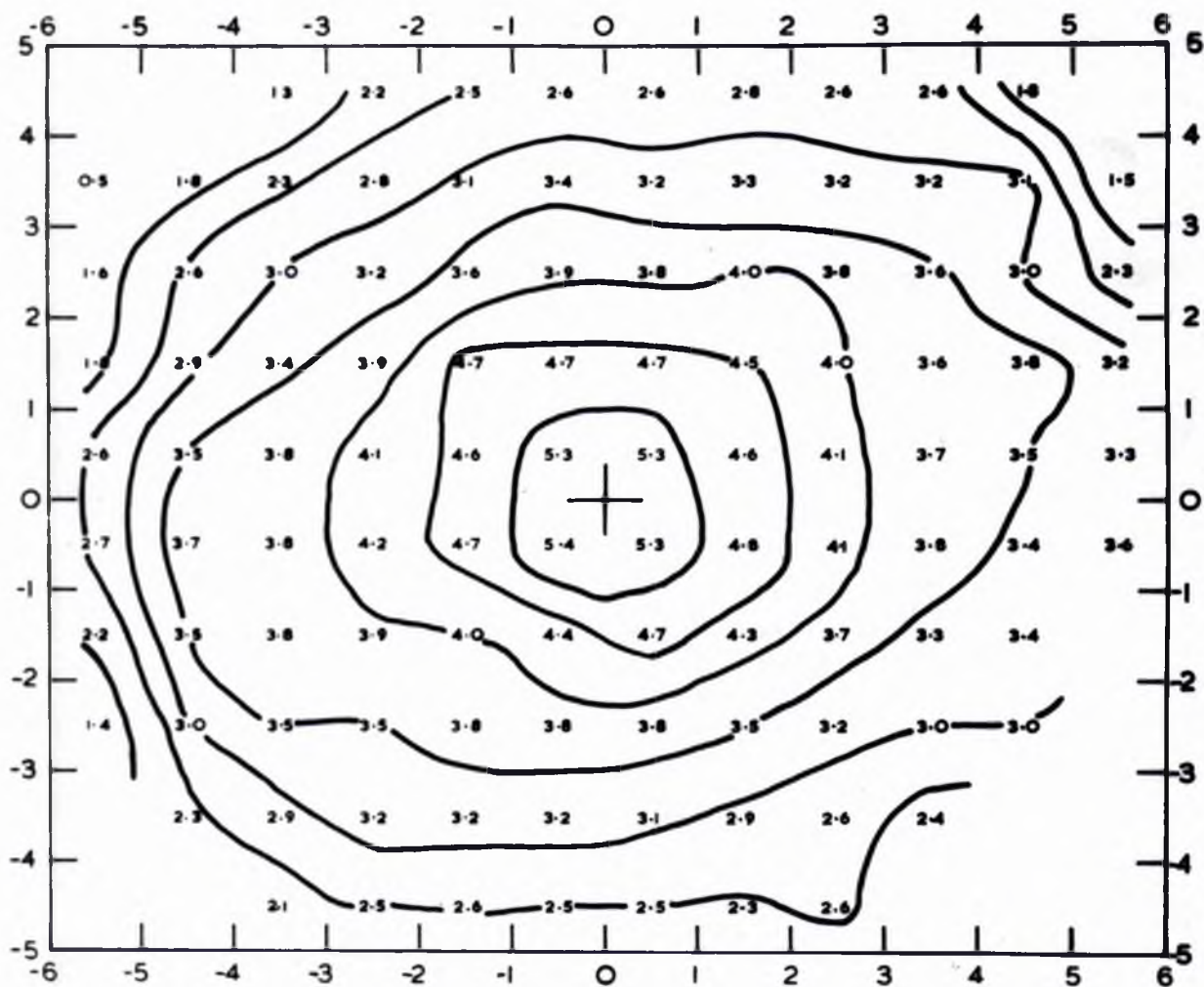
The first two measurements were to check the effect of the Rose rim and the last one to determine an experimental value for the leakage factor. These will now be considered in turn.

(a) Homogeneity of Field in Median Plane.

Measurements of the field variation over the median plane were made using the regenerative system described in section 2.2. This method is more flexible for such measurements than the bridge method, as the probe coil can be moved about in the field without any need for careful balancing at each point. The absence of any dispersion signal leads to accurate positioning of the line centre. A coil 2 cm long and 1 cm diameter enclosed a small quantity of paraffin oil in the form of a cylinder 1.2 cm long and 0.6 cm diameter. The nuclear resonance was displayed on a C.R.O. whose timebase was synchronous with the field modulation. The coil was positioned at various points in a network over the median plane of the magnet gap, and at each position the resonance was made central on the C.R.O. by adjustment of the frequency of oscillation. This frequency was measured by the BC221 frequency meter and converted into field values by the relation  $H = 2\pi\nu/\gamma$ . Readings were taken as far from the centre as possible, but at about 6 cm radius the signal became very broad and unsymmetrical, and the resulting absorption line could not

Figure 13

Field variation in median plane of gap



The dimensions of the network are in cm and the diagram is to be viewed looking through the gap towards the right-hand pole-face with the magnet as seen in figure 7

be positioned accurately on the C.R.O. screen.

The variation of the field in the median plane is shown in figure 13. The numerical readings are in gauss with an arbitrary zero, and contours are drawn at 0.5 gauss intervals. It is seen that the field is a maximum in the centre, and that the contours are drawn out at two positions on opposite sides of the centre. These positions were the most homogeneous parts of the field and gave the narrowest lines as shown by the probe signal. The radiofrequency coil, and hence the cylindrical specimen, had their long axes vertical. The line-widths at these two points were quite small enough for the present series of experiments described in section 4, and no attempt was made to decrease them further by mechanical treatment of the pole-faces. These line-widths were between 0.2 and 0.3 gauss, with a second moment correction of 0.02 to 0.04 gauss<sup>2</sup>, depending on the size and actual position of the specimen.

In addition to this variation in the median plane, measurements were taken at certain points near the left-hand face, central and near the right-hand face, and it was found that the field varied considerably across the gap. Due to the finite dimensions of the coil the measurements could not be made nearer than about 7 mm from each face, but nevertheless variations of 8-10 gauss were noted in some places, whereas in others the total variation was no more than 1 gauss.



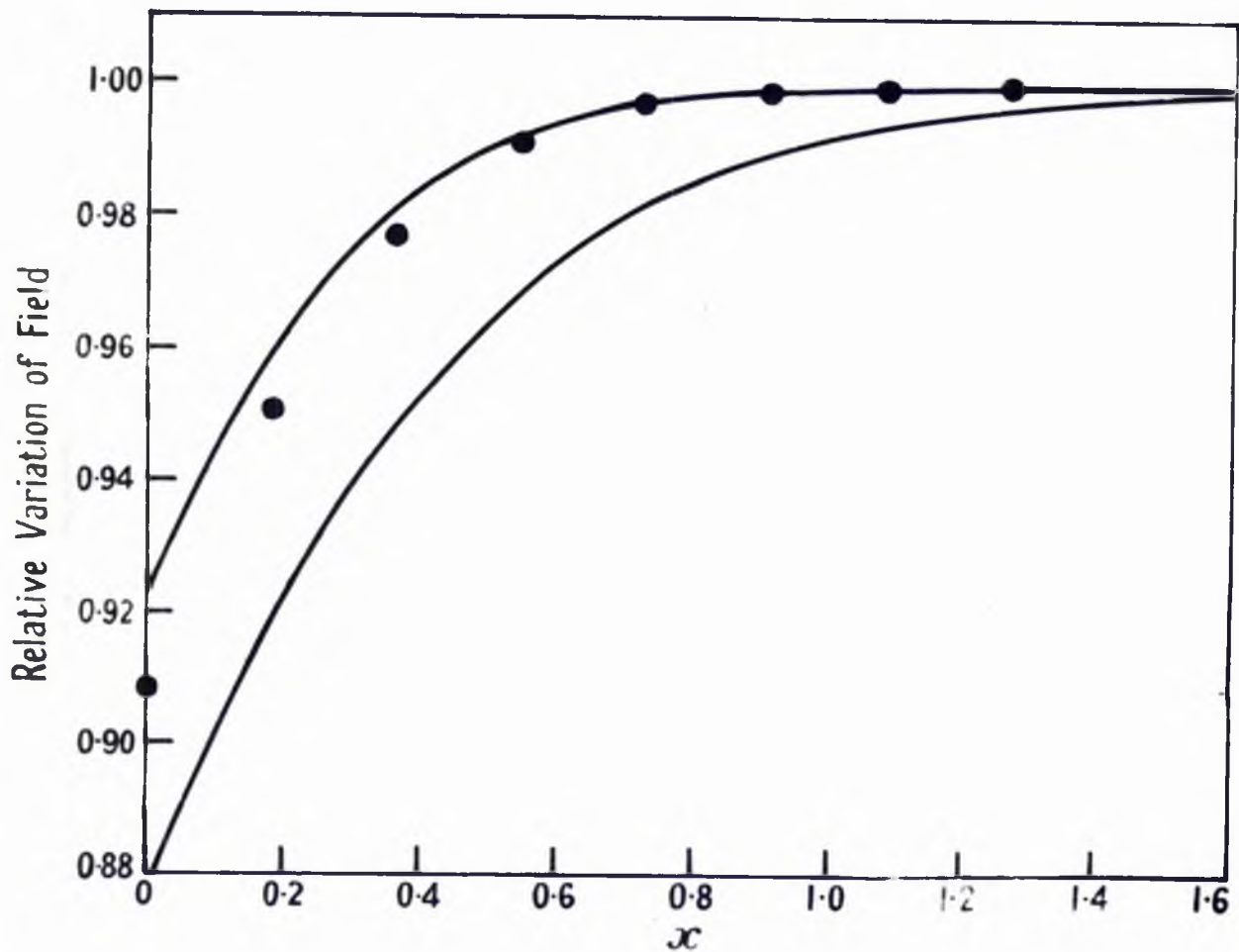


Figure 14

Comparison of actual and predicted performances of magnet

Circles: experimental points

Upper curve: predicted variation with shim

Lower curve: predicted variation without shim

This must be attributed to local variations in the iron, despite the precautions taken. In all cases the line-shape was very unsymmetrical in the positions near the pole-faces, indicating that the field variation was complex near these faces. This is confirmed in accurate tests on another magnet by Bruce (1953) where even an extremely small sample did not enable the field variation to be analysed near the pole-faces of that magnet. It would appear that if homogeneities of better than about one part in  $10^6$  over normal sample volumes are required, great attention must be paid to the polecap material, unless such a large gap is used that the local variations near the pole-faces do not affect the field in the median plane, and always provided that geometrical inhomogeneities are not the controlling factors.

(b) Effect of Shims on Field.

The field in the median plane near the edge of the gap has been measured with a search coil and fluxmeter. The rate of change of field is so great that a nuclear resonance method is not suitable; the resulting line-width would be too large, even with a very small sample. In figure 14 the field is shown plotted against  $x$ , the distance inward from the edge of the gap in half-gap units. The variation expected theoretically both with and without the ring shim has been calculated in the manner described by

Rose and is also shown in figure 14. While the agreement with the upper curve is not perfect, it is clear that the first order of inhomogeneity has been very largely removed. This is very satisfactory, since it might have been doubted whether the ratio of polecap diameter to gap-width, 3.6, was sufficient to satisfy assumption (b) in section 3.3 adequately; the relatively small value of this ratio may in fact be the main cause of the discrepancy between the experimental points and the upper curve in figure 14. The fact that the shim dimensions should be 2.6% larger will probably introduce a relatively small error.

#### (c) Leakage Flux Measurement.

The total flux provided by the material was determined using a search coil and fluxmeter to measure (i) the flux over the surface area of the yoke and (ii) the total flux passing across the median plane of the magnet. The leakage to the yoke was found to be 635,000 maxwells and the total flux across the median plane (including the gap) was 4,561,000 maxwells. The magnetic material therefore gave a total flux of 5,196,000 maxwells. The flux in the gap, neglecting any leakage and fringing effects, was calculated on the basis of the field in the centre of the gap as recorded by the fluxmeter, assumed constant over the total gap surface area (allowing for the slight narrowing of the gap by the shims). This was found to be 1,724,000 maxwells,

giving an experimental leakage factor for the magnet of 3.01. The calculated leakage factor (allowing for the 3% increase in material used over the calculated volume) was 2.72.

The discrepancy between the specified and observed values of the field must now be discussed. No ageing was done, as that would have reduced the field still further. The theoretical value of the field should therefore have been 7500 oersted, whereas the measured field was 5520 oersted.

The various factors which affect the value of the field are listed below, and it is unfortunate that they all work in the same direction, namely to decrease the field.

(i) increased gap length.

This was an increase of 2.6% over the specified value.

It affects the working (BH) point, and will decrease the field by ~ 2%, i.e. by ~150 oersted.

(ii) incomplete magnetisation.

From measurements made on a good specimen of Alcomax III, full magnetisation should produce a field ~ 3% higher than that achieved with 1250 ampere-turns per cm (Hoselitz, 1951). As the magnetic material used was in the form of large blocks and was not ideal, an estimate for the decrease in field due to incomplete magnetisation is about 4-5%, i.e. ~ 300 oersted.

(iii) underestimated leakage.

The measured leakage factor was 3.01 and the calculated

factor was 2.72. The gap field varies as  $(K_1 K_2)^{-\frac{1}{2}}$  and so will be about 400 oersted down due to this factor.

(iv) defects in magnetic properties of Alcomax III blocks.

The remainder of the discrepancy (~1150 oersted) must be ascribed to the magnetic material used. This can be approached from another aspect. On the basis of the measured field value of ~5500 oersted and the measured leakage factor of 3.01, the (BH) value of the material as calculated from the theory of appendix 1 is 3.09 mega-gauss-oersted. This can be shown to be made up from a  $B_m$  value of 7350 gauss and  $H_m$  value of 420 oersted. The field would be 4-5% higher on full magnetisation, giving a nominal (BH) value for the fully magnetised material of 3.40 mega-gauss-oersted. The average value of  $(BH)_{\max}$  for a normal specimen of Alcomax III is 4.75 mega-gauss-oersted (Jessop-Saville, 1950). The (BH) value of the blocks is therefore 28% below this value, and not the 10% we had been advised to allow. It has since been learned (Hoselitz, 1951) that a value of  $(BH)_{\max}$  greater than 3.5 mega-gauss-oersted in Alcomax III would be extremely difficult to achieve.

The field value of 5500 oersted rather than the 6700 oersted specified is no great drawback. The working frequency for proton resonance experiments in this field

is 23.4 Mc/s as opposed to the 28.5 Mc/s for the higher field. This new frequency is remote from any amateur radio band, whereas the higher frequency was in the centre of one of these bands and difficulty might have been experienced through radio interference.

The total weight of the magnet is about  $1\frac{1}{4}$  tons, and it is mounted on a wooden trolley at an angle of  $40^\circ$ . This gives access to the gap both vertically and horizontally. The experiments at present have only used a single Dewar tube in the gap (see figure 5) but the gap clearance was made large enough to accommodate a double Dewar for very low temperature work.

The magnet has been of great value in all the nuclear resonance work carried out since it was installed. The constancy of field compared with that of the electromagnet has enabled complicated lines, and lines with a poor signal-to-noise ratio, to be plotted and replotted with confidence.

## 4. EXPERIMENTAL RESULTS

### 4.1 Introduction

One of the main objects of the experiments was the study of molecular motion in the solid state. The choice of suitable substances for investigation by nuclear resonance methods is governed by several considerations, among the more important being the following.

- (i) Protons are used as the resonating nuclei because the high gyromagnetic ratio of the proton ensures a relatively large signal-to-noise ratio (BPP Appendix).
- (ii) The magnetic moments of all other nuclei within reasonable distances of the protons must be known. In this respect hydrocarbons are ideal substances because the magnetic moment of the  $C^{12}$  nucleus is zero.
- (iii) The substances should be of high purity, since the presence of impurities might influence both the second moment and relaxation time data.
- (iv) Physical properties such as specific heat, dielectric constant, crystal structure and infra-red and Raman spectra can often give an indication of suitable compounds for investigation.

There are other considerations relative to the apparatus in use - for instance the substance must be solid over a temperature range within the capabilities of the apparatus.

It may be remarked here that although a specific heat anomaly is generally accompanied by a related change in the width of the nuclear resonance spectrum, the reverse does not necessarily follow. The general criterion for a line-width change in a solid is that the reorientation frequency of the particular molecular motion occurring should be of the same order of magnitude as the value of the line-width expressed as a frequency. A more quantitative relation between these frequencies is given by Gutowsky and Pake (1950) and will be referred to in the discussion of n-pentane and n-hexane. The particular temperature at which this takes place is in a sense fortuitous, and this mechanism will not in general give rise to a specific heat discontinuity. The line-width transitions may thus be found in substances where their presence may not be indicated by specific heat data.



## 4.2 Anthracene and Ethylene Glycol

### 4.2.1 Introduction

Measurements of the nuclear magnetic resonance absorption spectrum of anthracene reported by Andrew (1950) showed a remarkable line-width change between  $180^{\circ}\text{K}$  and  $200^{\circ}\text{K}$ , when the absorption line narrowed by a factor of five and remained at this smaller value up to room temperature. Values for the experimental second moment of this narrow line could not be accounted for by postulating any simple molecular motion. The transition was also interesting in that naphthalene, which has very similar molecular and crystal structures, gave no indication of this behaviour.

### 4.2.2 Experiments

Further experiments have been made with anthracene and also with naphthalene and naphthacene, the two-ring and four-ring neighbours of anthracene. These latter compounds were examined for the presence of a narrow line similar to the anthracene line. No indication of a narrow line was found with these solids although the investigations were carried up to the melting points of both substances,  $80.2^{\circ}\text{C}$  for naphthalene and  $336^{\circ}\text{C}$  for naphthacene.

Experiments on the anthracene used by Andrew in his

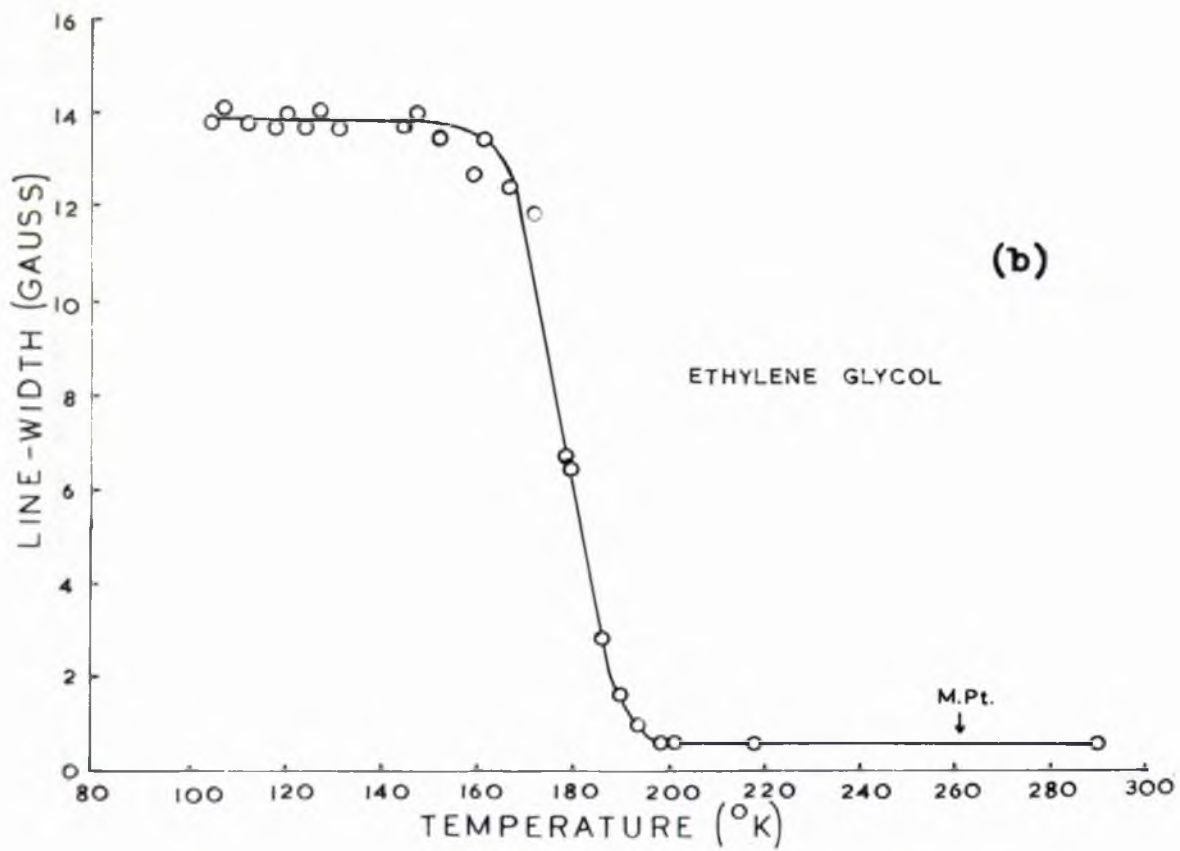
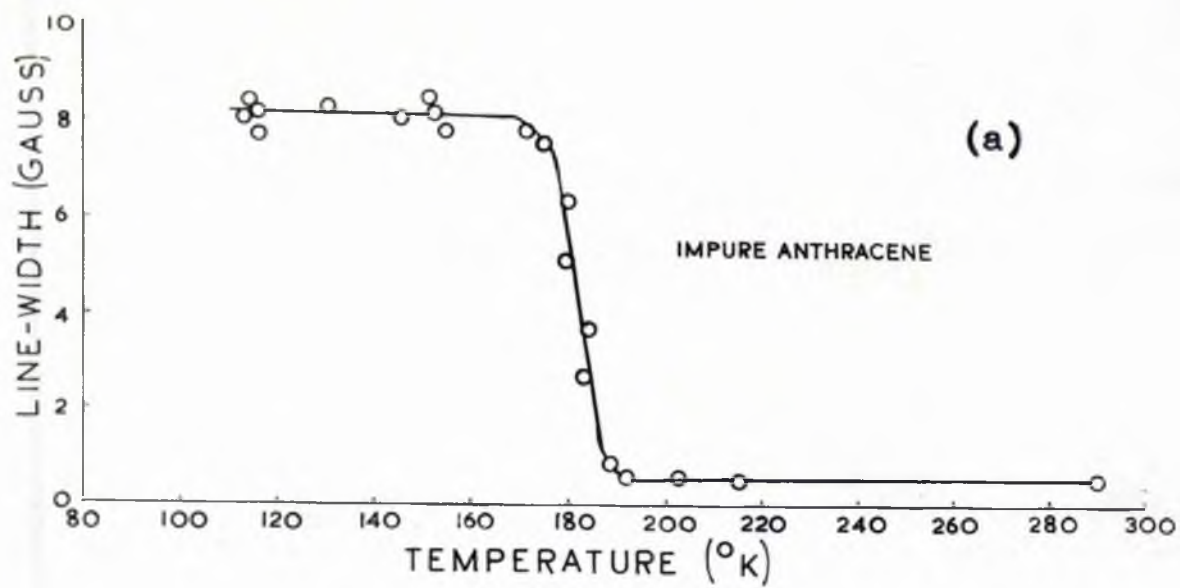


Figure 15

previous experiments (Eastman Kodak 480-X) gave substantially the same results as reported. However, this narrow line could not be found in several other samples of anthracene obtained from different sources, although all these other samples were nominally of lower purity than the original one. The line-width transition is shown in figure 15(a), and the line-width changes at about  $180^{\circ}\text{K}$  from 8.1 gauss to a value determined by the field inhomogeneity. On the basis that there might be an impurity in the original sample, attempts were made to purify this anthracene by chromatographic methods, but these were not very satisfactory, due mainly to the very insoluble nature of anthracene. It was found that if some of this anthracene was simply washed with distilled water, filtered and allowed to dry, the narrow resonance line could not be found. This pointed to some soluble impurity, and information was kindly supplied by the Eastman Kodak Company about their anthracene purification methods. The final step in the process was co-distillation with ethylene glycol, and so attention was turned to this substance.

Measurements of the line-width of ethylene glycol (distilled from B.D.H. material) are shown in figure 15(b) where it is seen that this substance undergoes a line-width transition in the solid state. The line-width decreases

from 13.7 gauss to the field inhomogeneity value over the same temperature region as the transition found for the original anthracene sample, this change occurring about  $80^{\circ}$  below the melting point of ethylene glycol. It is this transition which caused the narrowing of the line previously attributed to anthracene. Ethylene glycol has marked supercooling properties, and tests showed it could still be liquid  $30^{\circ}$  below its melting point. In all the line-width measurements below the melting point care was taken to ensure that the substance had actually solidified.

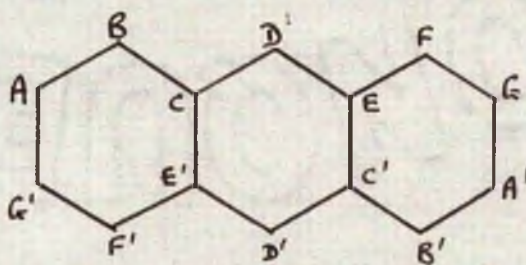
Two other anthracene samples were fully investigated over this temperature region, and neither showed any similar narrowing of the line-width from the value of about 8 gauss. One of these samples was from another batch of Eastman Kodak 480-X anthracene, showing that the original sample must have been from an unfortunate batch. The other sample was a very pure specimen kindly supplied by Professor J.W. Cook of Glasgow University.

A quantitative chemical analysis of the impure material was made with the assistance of Dr. Openshaw of the Chemistry Department. The method is given in appendix 2, and it showed that there was a 3.11% proportion by weight of ethylene glycol in the original sample, whereas none could be found to within the experimental limits (1 part in  $10^4$ ) in the other Eastman Kodak sample. Ethylene glycol

is miscible in all proportions with water, and so was easily removed by the washing process referred to previously.

#### 4.2.3 Molecular and Crystal Structure

The structure of anthracene has recently been re-determined by Mathieson, Robertson and Sinclair (1950). The analysis of these results (Sinclair, Robertson and Mathieson, 1950) showed that the three-ring structure is not composed of regular hexagons. The analysis of their experimental results has been carried further by Ahmed and Cruikshank (1952) with slightly modified values resulting for the various averaged C-C bonds. The results are shown in the following table, together with theoretical values for these anthracene bonds as derived by Coulson, Dandel and Robertson (1951).



Bond Lengths in Angstrom Units

	Experimental		Theoretical
	Sinclair et al.	Ahmed & Cruikshank	
G'A	1.390	1.408	1.410
AB	1.364	1.370	1.382
BC	1.419	1.423	1.420
CE'	1.440	1.436	1.430
CD	1.391	1.396	1.406

#### 4.2.4 Discussion

The broad line of the anthracene in the impure sample tends to be masked above  $190^{\circ}\text{K}$  by the superposed strong narrow line of the glycol impurity. This is partly due to the phase-sensitive method of detection. When a narrow line is found, the amplitude of the modulation field is reduced to a value less than that of the line-width in order to avoid spurious broadening. The signal strength of any broader line is consequently reduced, and may not be detected relative to the signal strength of the narrow line. Both lines have been found in the impure anthracene at about  $200^{\circ}\text{K}$  using a 2-gauss modulation, but with the narrow line necessarily broadened. Below  $180^{\circ}\text{K}$  the glycol line is broad and weak, and the true anthracene line then achieves prominence.

At the time the nuclear resonance experiments were made, the results of Ahmed and Cruikshank(1952) were not available and the second moment of anthracene was calculated on the basis of the data given by Sinclair et al.(1950). The C-H distance was taken to be 1.102 Å on the basis of the electron distribution plot given by these authors. Inter-proton distances up to 6Å were treated accurately, an estimate being made for the effects of protons at distances greater than 6Å from each particular proton considered.

The intramolecular contribution was calculated to be  $3.27 \text{ gauss}^2$ , and it is estimated that the later results of Ahmed and Cruikshank would decrease this value by about 2%. More uncertainty lies in the calculation of the intermolecular contribution to the second moment as an estimate must be made for the lattice contraction from the temperature of structure measurement (about  $20^\circ\text{C}$ ) to about  $100^\circ\text{K}$ . Measurements of the expansion coefficient of anthracene only exist in the region  $20^\circ\text{C}$  to  $180^\circ\text{C}$  (Klemm, 1928). Turning to the case of naphthalene, measurements are available from  $20^\circ\text{C}$  to  $70^\circ\text{C}$  (Klemm, 1928), and spot measurements of the density of naphthalene are quoted at  $-188^\circ\text{C}$  and  $17^\circ\text{C}$  (Dewar, 1905). Anthracene and naphthalene have very similar crystal structures, and their specific heats show very similar variations with temperature. It is reasonable to assume that the expansion coefficients vary in a similar manner. Combining all these results it was concluded that, if we assume isotropic expansion, the linear dimensions of the monoclinic cell would each be about 1.4% smaller at the temperature of second moment measurement than at room temperature. On this basis, the intermolecular contribution to the second moment is 4.88 gauss<sup>2</sup>. The results of Ahmed and Cruikshank would probably increase this value a little, so the total second moment of  $8.15 \text{ gauss}^2$  would not be changed by much. The mean of

several determinations of the second moment of pure anthracene at  $100^{\circ}\text{K}$  is  $8.2 \pm 0.2 \text{ gauss}^2$ , indicating that the lattice is effectively rigid at this temperature.

The mean experimental second moment of ethylene glycol at about  $100^{\circ}\text{K}$  was  $21.0 \pm 0.5 \text{ gauss}^2$ , but as the crystal structure is not known, an accurate theoretical value for the second moment cannot be calculated.

This work has been briefly reported (Rushworth 1952) and is an indication of the importance of using materials which are of the highest purity in these investigations. Unless the purities are known or can be found by melting point determinations, there is always the risk of effects of the kind found here. It is for this reason that some of the substances which on preliminary tests appeared interesting have not been investigated further.



### 4.3 Cyclopentane

#### 4.3.1 Introduction

Cyclopentane  $C_5H_{10}$  appeared to be a substance which might give interesting results since two specific heat transitions are found in the solid state. The relevant data in the following table is averaged from the later results quoted by Timmermans (1950).

	Temperature	Heats of Transition, Melting and Vaporisation
Transition I	$-150.77^{\circ}C(122.4^{\circ}K)$	16.64 Cal/gm
Transition II	$-135.09^{\circ}C(138.1^{\circ}K)$	1.18 "
Freezing Point	$-93.8^{\circ}C(179.4^{\circ}K)$	2.07 "
Boiling Point	$49.3^{\circ}C$	99.63 "

The sample used for the nuclear resonance experiments was obtained from the Chemical Research Laboratory, Teddington, and had a mole per cent purity of  $99.95 \pm 0.02$  as determined from the freezing point. It was transferred by distillation in vacuum from the standard ampoule in which it was supplied to a thin-walled sealed glass tube specially made to fit the nuclear resonance coil.

#### 4.3.2 Molecular and Crystal Structure

Although many earlier workers assumed a planar model with  $D_{5h}$  symmetry, it seems clear from recent evidence that

the five carbon atoms do not all lie in one plane, but the true molecular structure is not known. Aston, Fink and Schumann (1943) compared the experimental entropy with that calculated from statistical and molecular data and concluded that one carbon atom must lie out of the plane of the other four. Kilpatrick, Pitzer and Spitzer (1947) surveyed the published data from electron diffraction, Raman and infra-red spectra, entropy and specific heat measurements. These authors calculated the effect of the repulsions between hydrogen atoms on neighbouring  $\text{CH}_2$  groups which produce torsional forces about the C-C bonds tending to pucker the planar ring structure. The calculations, which involved certain approximations, indicated that the maximum displacement of one carbon atom from the plane of the other four is  $0.2\text{\AA}$ , and that this displacement is not localised at a given carbon atom but rotates round the ring. A thorough investigation of the infra-red and Raman spectra of cyclopentane has been made by Miller and Inskip (1951). The selection rules for the planar and non-planar forms should be different, and they concluded that the molecule cannot have  $D_{5h}$  symmetry but could give no definite evidence of the exact symmetry and geometry of the molecule. These authors stated that it is not necessary to adopt the puckered ring model of Kilpatrick et al. (1947) to interpret the data, but this does not rule out the possibility of this model being correct.

Electron diffraction experiments by Hassell and Viersvoll (1946) gave the C-C bond length to be 1.54A and the C-H bond length 1.09A, normal lengths for a saturated compound. Although they assumed a planar model in the interpretation of their data, good agreement was obtained. The puckered ring model would only introduce a minor effect.

The molecular structure of cyclohexane ( $C_6H_{12}$ ) is known to be a chair model with  $D_{3h}$  symmetry, tetrahedral angles and C-C bond length of 1.54A (see discussion by Andrew and Eades 1953). A recent determination of the structure of the other neighbour, cyclobutane ( $C_4H_8$ ) has been reported by Dunitz and Schomaker (1952) using electron diffraction methods. The bond distances were C-C=1.56 $\pm$ 0.02A, C-H=1.09 $\pm$ 0.04A and H-C-H angle = 114 $^\circ$   $\pm$  8 $^\circ$ . On the average the ring was non-planar with dihedral angle 20 $^\circ$  (+10 $^\circ$ , -20 $^\circ$ ) but the equilibrium symmetry may be either  $D_{2h}$  (puckered ring) or  $D_{4h}$  (planar ring subject to bending). The long C-C bond was discussed by these authors.

Single crystal X-ray diffraction methods have been applied to cyclopentane by Post, Schwartz and Fankuchen (1951). Between transition II and the melting point they found the structure to be hexagonal with two molecules per unit cell in close-packed positions. The lattice parameters were  $a = 5.83 \pm 0.05A$  and  $c = 9.33 \pm 0.05A$ , with a unit cell volume of 270 cubic angstroms. The symmetry of the crystal and the

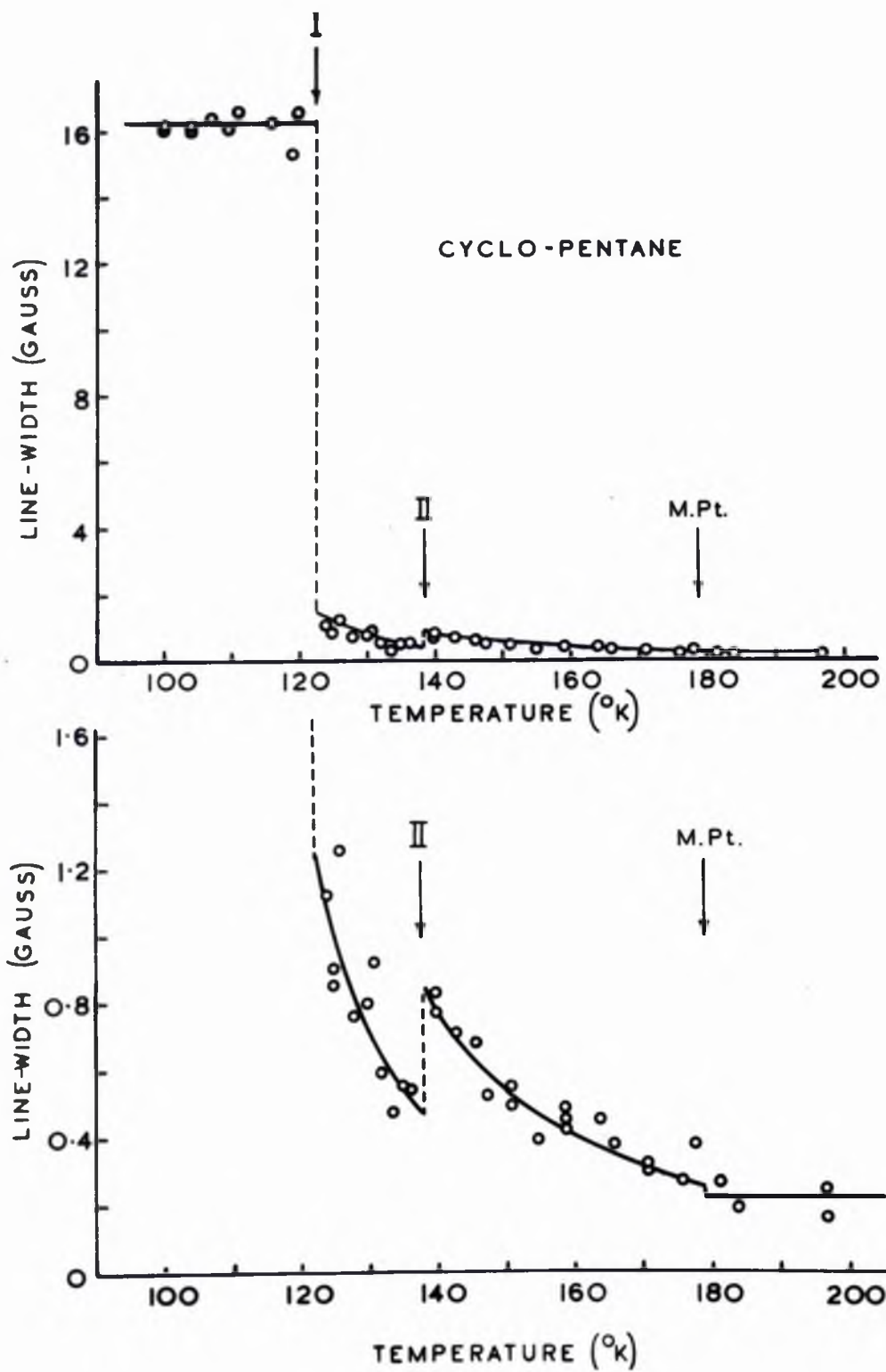


Figure 16

intensities of the reflections indicated that there was considerable molecular disorder above transition II. Comparison of observed structure factors with computed structure factors for several types of motion showed that the best agreement was obtained if this motion was free rotation with spherical symmetry. Examination of the crystal with a polarising microscope suggested that below the temperature of this transition a change occurred to a polycrystalline form of lower symmetry.

#### 4.3.3 Experimental Results

##### (a) Line-width and second moment.

The variation of the nuclear resonance absorption line-width with temperature is shown in figure 16(a). A sudden decrease by a factor of about 12 occurs at transition I, and the line-width then decreases further in the interval between transitions I and II. The line-width above transition I is plotted on a larger scale in figure 16(b), where this decrease is more evident. At transition II the line-width appears to increase from 0.5 gauss to 0.8 gauss. This increase is considered to be a real effect outside experimental error and will be discussed later. The line-width above transition II decreases slowly with increasing temperature to about 0.3 gauss just below the melting point. The liquid line, a measure of the field inhomogeneity, is about 0.25 gauss wide.

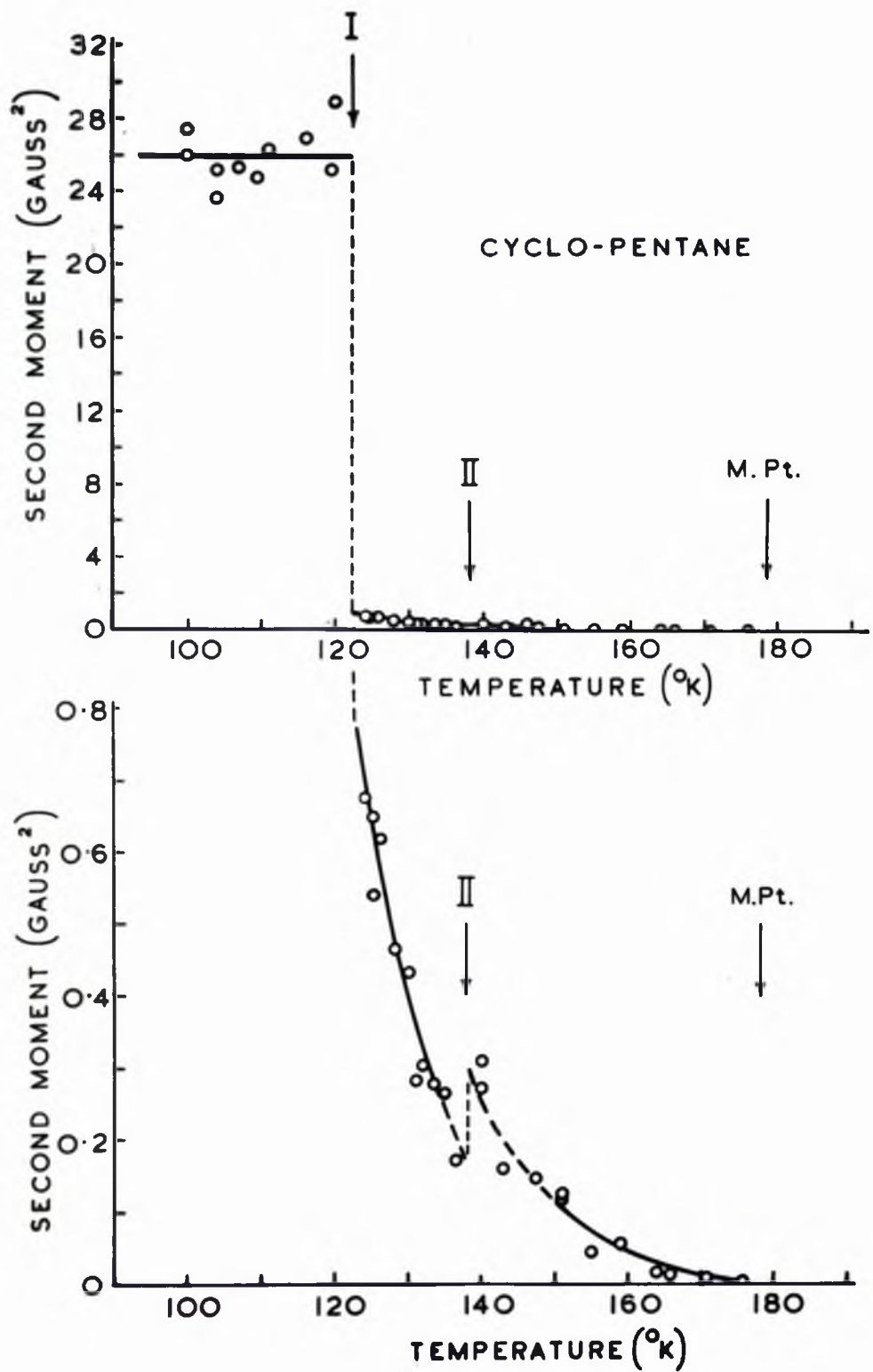


Figure 17

The recorder traces shown in figure 4 are for cyclopentane. The line-width in (a) was 16.1 gauss and in (b) 0.56 gauss, the recorder paper speed being greater in this latter case.

The line-width change at transition I is reflected in the change in second moment as shown in figure 17. The second moment decreases as the temperature rises between transitions I and II, but the second moment increase at transition II is not as marked as the line-width increase. The second moment values are very low and the uncertainty in each point is  $\pm 0.03$  gauss<sup>2</sup> at temperatures near transition II. There is a further gradual decrease in the second moment value between transition II and the melting point.

(b) Spin-lattice relaxation time.

The variation of the spin-lattice relaxation time with temperature is shown in figure 18. Below transition I the relaxation time was large enough to observe the recovery from saturation on the meter. Above 130°K the absorption line was narrow enough to give a relatively strong trace on the C.R.O. and the relaxation time was measured by the cine-camera method. The most difficult region was the small interval between transition I (122.4°K) and 130°K. The line-width was changing rapidly in this region and the signal was not of sufficient strength for the cine-camera method to be of use. The relaxation time was too short for visual observation of

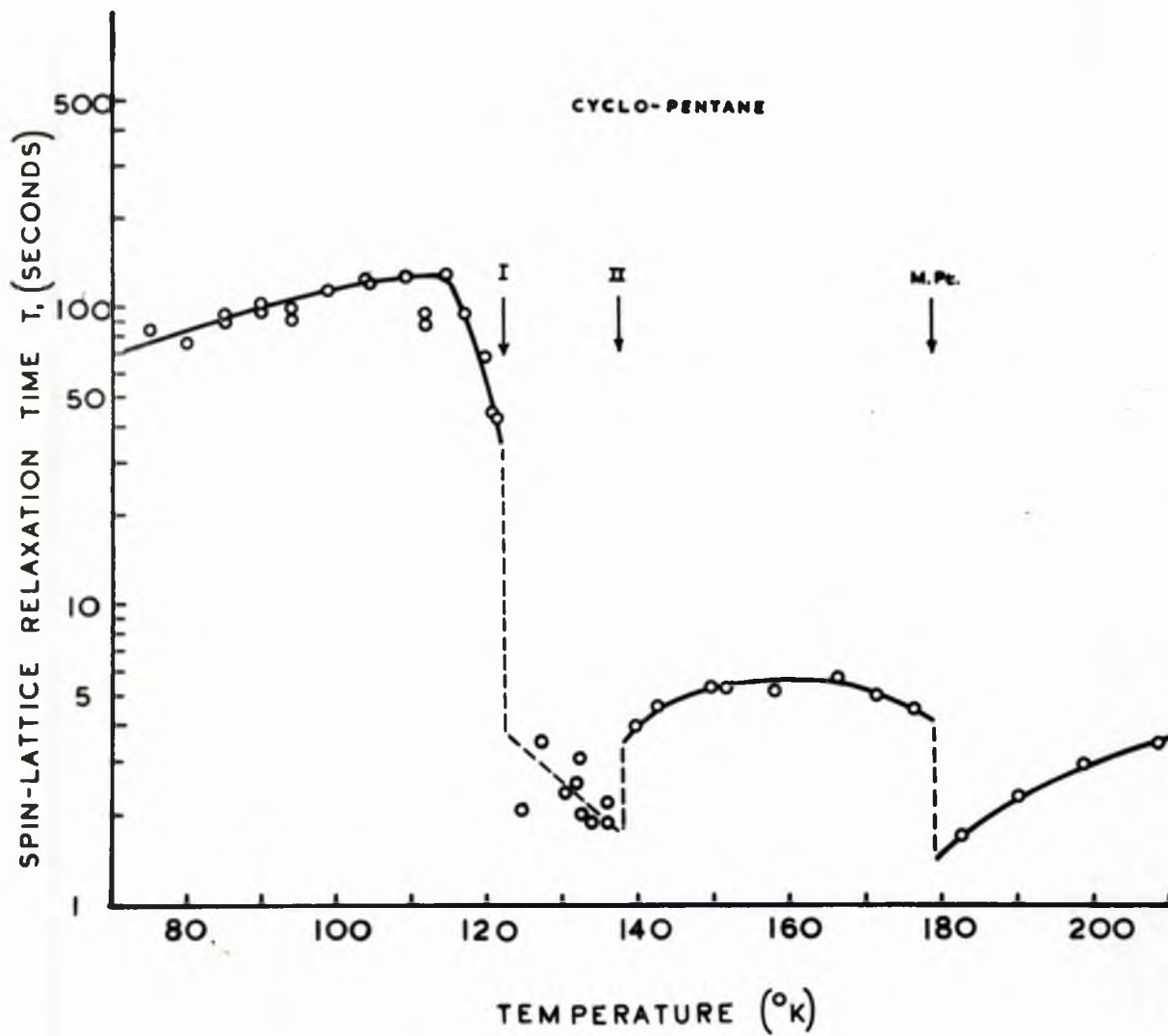


Figure 18



the meter recovery, and recourse had to be made to the progressive saturation method. It will be recalled that a knowledge of  $T_2$  is required, which depends on the line-width provided the line-shape is of the same form throughout. The line-width change was so rapid over this region, and the line-shape may not have been exactly the same throughout due to possible field inhomogeneity effects, that the measurements in this region are not accurate enough to ensure a full knowledge of the  $T_2$  variation. The dashed curve must only be taken as an indication of the probable general shape of the curve, but it is highly likely that a discontinuity does occur at transition I.

#### 4.3.4 Discussion

It is obvious that a major change occurs at transition I and that the changes at transition II and the melting point are small in comparison. This is reflected in the large heat of transition I, which is 14 times greater than the heat of transition II and 8 times greater than the heat of melting.

Below transition I the second moment is constant at  $26.2 \pm 1.5 \text{ gauss}^2$ . This value has to be compared with the theoretical value for a rigid structure as calculated from equation (8). The intramolecular contribution can be calculated on the basis of a plane pentagon model with tetrahedral H-C-H angles, C-C bond length 1.54 Å and C-H bond

length 1.09A (Hassel and Viervoll, 1946) and is found to be 18.0 gauss<sup>2</sup>. Although it is not strictly correct to take a planar ring model, the puckered ring version of Kilpatrick et al. (1947) will not introduce much change. Assuming the relative positions of the protons attached to the four coplanar carbon atoms are not affected due to the displacement of the fifth carbon atom by 0.2A, the part of the intramolecular contribution due to their mutual interactions will not change. This amounts to 73% of the total. A further 12% comes from the mutual interaction between the two protons attached to the displaced carbon atom, and this will not be affected provided the C-H bond length and the H-C-H angle remain the same. This leaves 16% as due to the interactions of the two displaced protons with the protons in the rest of the molecule. Displacement of the carbon atom by only 0.2A will not greatly affect this fraction, and the intramolecular contribution to the second moment can be quoted as  $18.0 \pm 0.5$  gauss<sup>2</sup> with a fair degree of confidence.

Lack of knowledge of the crystal structure below transition I means that the intermolecular contribution can only be estimated from other evidence. The relevant information used by Andrew and Eades (1953) for cyclohexane can be applied to the case of cyclopentane. The similarity between the sums of the heats of transition, melting and vaporisation of cyclopentane and cyclohexane (120 cal/gm and 121 cal/gm

respectively) suggests that the packing of the molecules in the crystal lattices is similar, and that the intermolecular parts of their respective second moments might be similar. Other data for cyclohexane led to a value for its intermolecular contribution to the second moment being quoted by these authors as  $10.0 \pm 1.5$  gauss<sup>2</sup>, and we shall assume this value for cyclopentane.

The total calculated second moment is therefore  $28.0 \pm 2.0$  gauss<sup>2</sup>, compared with the experimental value below transition I of  $26.2 \pm 1.5$  gauss<sup>2</sup>. The lattice is thus effectively rigid at these temperatures. The estimation of the intermolecular contribution may be a little high, since with both cyclopentane and cyclohexane the theoretical value is greater than the experimental value, although in both cases the discrepancy is within the combined limits of uncertainty.

The second moment drops to about  $0.8$  gauss<sup>2</sup> at transition I and continues to fall thereafter, apart from the possible slight increase at transition II. This value is very low for a solid and means that there must be considerable molecular motion in the lattice. Rotation about an axis perpendicular to the plane of the four carbons would not result in sufficient reduction of the second moment. This motion would have no effect on the contribution of the mutual interaction between the protons of each CH<sub>2</sub> group. These interactions represent over 60% of the intramolecular

contribution of  $18.0 \text{ gauss}^2$ , and so the second moment resulting from a reorientation process about this axis must be greater than this value, which is  $11.3 \text{ gauss}^2$ . This is too high by a factor of 10 or more, and so motion of a more serious nature must be considered.

Free spherical rotation of the molecule was suggested by Post, Schwartz and Fankuchen (1951) to be the type of molecular disorder most consistent with their X-ray results. On the basis of their structure determination at  $-110^\circ\text{C}$  ( $163^\circ\text{K}$ ) calculations have been made for the second moment resulting from the picture of rotating balls. Provided this random rotation is fast enough, the intramolecular contribution to the second moment will be effectively zero. The intermolecular contribution can be approached in two ways.

(a) The protons can be considered clustered together at the centre of gravity of the molecule. The values of  $r_{jk}$  in equation (8) are now replaced by values of  $c_{jk}$  the distances between the centres of gravity of two molecules. The mean value of  $r_{jk}^{-6}$  will be greater than  $c_{jk}^{-6}$ , but the neglect of angular factors partly compensates for this. The resulting second moment value is  $1.4 \text{ gauss}^2$ , treating values of  $c_{jk}$  up to  $12\text{A}$  accurately and making an estimate for the effect of molecules where  $c > 12 \text{ A}$ .

(b) A more accurate method is to use the theory developed by Andrew and Eades (1953) when calculating the second moment

of cyclohexane resulting from free spherical rotation of those molecules. Some approximations are necessary to reduce the calculations to reasonable proportions and, after allowing for an angular factor of 0.6, a value of  $1.7 \text{ gauss}^2$  is obtained.

Although both these calculations are subject to a certain amount of error, the experimental second moment at  $163^\circ \text{K}$  is only about  $0.03 \text{ gauss}^2$  at most, about 50 times smaller than the two values calculated on the basis of completely free rotation. This small second moment can only be accounted for by the introduction of further molecular motion. We have used up all the three rotational degrees of freedom and are left with translational degrees of freedom. The suggestion is, therefore, that the molecules diffuse bodily through the lattice. In order to affect the line-width and second moment values, the molecules must change their positions at a rate greater than the line-width expressed as a frequency. This means that at  $163^\circ \text{K}$  each molecule changes its position at least 1600 times per second on the average. This frequency will be too low for the diffusion process to be noticeable in the X-ray crystal structure measurements, and no suggestion of diffusion was made by Post et al. (1951).

We will now consider the spin-lattice relaxation time data and analyse it in relation to the second moment arguments outlined above.

CYCLO-PENTANE

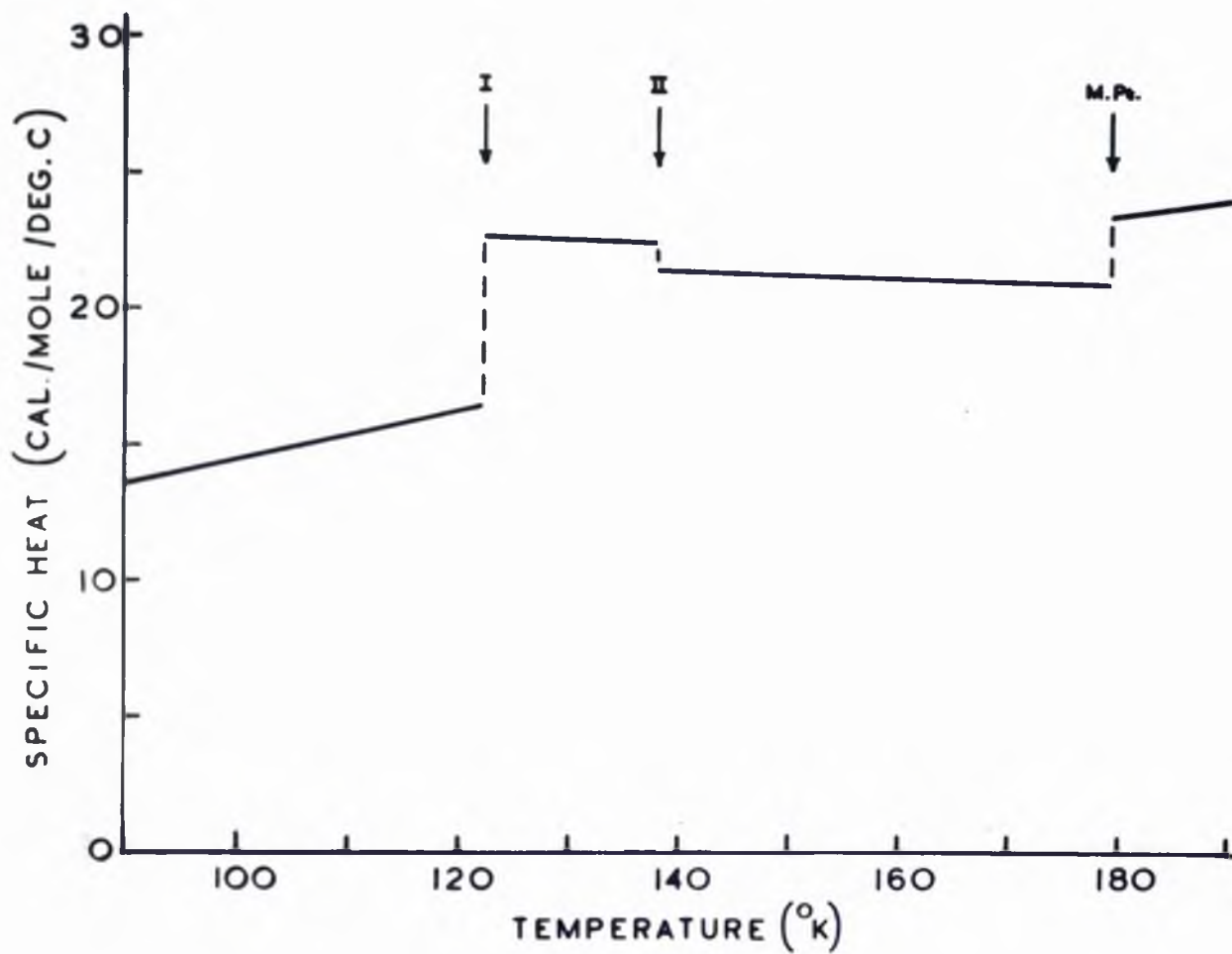


Figure 19

Below about  $110^{\circ}$  K the spin-lattice relaxation time is decreasing as the temperature decreases. This is a little unusual as the second moment value at these temperatures agrees with the theoretical value for a rigid system. Any motion which is present must be small and at a low frequency (in general a frequency less than the line-width). For this low frequency motion it can be shown that  $T_1$  normally increases with decreasing temperature. One might expect the spin-lattice interaction to become small at very low temperatures, and so presumably  $T_1$  will begin to increase at some temperature lower than  $70^{\circ}$  K. It is hoped to carry out experiments at these temperatures using liquid hydrogen as coolant.

At about  $110^{\circ}$  K the relaxation mechanism appears to anticipate the phase change at  $122.4^{\circ}$  K and begins to decrease rapidly. As explained previously, the values of  $T_1$  between  $122.4^{\circ}$  K and  $130^{\circ}$  K are not reliable, but there is a probable increase in  $T_1$  at transition II. This is to be compared with the increase in line-width and second moment at this temperature, all these effects being unusual. Turning to specific heat data, figure 19 shows the variation of specific heat with temperature from  $90^{\circ}$  K to above the melting point. This curve is based on results given by Aston, Fink and Schumann (1943). Later results of Douslin and Huffman (1946) are substantially the same over this temperature region. It will be seen that the value of the specific heat above transition II is lower than below transition II.

This again is unusual.

A tentative explanation of these phenomena can be given on the basis of a change in crystal structure. Post, Schwartz and Fankuchen (1951) observed the crystal structure below transition II with a polarising microscope. They stated that in this temperature region the structure was of lower symmetry than the hexagonal symmetry found above transition II. In order to form this pattern of close-packed hexagonal unit cells with the observed axial ratio, the molecules must act like spheres. This is quite probable because we have shown they must be freely rotating and that this motion must commence at transition I. The rotational frequency will increase with increasing temperature, and at  $138.1\text{ K}^{\circ}$  the rotation is sufficient for the molecules to act effectively as balls and prefer to form the close-packed hexagonal structure. This new structure is of higher symmetry than the lower temperature modification, and the centres of gravity of the molecules are very probably closer together in the higher symmetry form. Thus the second moment, although still decreasing regularly with increasing temperature, will suddenly jump to a higher absolute value.

It is unfortunate that there are no measurements of the density of cyclopentane in this region, since the above argument requires an increase in density as the temperature increases through transition II. If an increase in density were found, the argument would be considerably strengthened.



In passing, reference must be made to the transition from ice to water. Above  $0^{\circ}\text{C}$  the specific heat is lower than below  $0^{\circ}\text{C}$ , as in the case of cyclopentane above and below transition II. A further similarity is that in both cases the specific heats above the transitions decrease with increasing temperature. The density of water at  $0^{\circ}\text{C}$  is known to be greater than that of ice, and although there is no suggestion that the cyclopentane change is exactly analogous to the melting of ice, the similarities in their behaviour imply that the required increase in the density of cyclopentane may not be improbable.

It will be noticed that just below transition II the spin-lattice relaxation time is decreasing, while just above transition II it is increasing, with increasing temperature. If we can assign a single correlation time  $\tau_c$  to the rotation motion, the relation between  $T_1$  and  $\tau_c$  should be of the form given by BPP equation (51)

$$\frac{1}{T_1} = C_1 \left[ \frac{\tau_c}{1 + \omega^2 \tau_c^2} + \frac{2\tau_c}{1 + 4\omega^2 \tau_c^2} \right] \quad (24)$$

where  $C_1$  is a constant and  $\omega/2\pi$  the radiofrequency used. This expression will give a minimum value for  $T_1$  when  $\omega\tau_c = 1/\sqrt{2}$ . When  $\omega\tau_c > 1$ ,  $T_1$  will decrease as  $\tau_c$  decreases, and when  $\omega\tau_c < 1$ ,  $T_1$  will increase as  $\tau_c$  decreases. In general  $\tau_c$  will become smaller as the temperature rises - the

rotational motion becomes easier at higher temperatures. The decrease of  $T_1$  with temperature below transition II corresponds to the case when  $\omega\tau_c > 1$ , or when the correlation frequency  $\nu_c$  (defined as  $1/2\pi\tau_c$ ) is less than the radio-frequency used. Above transition II the molecules are now in their preferred crystal positions and can rotate more freely. Thus we might have jumped across the minimum and reached the state when  $\omega\tau_c < 1$ , in which case  $T_1$  will increase with increasing temperature. As an increase of  $T_1$  occurs, this change must be greater than the change in the opposite sense which might be expected from the closer packing. The phase transition prevents  $T_1$  from reaching its minimum value, just as a phase change did in the case of cyclohexane (Andrew and Eades, 1953). The short temperature interval between transitions I and II, coupled with the inaccuracy of the relaxation time values in this interval, prevent a reliable estimate being made of the barrier height to reorientation.

If a further relaxation process is occurring due to the diffusion mechanism, then the full reorientation process cannot be described by a single correlation time. As the temperature rises towards the melting point, so does the molecular mobility increase and this new relaxation mechanism will have a greater effect. We have seen that this new type of molecular motion must be occurring at a relatively low frequency (of the order of the line-width) and will almost

certainly be less than  $\omega/2\pi$ . This would make  $T_1$  decrease with increasing temperature, and the gradual decline of  $T_1$  above 150°K does suggest that this new relaxation process is becoming more and more appreciable.

#### 4.3.5 Summary

Experiments have been described which give a new approach to the complex problem of the behaviour of solid cyclopentane. The main points which arise are:

- (i) Below transition I the lattice is effectively rigid.
- (ii) At transition I a major change occurs and a large amount of molecular freedom sets in. The molecules are freely rotating in the crystal and probably diffusing bodily through the lattice.
- (iii) At transition II it is suggested that the change in crystal structure is due to the effectively spherical symmetry of the rotating molecules.
- (iv) The accuracy of the experiments is not sufficient to distinguish between the plane and puckered molecular models. The greatest part of the inaccuracy arises from lack of knowledge of the crystal structure below transition I.

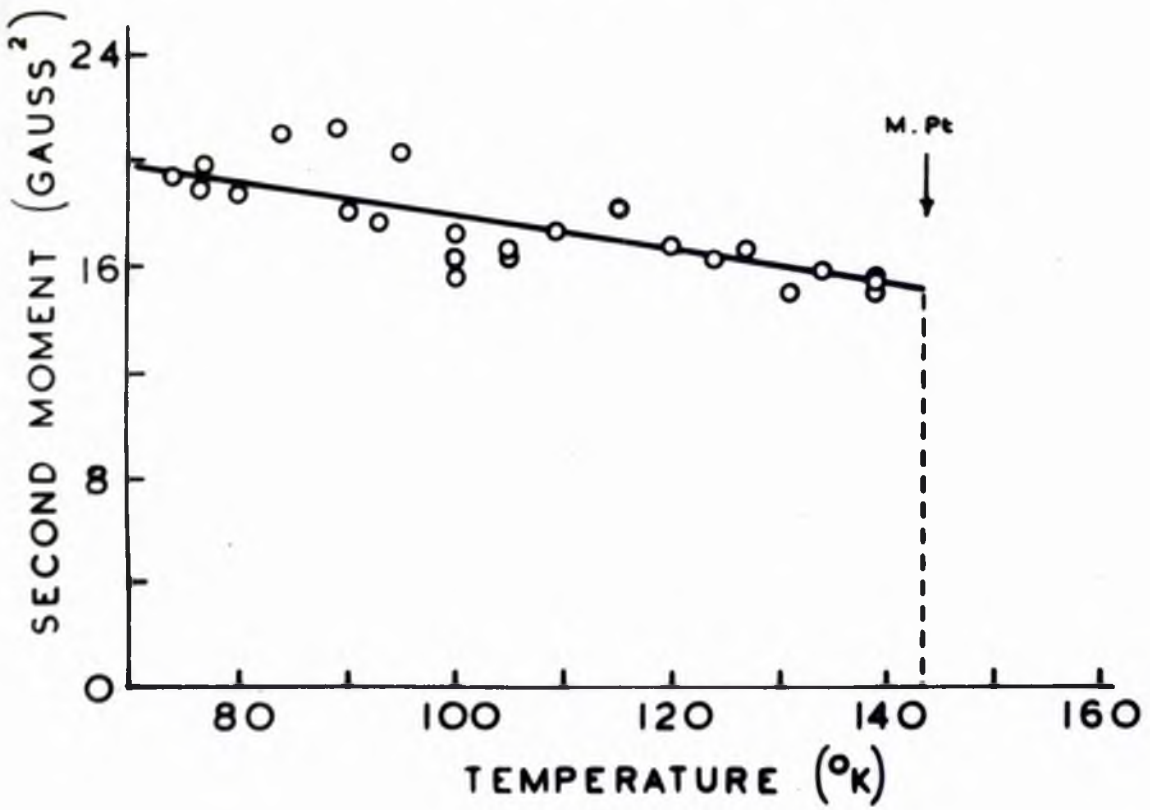
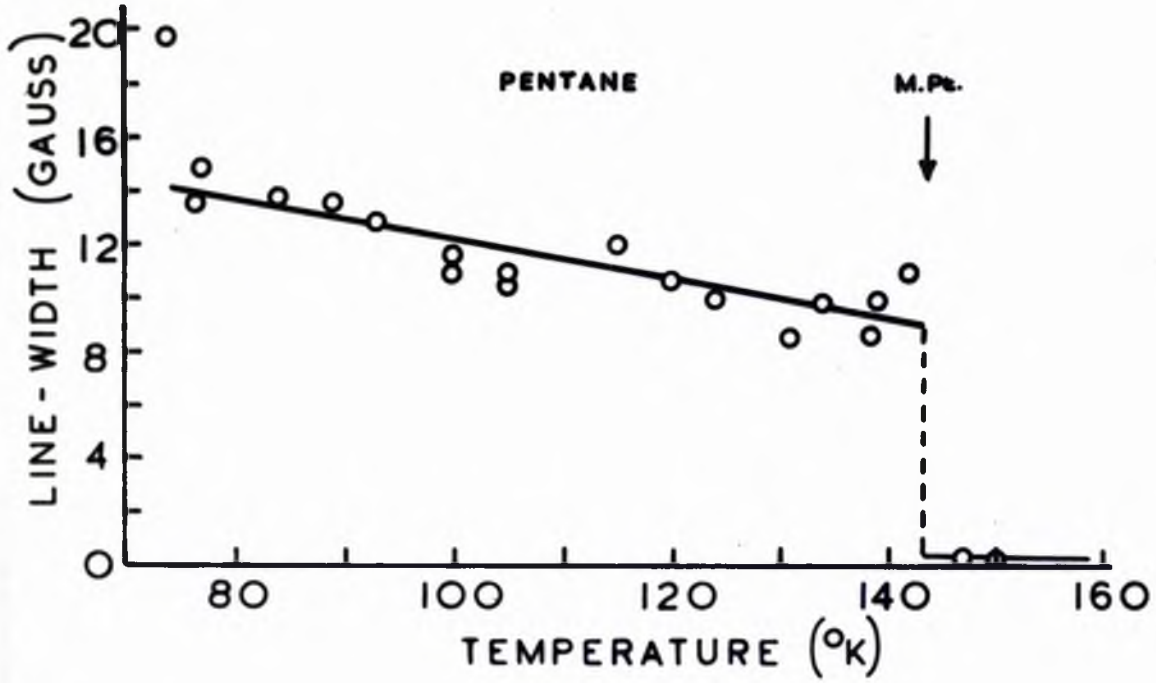


Figure 20

#### 4.4 n-Pentane and n-Hexane

##### 4.4.1 Introduction

These two normal paraffins are considered together since their behaviour is very similar and the theoretical discussion of the results applies to both substances.

No specific heat transitions are reported in the solid state for either substance, and the following data is taken from the more recent results quoted by Timmermans (1950).

	Temperature	Heats of Melting and Vaporisation
n-pentane	Freezing pt. $-129.7^{\circ}\text{C}(143.4^{\circ}\text{K})$	27.9 cal/gm
	Boiling pt. $36.1^{\circ}\text{C}$	86.8 "
n-hexane	Freezing pt. $-95.3^{\circ}\text{C}(177.8^{\circ}\text{K})$	36.3 "
	Boiling pt. $68.7^{\circ}\text{C}$	79 "

Both samples were obtained from the Chemical Research Laboratory, Teddington, and were distilled in vacuum from the standard ampoules into suitable thin-walled sealed glass tubes. The quoted purities in mole per cent were

(i) n-pentane  $99.88 \pm 0.06$

(ii) n-hexane  $99.85 \pm 0.05$

as determined from the freezing points.

##### 4.4.2 Molecular and Crystal Structure

The structure of the n-paraffin series  $\text{C}_n\text{H}_{2n+2}$  has been investigated by Müller (1928, 1930, 1932) using X-ray diffraction methods. He determined the structure of  $\text{C}_{29}\text{H}_{60}$  in the form

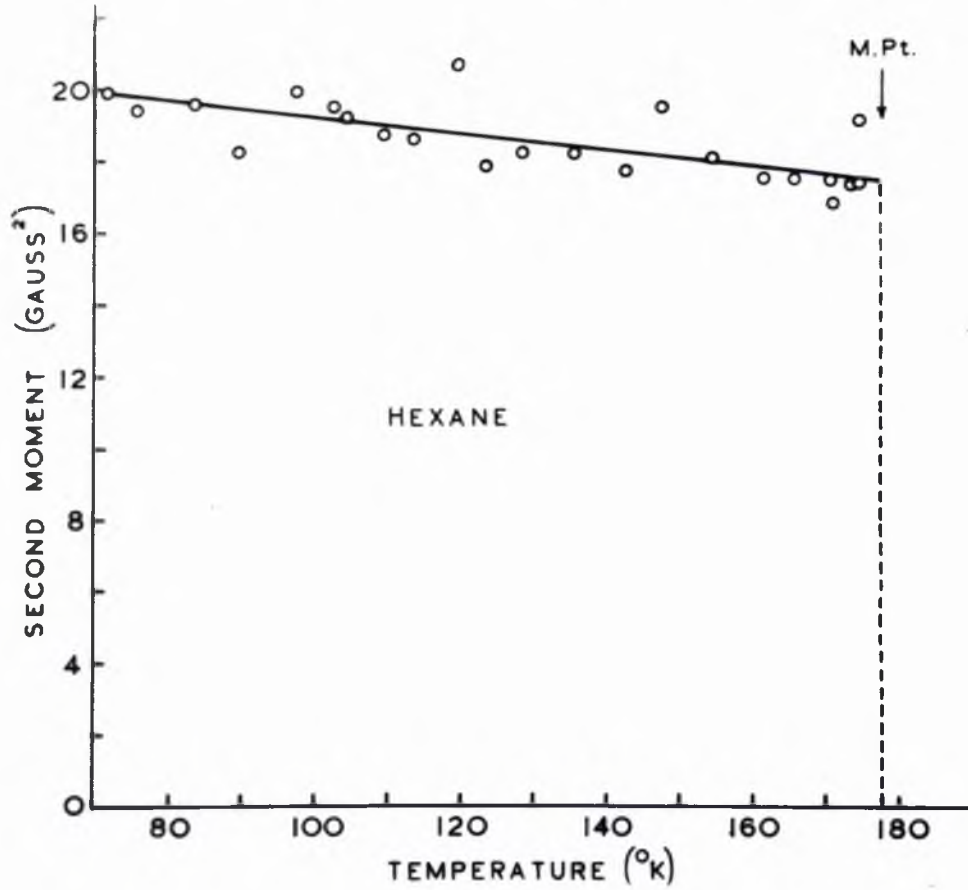
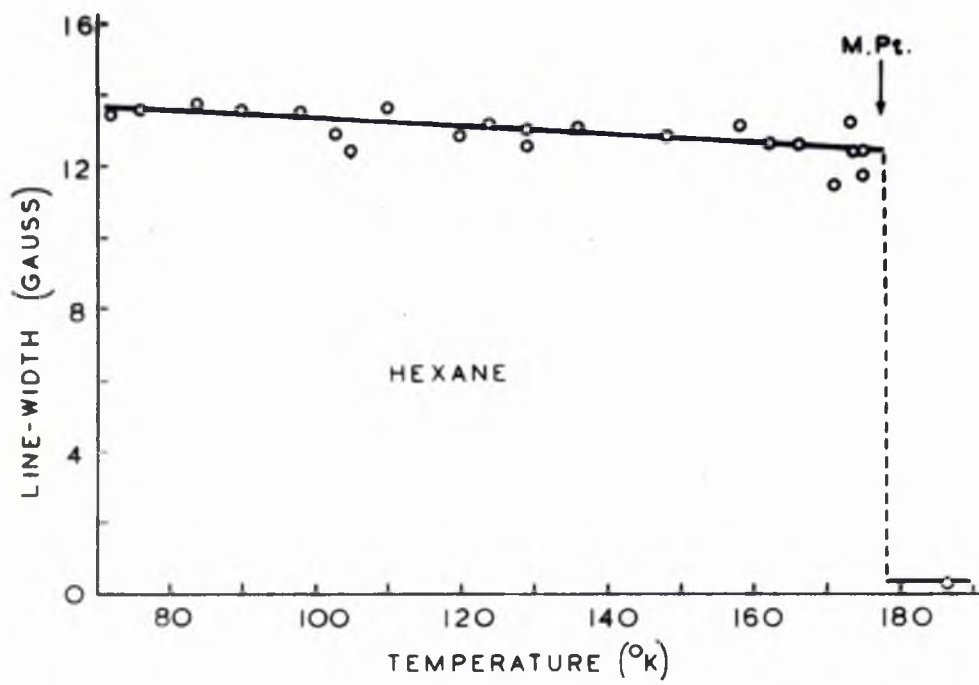


Figure 21

of a single crystal, and from powder photographs gave indications of the probable structures of the other members of this series. The molecules consist of plane zig-zag chains of carbon atoms with tetrahedral angles between the C-C bonds. The carbon chains, <sup>of C<sub>29</sub>H<sub>60</sub></sup> are all arranged parallel to the c-axis of an orthorhombic unit cell. Müller showed that for values of n from 5 to 30 in the general formula C<sub>n</sub>H<sub>2n+2</sub>, the a and b dimensions of the cell remain effectively constant, the c distance changing according to the number of CH<sub>2</sub> groups present. A full discussion of Müller's work in relation to the second moments of the n-paraffin series has been given by Andrew (1950) who investigated homologues with n = 18, 28 and 32.

In the present work, the C-C bond length has been taken as 1.54Å, the C-H bond length as 1.10Å with tetrahedral angles throughout, on the basis of a recent determination of the bond lengths and angles in ethane by Hansen and Dennison (1952).

#### 4.5.3 Experimental results

##### (a) Line-width and second moment.

The nuclear resonance spectrum for n-pentane showed evidence of fine structure, which became more noticeable at temperatures near the melting point. The variations of the line-width and second moment with temperature are shown in figure 20. These show no violent change over the

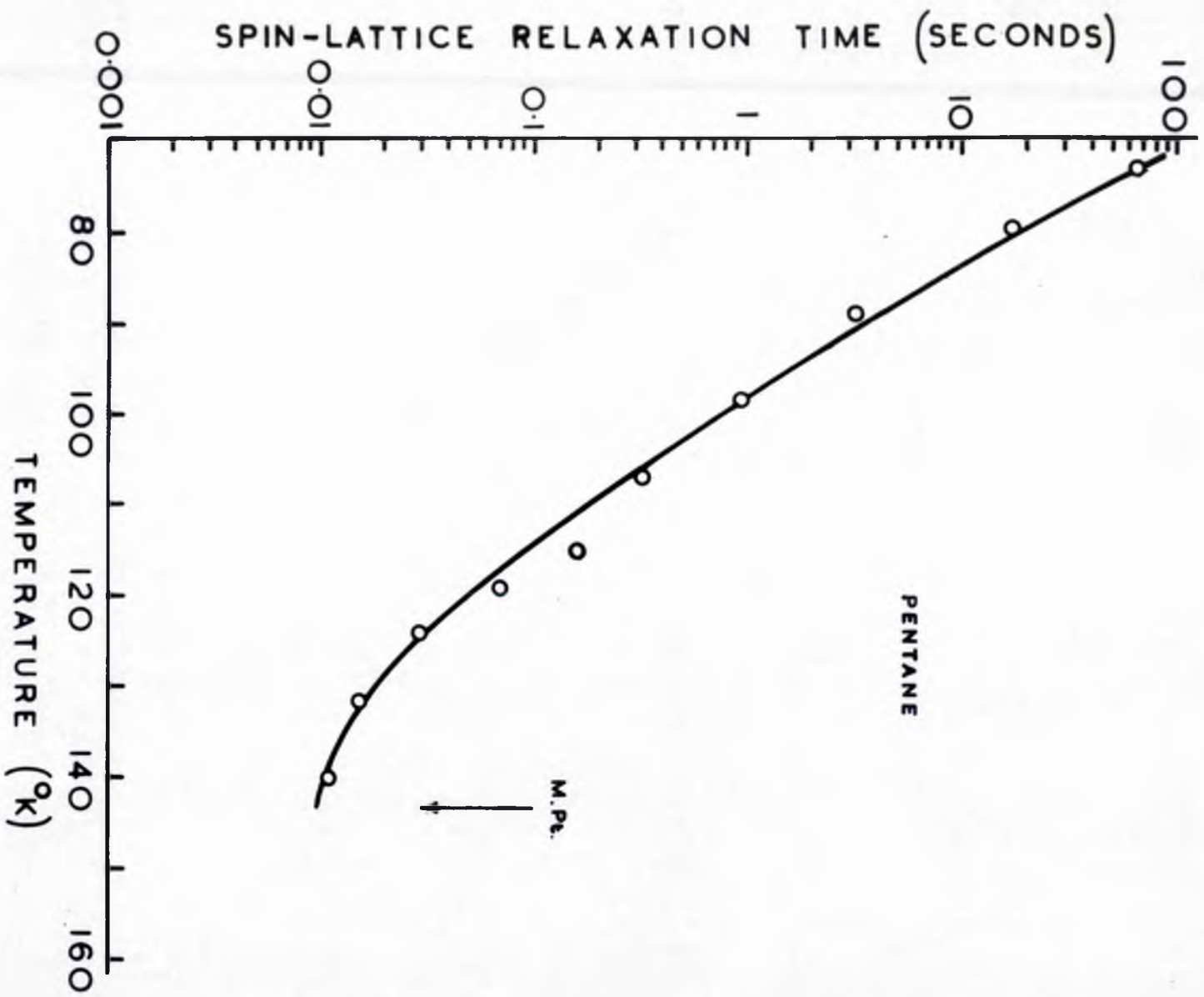


Figure 22



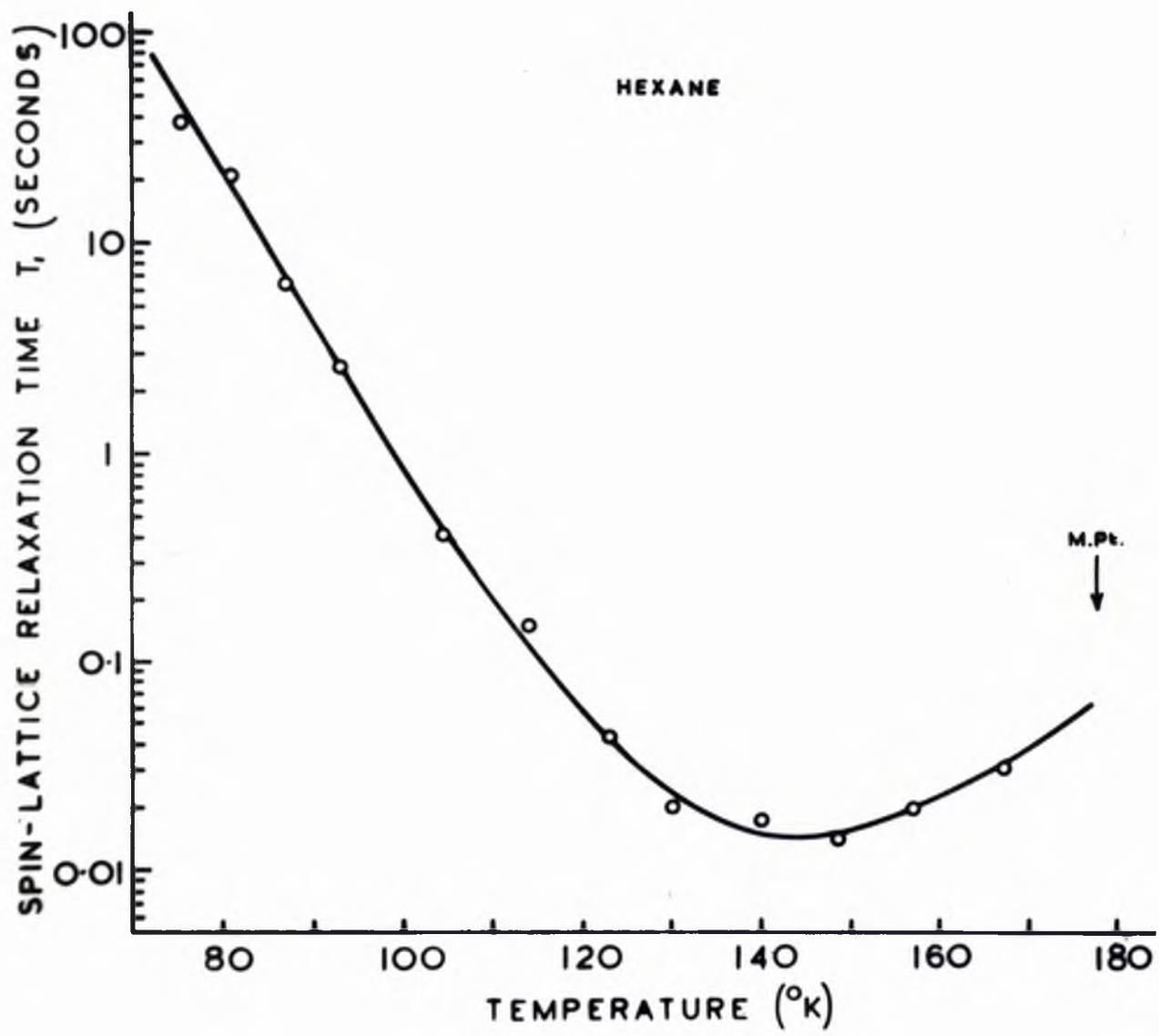


Figure 23

temperature region of measurement, but slowly decrease as the temperature rises.

As with n-pentane, fine structure was observed in the spectrum of n-hexane. The line-widths and second moment are plotted as a function of temperature in figure 21, where the variation is similar to that found in n-pentane.

The fine structure can be seen in the photograph of recorder plots shown in figure 24. The upper curves show the derivative plots for n-pentane at temperatures of  $131^{\circ}\text{K}$  and  $105^{\circ}\text{K}$ , i.e.  $13^{\circ}$  and  $39^{\circ}$  below the melting point. The fine structure can clearly be seen at  $131^{\circ}\text{K}$ , and at  $105^{\circ}\text{K}$  it is still evident in that the derivative plot is not of the symmetry one might expect from a simple absorption curve. The peak-to-peak value of the modulation was 3 gauss in each case, and is shown by the arrowed line. The lower curves are for n-hexane, the right-hand curve being the one showing the fine structure under normal circumstances. The left-hand curve will be referred to later.

(b) Spin-lattice relaxation time.

The variation of the spin-lattice relaxation times with temperature for n-pentane is shown in figure 22 and for n-hexane in figure 23. The general shape of the curves is similar, but whereas the n-hexane curve has a definite minimum, the n-pentane curve does not reach a true minimum value due to the onset of melting.

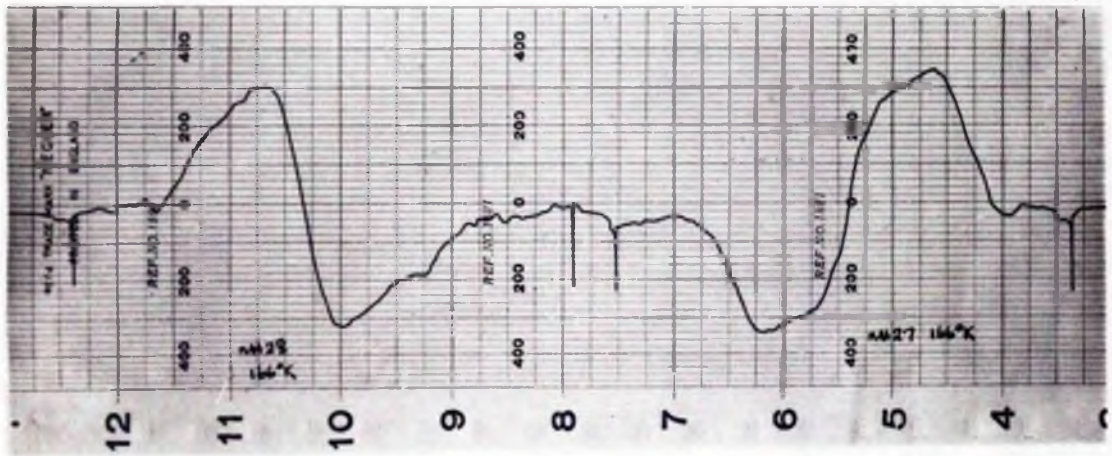


Figure 24

In both cases the relaxation times at the lowest temperatures of measurement ( $73.5^{\circ}$  K for n-pentane and  $75.5^{\circ}$  K for n-hexane) could be found by direct visual observation of recovery from saturation. At higher temperatures the relaxation time was too short for this method and the progressive saturation method was used for the remainder of the points, taking this lowest temperature as a calibration point. As explained in section 2.5, the progressive saturation method only gives relative values of T, and if absolute values are required at least one determination by the direct recovery method must be made.

One aspect which may be remarked on here is the change in line-shape as the value of the r.f. field was increased during the progressive saturation measurements. The derivative curve is a very sensitive indication of line-shape to the eye, more so than a plot of the actual line-shape itself. The two n-hexane plots shown in the lower half of figure 24 were taken at the same temperature, but the r.f. field in the left-hand plot was 10 times greater than in the right-hand plot. The line-widths differ by a factor of 2 and the line-shape also changes. As might be expected, the left-hand line is unsymmetrical due to saturation and an accurate value of the second moment cannot be calculated, but it is of the same order as the second moment of the unsaturated right-hand line. This change of line-shape is a little

disturbing as it might have an effect on the validity of the progressive saturation results.

The values of the relaxation time near the minimum may also be in error because of their very low values. The theory of the progressive saturation method given in section 2.5 assumes that the manner in which the meter deflection depends on  $\gamma^2 H_1^2 T_1 T_2$  is the same for all the measurements. This may not hold when  $T_1 \sim \frac{1}{\omega_m}$ , where  $\omega_m/2\pi$  is the modulation frequency, as the conditions are slowly changing during a modulation cycle. In general the line-width is greater than the field inhomogeneity and two cases are distinguished by BPP; case 1 where  $\omega_m T_1 \ll 1$  and case 2 where  $\omega_m T_1 \gg 1$ . The progressive saturation method can be used in either of these two cases, but the relative type of measurement made cannot be carried over directly from one case to another. The difference between these cases is shown in figure 7 of BPP (where there is a minor error in nomenclature). In the intermediate state when  $\omega_m T_1 \sim 1$  the analysis becomes complex, but the variation of the meter deflection with  $\gamma^2 H_1^2 T_1 T_2$  presumably lies between the two limiting curves.

For n-pentane and n-hexane case 2 applies in general and  $\omega_m T_1 \gg 1$ . At the lowest measured values of  $T_1$ , however, the corresponding values of  $\omega_m T_1$  are 1.6 for n-pentane and 2.4 for n-hexane. The condition  $\omega_m T_1 \gg 1$  is not adequately met at these temperatures and the absolute values of  $T_1$  may therefore be in error. This point will be raised again when quantitative conclusions are drawn from the experimental results.

#### 4.4.4 Discussion

The fine structure observed for both n-pentane and n-hexane probably arises from the triangular arrangements of protons in the end methyl groups. The theoretical line-shape for an isolated rigid triangular configuration of nuclei and for an isolated rotating triangular group has been given by Andrew and Bersohn (1950). The effects of using polycrystalline material and of broadening by neighbours were also computed. The analysis shows that a small central peak will be formed in the absorption curve which will show up as a subsidiary maximum and minimum in the derivative curve. In the cases of n-pentane and n-hexane there will be an appreciable contribution to the second moment due to mutual interaction of the protons in the methylene groups. For n-pentane the part of the intramolecular contribution due to this interaction is  $7.2 \text{ gauss}^2$  and for n-hexane  $8.8 \text{ gauss}^2$ . This will tend to mask the fine structure effect - more so for n-hexane than for n-pentane. The fine structure can be seen in figure 24. It should be noted that at the temperatures at which these line plots were made the values given above for the intramolecular contribution of the methylene groups represent almost half the total second moment in both cases.

The second moments of n-pentane and n-hexane rise steadily as the temperature decreases, and at  $120^\circ \text{K}$  have the values  $16.7 \pm 0.7 \text{ gauss}^2$  and  $18.8 \pm 0.7 \text{ gauss}^2$  respectively. These values have to be compared with the theoretical second moments

as calculated from equation (8).

The intramolecular contribution in the two cases can be calculated on the basis of the molecular structure described in section 4.4.2, and are found to be 21.4 gauss<sup>2</sup> for n-pentane and 21.0 gauss<sup>2</sup> for n-hexane. The intermolecular contributions present more difficulty since the exact positions and spacing of the protons in neighbouring methyl groups along the c-axis are uncertain. For n-pentane the long spacing between the molecules has been quoted by Müller (1930) as 7.35A. If we make use of our assumed molecular structure and take the molecules as having their long axes parallel to the c-axis of the crystal, the closest distance of approach between protons attached to neighbouring methyl groups is only 0.52A. This would be a very close approach, and Müller suggests ways by which this distance could be eased. The molecules may shorten, or may tilt relative to the base of the unit cell, or the end groups may suffer some rearrangement, or, of course, a combination of these effects may take place. The positions of the methyl group protons are therefore uncertain, but they must be known if an accurate value for the intermolecular contribution is to be calculated, as their mutual interaction will represent an appreciable part of the whole.

An estimate for this contribution, which will be substantially correct in the case of long chain molecules, can be made on the following basis. We have mentioned that the a and b dimensions of the unit cell for paraffins

$C_5H_{12}$  to  $C_{30}H_{62}$  are effectively the same (Müller, 1930). The measured values of  $a$  and  $b$  for  $C_{24}H_{50}$  thus apply to  $C_5H_{12}$  and  $C_6H_{14}$ . Suppose we only consider the intermolecular contribution due to the interactions of protons attached to one of the central methylene groups of one molecule with protons of other molecules in the same and neighbouring unit cells, and we assume these two protons are typical of the general behaviour. Because we are computing  $r_{jk}^{-6}$  we need only treat distances below  $5\text{\AA}$  accurately. For interproton distances greater than  $5\text{\AA}$  the usual method can be employed of replacing the summation by an integral and assuming the distant protons to be uniformly distributed in space according to the known proton density. If we take long enough molecules, then we need not consider protons of molecules in layers above or below the typical molecule as these distances will be  $> 5\text{\AA}$ . Thus we need only make use of the known distances  $a$  and  $b$ , together with the molecular structure, and consider molecules at about the same level as the typical one.

Using this method for *n*-hexane and taking a reasonable value for lattice contraction, Andrew and Eades (1953) calculated the intermolecular contribution at  $120^\circ\text{K}$  to be  $9.6 \text{ gauss}^2$ . The value for *n*-pentane will be the same. Obviously the accuracy of this figure will be poorer the shorter the molecule, but an error of  $\pm 1.5 \text{ gauss}^2$  is reasonable

The total rigid lattice values for the second moments



of n-pentane and n-hexane at  $120^{\circ}$  K are therefore  $30.0 \pm 1.5$  gauss<sup>2</sup> and  $29.6 \pm 1.5$  gauss<sup>2</sup> respectively, to be compared with the experimental values of  $16.7 \pm 0.7$  gauss<sup>2</sup> and  $18.8 \pm 0.7$  gauss<sup>2</sup>. Discrepancies of  $> 10$  gauss<sup>2</sup> appear, and it is clear that this large difference must be explained on the basis of one or more types of molecular motion.

Possible motions which must be considered are

(i) rotation of the molecule as a whole about its long axis.

(ii) rotation of the methyl groups about the end C-C axes.

The effects of these motions on both the intramolecular and intermolecular contributions must be worked out. It will be seen that the intramolecular contribution is about 70% of the total second moment so this will be the most important contribution to consider. It is fortunately the one for which a reasonably accurate rigid value can be calculated.

The effect on the intramolecular contribution of rotation of the whole molecule can be calculated on the basis of the theory given by Gutowsky and Pake (1950). This contribution for n-pentane is reduced from  $21.4$  gauss<sup>2</sup> to  $4.9$  gauss<sup>2</sup>, a reduction of  $16.5$  gauss<sup>2</sup> which is itself greater than the discrepancy to be explained. As the intermolecular contribution will also be decreased, the total reduction would be too great. We must therefore rule out a reorientation process of this type which involves all the molecules. If we postulate that only a

fraction of the molecules are rotating as a whole, then the intramolecular contribution would be reduced by less than the amount quoted above and the two values could be made to agree. This would explain the second moment results but the exact mechanism is uncertain and this type of motion is considered to be improbable.

We must now consider motion (ii), where the supposition is that the methyl groups rotate about the end C-C axes. The effect on the intramolecular contribution of such motion can be determined. For cyclohexane, Andrew and Eades (1953) calculated the effect on the intermolecular contribution due to rotation of the molecules about their triad axes, the crystal structure being known. This theory can be readily applied to determine the effect of rotation of the methyl groups on the intramolecular contribution of the n-pentane and n-hexane molecules. The effect of motion of the three protons of each methyl group on their own part of this contribution is known to be reduction by a factor of four, as the axis of motion is at right angles to the interproton axes (Gutowsky & Pake, 1950). The complete calculation for n-pentane gives the new intramolecular contribution as  $11.5 \text{ gauss}^2$ , a reduction of  $9.9 \text{ gauss}^2$  from the rigid value. This means that the intermolecular contribution must be reduced by about  $3.4 \text{ gauss}^2$  if this motion is to be a correct description of the processes

involved. It has been mentioned that an accurate theoretical value for the intermolecular contribution cannot be made as it is the relative positions of the methyl groups which are uncertain. The reduction of  $3.4 \text{ gauss}^2$  is reasonable, since only half the protons of each molecule would be in motion. From the second moment data it seems a fair deduction to say that over the temperature range of measurement the methyl groups of the n-pentane molecules are executing rotational motion about the neighbouring C-C axes.

In the case of n-hexane, the difference between the observed and calculated second moments at  $120^\circ \text{K}$  is  $10.8 \text{ gauss}^2$ . Motion of all the molecules as a whole about their long axes again results in too large a decrease in the second moment. The calculations for the effect of methyl group rotation follow the same lines as for n-pentane, and the new intramolecular contribution is  $12.9 \text{ gauss}^2$ , a reduction of  $8.1 \text{ gauss}^2$ . This means that the intermolecular contribution is to be reduced by  $2.7 \text{ gauss}^2$  if this motion is a correct description of the reorientation process which must be occurring. This is rather less than the required reduction for the n-pentane intermolecular contribution, as might be expected. We can therefore say it is highly likely that this type of motion is also occurring in n-hexane.

A study of the spin-lattice relaxation time data gives further information about this proposed molecular motion.

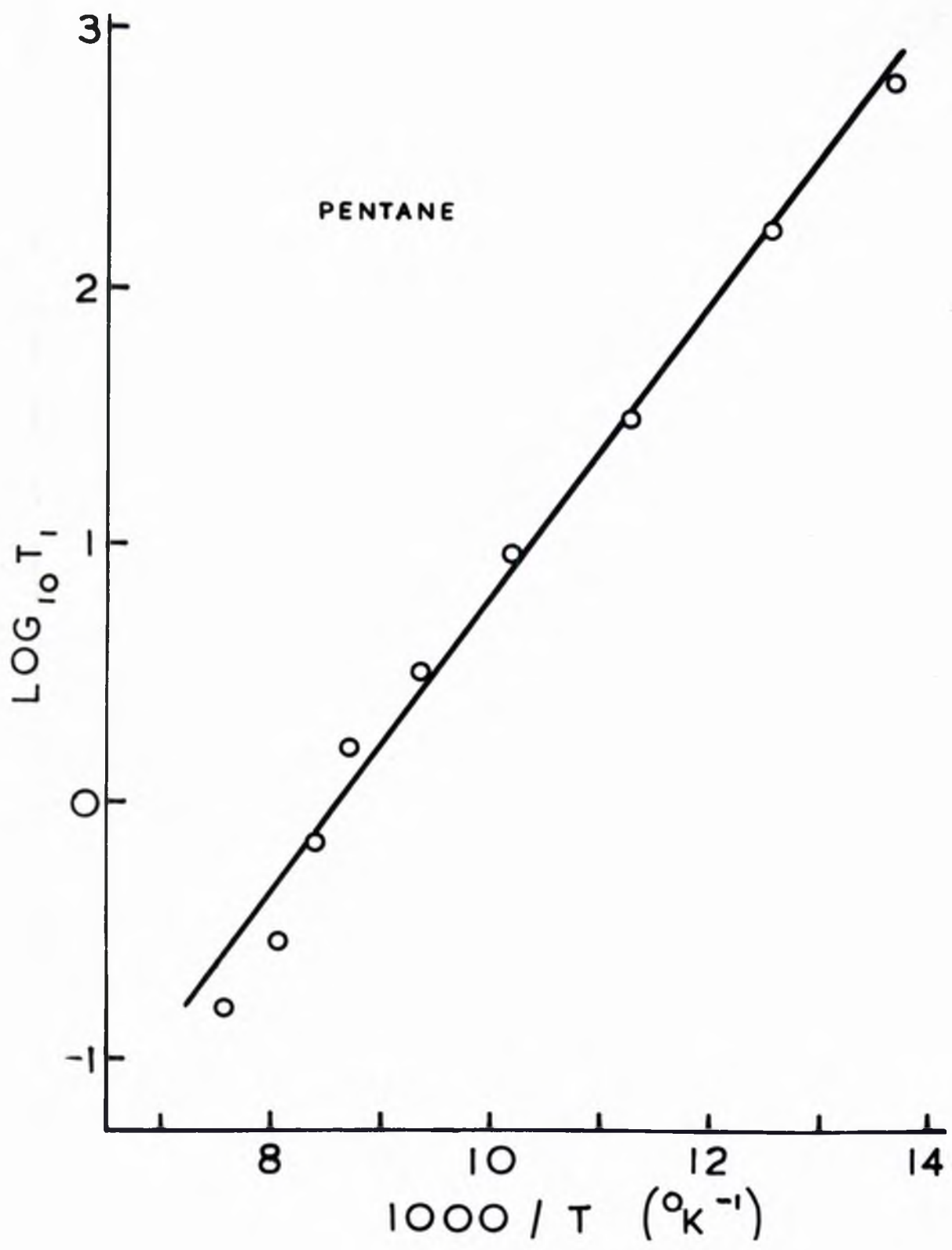


Figure 25

If the reorientation rate can be described by a single correlation time  $\tau_c$ , the relation between  $T_1$  and  $\tau_c$  should be of the form derived by BPP and quoted earlier as equation (24)

$$\frac{1}{T_1} = C_1 \left[ \frac{\tau_c}{1 + \omega^2 \tau_c^2} + \frac{2\tau_c}{1 + 4\omega^2 \tau_c^2} \right]$$

where  $\omega/2\pi$  is the radiofrequency used and  $C_1$  is a constant.

This expression has a minimum value for  $T_1$  when  $\omega\tau_c = 1/\sqrt{2}$ .

If the reorientation process is hindered by a potential barrier of height  $E$  per mole, the variation of  $\tau_c$  with temperature should be of the form

$$\tau_c = \tau_0 e^{E/RT} \quad (25)$$

where  $R$  is the gas constant per mole. The barrier height can be determined in two ways.:

(a) Since  $\omega\tau_c = 1/\sqrt{2}$  for the minimum value of  $T_1$ , then

$$T_{\min} = 3\omega/2\sqrt{2}C_1$$

and if the minimum is found experimentally, a value of  $C_1$  can be determined. Knowing  $C_1$ , values of  $\tau_c$  corresponding to the various measured  $T_1$  values can be found from equation (24) and a graph of  $\log \tau_c$  against  $1/T$  should give a straight line from whose slope  $E$  may be found.

(b) If we only consider measurements at temperatures where  $\omega^2\tau_c^2 \gg 1$ , then equation (24) reduces to

$$T_1 = 2\omega^2\tau_c/3C_1 = \frac{2\omega^2\tau_0}{3C_1} e^{E/RT}$$

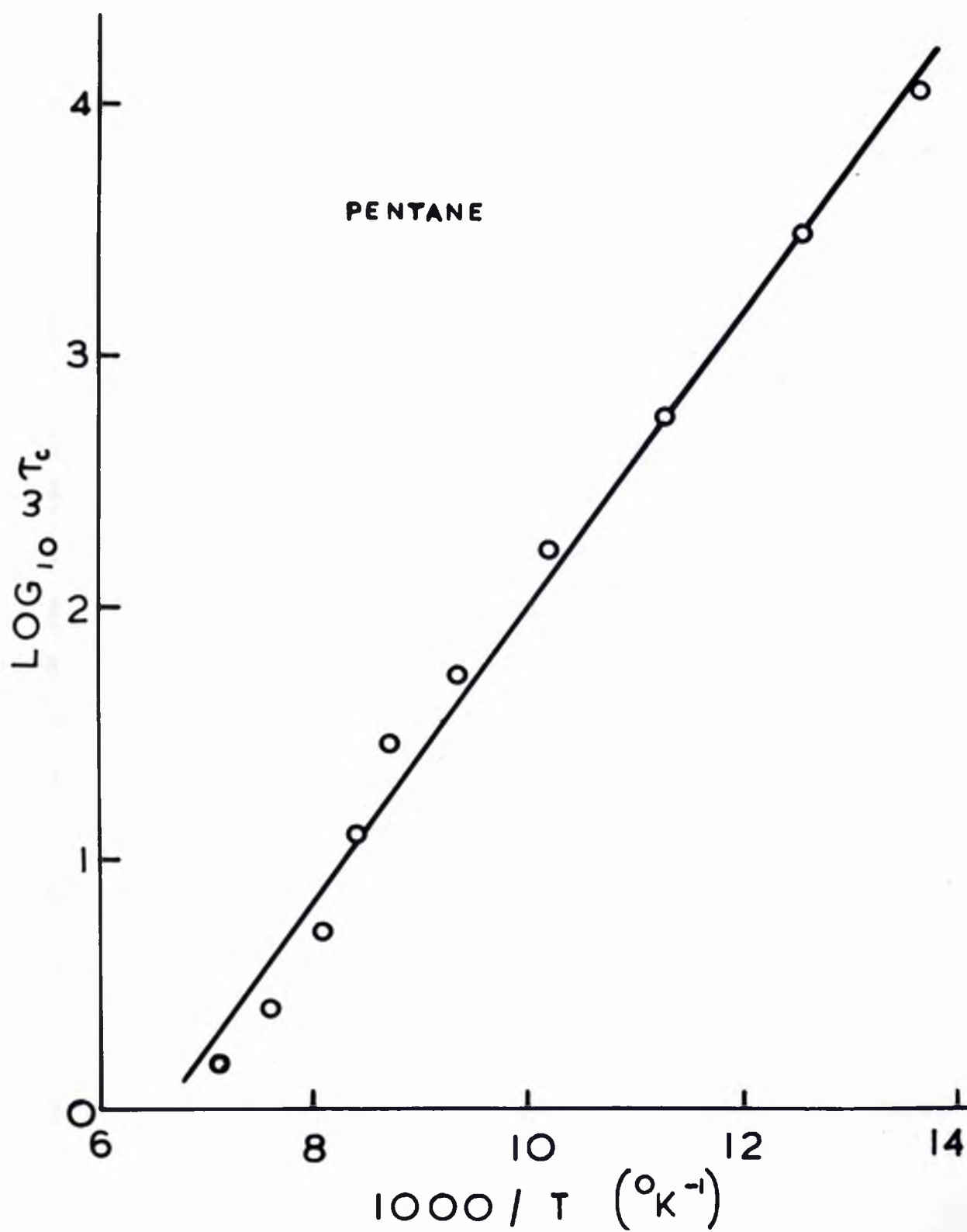


Figure 26

and a plot of  $\log T$ , against  $1/T$  should give a straight line from whose slope  $E$  can be found.

For the case of n-pentane, method (a) might be unreliable, firstly because an extrapolation is needed to find the minimum value of  $T$ , but more so because of the very low value of  $T$ , near the minimum. This has been mentioned in section 4.4.3. The lowest measured value of  $T$ , was 0.01 sec, resulting in  $\omega_m T = 1.6$ . This might lead to an error of  $\sim 40\%$  in the actual values of  $T$  near the minimum, although it must be remembered that the curve is plotted on a logarithmic scale, and so this error is not as serious as might appear at first sight. At temperatures below about  $130^\circ\text{K}$  the value of  $\omega_m T$ , is always greater than 5, and so the condition that  $\omega_m T \gg 1$  will be complied with. Method (b) is therefore used first, and figure 25 shows a plot of  $\log T$ , against  $1/T$  with the smaller values of  $T$ , omitted. A least squares calculation gives the slope, from which the barrier height  $E$  is found to be 2700 calories per mole.

Turning to method (a) and calculating the values of  $\omega\tau_c$  on the basis of a minimum  $T$ , value of  $8.9 \times 10^{-3}$  sec, the values of  $\log \omega\tau_c$  are plotted against  $1/T$  in figure 26 and a straight line fitted whose slope is that calculated from figure 25. The good fit suggests that the minimum value of  $T$ , cannot be greatly in error despite the fears expressed.

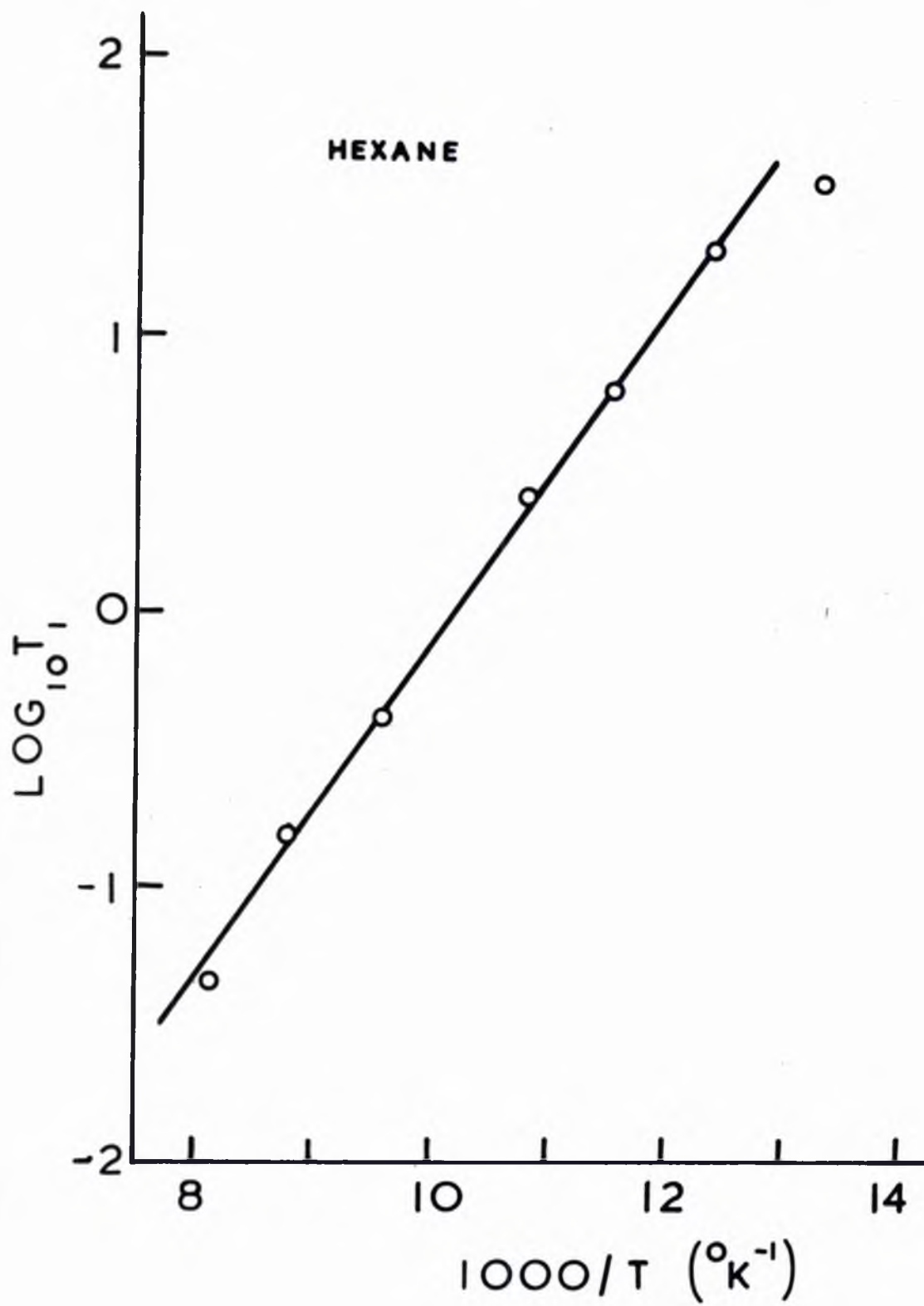


Figure 27



The theory can be applied to n-hexane, where a minimum does occur in the spin-lattice relaxation time curve. Again the smallest values of  $T_1$  are neglected when plotting  $\log T_1$  against  $1/T$  in figure 27. The slope of this line gives  $E = 2900$  calories per mole. One point has been omitted in the least squares calculation, the point at the lowest temperature  $75^\circ\text{K}$ . This fell off the best line through all the other 6 points and there is a certain amount of justification for doubt. It will be recalled that the accuracy of the temperature determination decreased as the temperature decreased. A small error at  $75^\circ\text{K}$  would appear as a comparatively large error in the  $1/T$  plot compared with the same error at, say,  $150^\circ\text{K}$ . This calculated slope fits the  $\log \omega\tau_c$  against  $1/T$  graph in figure 28, again indicating that the  $T_1$  values near the minimum must be reasonably accurate.

The values of the potential barriers restricting rotation of the methyl groups are 2700 cal/mole for n-pentane and 2900 cal/mole for n-hexane. The accuracy of these determinations will not be high as doubts have been expressed about the accuracy of the relaxation times on which this data is based. It is interesting to compare these values with those obtained by other methods. The determination of potential barriers hindering rotation can be made from thermodynamical considerations and recent reviews by Aston (1951) and Pitzer (1951) cover the field very well. For the

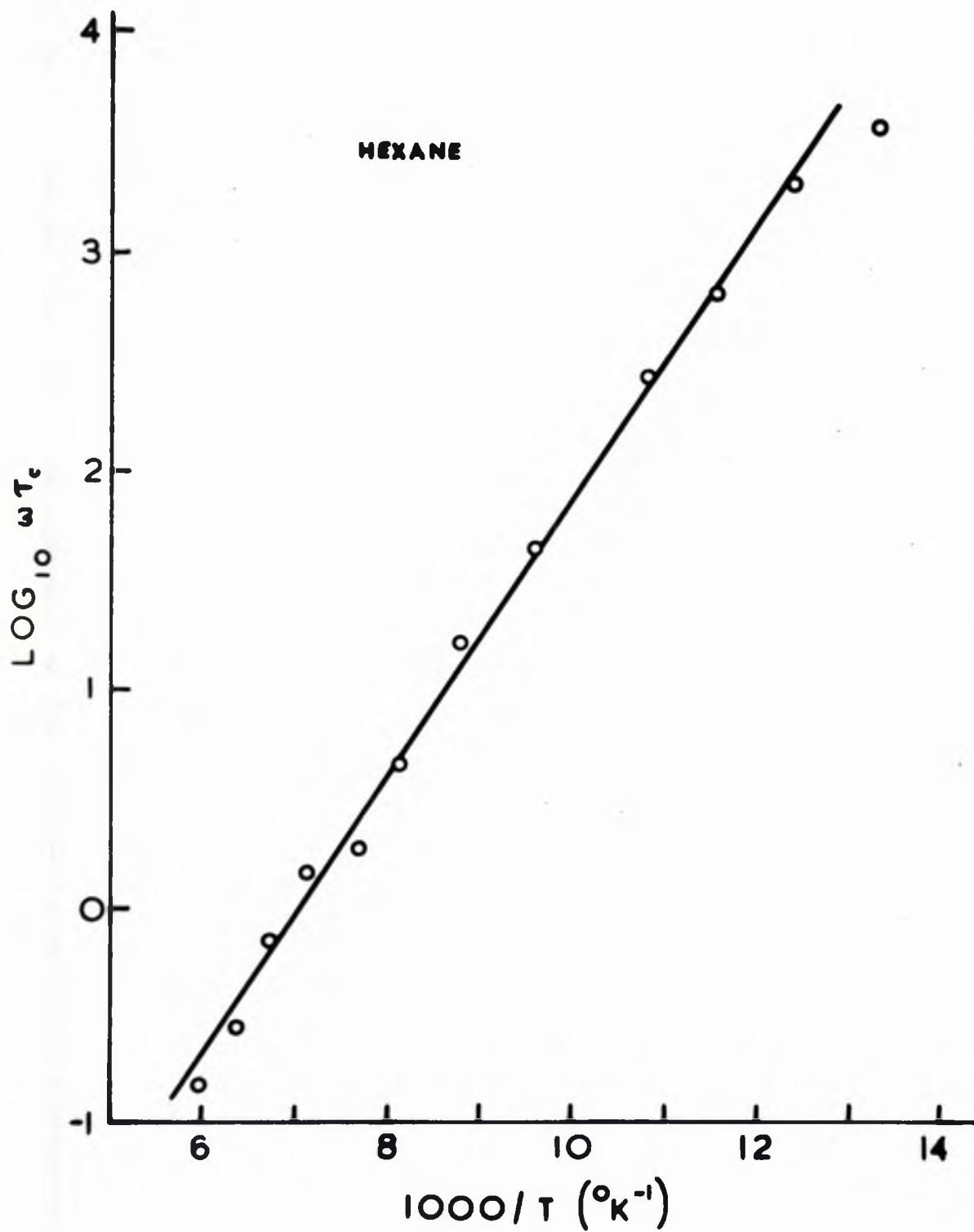


Figure 28

n-paraffin series, experimental and theoretical values are available for ethane (2750 cal/mole) and propane (3300 cal/mole) (Aston, 1951). Our experimental results are therefore of the correct order of magnitude. The nature of these barriers has been a source of speculation, but it is believed they are mainly due to the effect of repulsions of nearby hydrogen atoms in the same molecule. For ethane, therefore, the most stable configuration will be one where the  $\text{CH}_3$  groups are "staggered" rather than "eclipsed", and the effect of each hydrogen atom at one end of the molecule on rotation of the methyl groups at the other end is 2750/3 cal/mole. French and Rasmussen (1944) have taken this line of argument a little further, and from experimental data have devised a method of calculating these potential barriers. The minimum distance of each proton in the molecule from the rotation circle of the methyl group protons is taken as a measure of the restriction to rotation due to that proton. The effect will naturally fall away with increasing distance and these authors give an empirical curve showing the manner in which this restricting barrier depends on these distances. For n-pentane and n-hexane the effects of the four hydrogen atoms attached to the two methylene groups nearest to each methyl group will give the dominant contributions to the total barrier. The relevant distances have been calculated from the assumed molecular structure and the resulting value for the potential barrier

is 3270 cal/mole. This should be effectively the same for n-butane, n-pentane, n-hexane etc. as the extra methylene groups will have a negligible effect.

The experimental values are thus lower than this calculated value, but at least it is satisfactory that this new method of approach to the determination of potential barriers does give results in reasonable accord with those obtained by other methods.

Further information can be obtained from the graphs in figures 27 and 28. The fact that the points on these graphs fall on straight lines suggests that the relaxation time values are substantially correct over the whole temperature range. A least squares calculation gives the slope and intercept in each case. Using method (a), the calculated potential barriers to rotation are 2800 cal/mole for n-pentane and 3000 cal/mole for n-hexane, in good agreement with the previous results as was to be expected.

We have mentioned before that a line-width change is linked with the reorientation frequency of the molecular motion which is taking place. Since this frequency will diminish as the temperature falls, there will come a time when it is less than the line-width (expressed as a frequency). The motion may then not affect the line-width to the same extent and the line may begin to broaden and reach its rigid lattice value. Gutowsky and Pake (1950) have used the theory

of BPP and put this argument on a quantitative basis. They relate the line-width  $\Delta\nu$  with the reorientation frequency  $\nu_c$  (defined as  $1/2\pi\tau_c$ ) by the equation

$$(\Delta\nu)^2 = A^2(2/\pi) \tan^{-1}(\alpha\Delta\nu/\nu_c)$$

where  $A$  is the line-width for a rigid lattice ( $\nu_c \rightarrow 0$ ) and  $\alpha$  a constant "the order of unity". According to this expression the line should be in the process of broadening when  $\alpha = \nu_c/\Delta\nu$ . For n-pentane and n-hexane at  $75^\circ\text{K}$  we know the line is not in the process of broadening in either case, and so at this temperature  $\alpha < \nu_c/\Delta\nu$ . We can find values of  $\nu_c$  at  $75\text{ K}$  from figures 27 and 28, using the least squares calculations, and we know the values of  $\Delta\nu$  from figures 20 and 21. The quantity  $\nu_c/\Delta\nu$  for n-pentane turns out to be 0.035 and for n-hexane 0.031, so we can say that  $\alpha$  must be less than about 0.03 in both cases. This is unusual as although values of  $\alpha$  ("the order of unity") have been reported as 0.6 for cyclohexane and 0.3 for benzene (Andrew and Eades 1953) it has never been found as low as 0.03 before. It is clear that experiments must be carried out below  $75^\circ\text{K}$  to find if, and at what temperatures, the lines do broaden and hence determine an absolute value for  $\alpha$  in the two cases.

The constant  $\alpha$  is introduced for two reasons. Firstly the line-shape may not be a simple curve and  $\Delta\nu$  may not be an adequate description of this shape; secondly  $\alpha$  is introduced to cover uncertainties in the integration limits

of BPP equation 35. It is hoped to investigate the theoretical significance of this low value of  $\alpha$ .

One further point must be raised concerning motion of the molecules about their long axes. The second moment at 120°K is intermediate between the rigid value and the value it should take if all the molecules were rotating. It might be considered that a very gradual transition is occurring. We know that where  $T_c$  is a minimum the reorientation frequency is of the same order as the radiofrequency used. This means that  $\Delta\nu/\nu_c \sim 0.002$  and so  $\alpha \sim 500$  if this transition is taking place. Such a high value means that this idea is not tenable.

#### 4.4.5 Summary

Two normal paraffins  $C_5H_{12}$  and  $C_6H_{14}$  have been investigated by nuclear resonance methods at temperatures from 75°K to their melting points. The following main conclusions can be drawn.

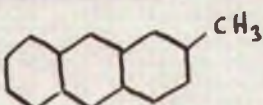
- (i) Molecular motion is occurring in both substances down to the lowest temperature reached.
- (ii) This motion is very probably reorientation of the CH groups of the molecules about the end C-C axes.
- (iii) The potential barriers to this motion are 2700 cal/mole for n-pentane and 2900 cal/mole for n-hexane. These are slightly less than might be predicted.
- (iv) The effect of this motion on the line-width leads to differences with theory which are being investigated.

#### 4.5 Early Qualitative Investigations

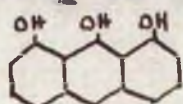
A large number of substances were investigated qualitatively using the apparatus described in section 2.2. Many of these substances were related to anthracene, as at the time it was thought that the narrow anthracene line was a real effect. Other compounds were chosen on the grounds of having a long axis of symmetry about which motion might take place. All were solids at room temperature and in most cases were taken up to their melting points in the furnace.

Visual observation of the C.R.O. trace was always used, with more detailed investigation by the phase-sensitive amplifier in promising cases. Narrow lines ( $< 10$  gauss) were the prime object of the search. These lines are generally seen on the C.R.O. but saturation might easily occur during a detailed plot of the line derivative.

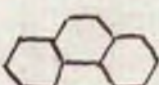
These results are qualitative and exploratory and are given here just to be recorded.

2-Methyl anthracene  M.pt.  $205^{\circ}\text{C}$

No resonance was detected up to the melting point.

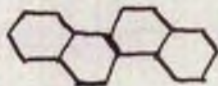
Dithranol  M.pt.  $^{\circ}\text{C}$

No resonance at  $20^{\circ}\text{C}$ .

Phenanthrene  M.pt.  $98^{\circ}\text{C}$

No narrow line was visible at room temperature, but a line

~ 1 gauss wide appeared at 87° C which became stronger up to the melting point. This may be due to poor temperature control or an impure sample.

Chrysene

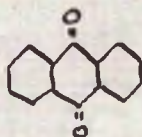
M.pt. 254° C

A very weak line ~ 4 gauss wide was detected on the meter at 197 C, but saturation was probably occurring.

Pyrene

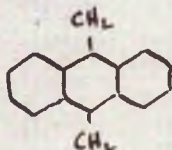
M.pt. 149° C

A line ~ 6 gauss wide was detected at room temperature, and this line narrowed to ~ 4 gauss just below the melting point.

Anthraquinone

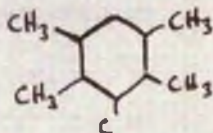
M.pt. 285° C

A very weak line ~ 3 gauss wide was detected which did not change up to 200° C.

Anthrone

M.pt. 154° C

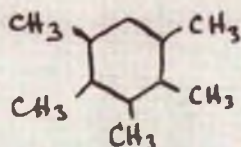
No narrow line found up to melting point.

Durene

M.pt. 80° C

A narrow line about 7 gauss wide was seen on the C.R.O. and detected on the meter. This appeared to narrow to about 5 gauss just below the melting point. There are a large number of short interproton distances and motion of the methyl groups is very probable in view of the relatively narrow line.

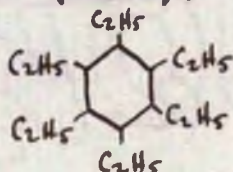


Pentamethylbenzene

M.pt. 51-55°C

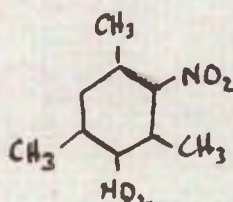
A narrow line 2.8 gauss wide was detected on the C.R.O. and by the meter. Again the narrowness of this line suggests methyl group motion.

The related compound hexamethylbenzene has been investigated by Andrew (1950).

Hexaethylbenzene

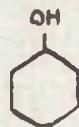
M.pt. 128°C

At 25°C the line width was 7.6 gauss, narrowing as the temperature was increased. Again the many short interproton distances would lead to a greater line-width for the rigid lattice and so some kind of motion is probable. Rotation of the methyl groups is more likely than rotation of the ethyl groups as this latter motion would require much more room in the crystal and would probably be hindered by neighbouring molecules.

2,4-Dinitromesitylene

M.pt. 85°C

A narrow line appeared at 81°C, again probably due to melting.

Phenol

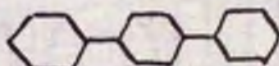
M.pt. 42°C

A very weak line ~ 3 gauss wide was detected at room temperature, no change occurring up to the melting point.

Diphenyl

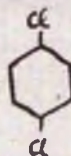
M.pt. 70°C

No resonance was visible at room temperature, and one ~ 3.5 gauss wide 3° below the melting point may have been caused by poor temperature control and the onset of melting. If the sample was not pure, the melting would occur at a lower temperature than 70°C.

para-Diphenylbenzene

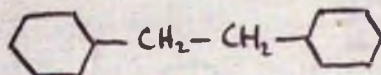
M.pt. 212-3°C

No line visible up to melting point.

para-Dichlorobenzene

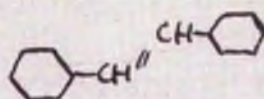
M.pt. 50°C

No line detected below melting point.

Dibenzyl

M.pt. 50°C

A line about 5 gauss wide was detected at 43°C, but became very sharp at 46°C, probably due to melting.

trans-Stilbene

M.pt. 121-2°C

A resonance line ~ 7 gauss wide was seen at 71°C which narrowed slightly up to the melting point.

In several cases it will be seen that these results, although very qualitative, did give indications of possible molecular reorientations, particularly methyl group rotation. As the purity of every substance was suspect further accurate investigations were postponed until either purer samples could be obtained or chemical purification processes carried out.

APPENDIX IMAGNET DESIGN THEORY

**Symbols:** The general symbols used are

H = magnetic field strength

B = magnetic induction

L = length

A = cross-sectional area.

Suffix m refers to the magnetic material,  
g to the gap and y to the yoke.

Simple Theory

(a) The magnetomotive force provided by the magnetic material must be sufficient to drive the flux across the gap. Taking any closed magnetic circuit,

$$H_m L_m = H_g L_g$$

$$\text{or } L_m = H_g L_g / H_m$$

provided the reluctance of the yoke is small enough to make  $H_y$  small and the product  $H_y L_y$  negligible in comparison with  $H_m L_m$  and  $H_g L_g$ .

(b) The cross-sectional area of the magnetic material must be sufficient to produce the necessary flux in the gap, with coning of polecaps if necessary.

$$B_m A_m = K \cdot H_g A_g$$

where K is a leakage factor to account for the flux lost.

The volume of magnetic material is therefore given by

$$L_m A_m = K \frac{H_g L_g A_g}{B_m H_m}$$

and for minimum volume of material we must have the product  $B_m H_m$  as large as possible.

This is the theory usually given. However there are one or two points to be considered which modify the conception of leakage factor. This factor can conveniently be split into two parts:

- (1)  $K_1$ , covering leakage from the surfaces of magnetic material, i.e. from points of differing magnetic potential.
- (ii)  $K_2$ , covering leakage from the polecaps, i.e. from surfaces of constant potential.

It is desirable to have  $B_m$  constant throughout the material. To allow for the increased leakage which must take place from magnetic surfaces near the gap, the magnetic material would need to be tapered in order to keep  $B_m$  constant. If the area where the polepiece abuts on to the yoke is  $A_{m1}$ , and where it joins the polecap  $A_{m2}$ , then we can define  $K_1$  as

$$K_1 = \frac{B_m A_{m1}}{B_m A_{m2}} = \frac{A_{m1}}{A_{m2}} \quad \text{if } B_m \text{ is constant.}$$

The area of the gap  $A_g$  may be smaller than  $A_{m2}$  due to possible coning of the polecaps, and the polecap leakage factor  $K$  can be defined as

$$K_2 = \frac{B_m A_{m2}}{H_g A_g} \quad \text{or} \quad H_g = B_m \frac{A_{m2}}{A_g} \frac{1}{K_2}$$

As we increase the polecap coning, i.e. increase the ratio  $A_{m_2}/A_g$ , so will  $H_g$  tend to increase. But there will also be more leakage, and the increase in  $K_2$  will offset this gain. An optimum coning angle must be found consistent with reasonable polecap thickness.

The measured leakage factor is given by  $K_1, K_2$  as

$$K_1, K_2 = \frac{B_m A_m}{H_g A_g} = \frac{\text{Total flux available}}{\text{Flux in gap}}$$

The quantity  $H_g A_g$  is greater than the actual gap flux as  $H_g$  is taken as the central field. This loss is included as part of  $K_2$ .

In the case of the permanent magnet whose design is discussed in section 3.2, values of  $K_1$  and  $K_2$  were calculated by Dr. E. R. Andrew.  $K_1$  was found from the method given by Evershed (1920) to be 1.65 and  $K_2$  was found by a Schwarz transformation method to be 1.60. An allowance was made for the yoke reluctance and the actual value of  $L_m$  was 2% greater than that calculated from the theory given above.

APPENDIX IIEstimation of Ethylene Glycol in Anthracene

Ethylene glycol is oxidised by potassium periodate to formaldehyde. If excess periodate is added to the ethylene glycol, the excess can be titrated against potassium arsenite using KI provided the reactions occur in neutral solution.



The potassium periodate was made up as follows.

4.6 gm was dissolved in boiling water diluted to 900 c.c. and filtered. A further 100 c.c. distilled water was added. This solution was not stable and had to be standardised against  $\text{KAsO}_2$  solution each time it was used.

The potassium arsenite was made up by dissolving 1.2209 gm arsenious oxide in caustic potash solution. A drop of phenolphthalein was added and the solution neutralised with HCl. The solution was now made up to 1000 c.c. with concentrated sodium bicarbonate solution.

The  $\text{KIO}_4$  was standardised as follows:

20 c.c. of the  $\text{KIO}_4$  was placed in a beaker with 0.5 gm  $\text{NaHCO}_3$  and 0.2 gm KI, the KI liberating the iodine from the  $\text{KIO}_4$ , which was titrated against the standard  $\text{KAsO}_2$  solution. An accurate end-point was obtained using starch solution as an indicator.

As a trial of the method, a solution of ethylene glycol

was made up so that it did not contain more than 45 mg.  $(\text{CH}_2\text{OH})_2$  in a 10 c.c. sample of the solution. Such a sample was placed in a 100 c.c. graduated flask, a known volume of  $\text{KIO}_4$  which would be in excess for the reaction was added, and the whole made up to 100 c.c. and allowed to stand for 1 hour. 20 c.c. samples of this were removed and titrated against  $\text{KAsO}_2$  solution as described above. This was repeated using different concentrations etc.. From the titrations, the number of mg. of  $(\text{CH}_2\text{OH})_2$  present was calculated and could be compared with the weighed amount. After the conditions had been adjusted to give sufficiently large titre values, the two sets of results were in fairly good agreement.

The anthracene was weighed out (approximately 0.5 gm) and 2 c.c. of distilled water was added. The mixture was shaken in a small tube and filtered through a very small Buchner funnel. A known volume of the filtrate was taken and placed in a 100 c.c. flask, a known volume of  $\text{KIO}_4$  solution was added and the whole made up to 100 c.c. with distilled water. The titration was carried out as above and the percentage of ethylene glycol present was calculated.

This was done for the two different samples of Eastman-Kodak 480-X anthracene. In the first one, 3.11% by weight of ethylene glycol was found. In the second one no trace of ethylene glycol could be found, the  $\text{KIO}_4$

present in solution after 1 hour being exactly the same as that originally present.

This analysis was carried out by a chemistry student under the supervision of Dr.H.T.Openshaw.



REFERENCES

- Ahmed, F.R. & Cruickshank, D.W.J. 1952 Acta Cryst. 5, 852.
- Andrew, E.R. 1950 J. Chem. Phys. 18, 607.
- Andrew, E.R. & Bersohn, R. 1950 J. Chem. Phys. 18, 159.
- Andrew, E.R. & Eades, R.G. 1953 Proc. Roy. Soc. A, 216, 398.
- Andrew, E.R. & Rushworth, F.A. 1952 Proc. Phys. Soc. B, 65, 801.
- Arnold, J.T., Dharmatti, S.S. & Packard, M.E. 1951  
J. Chem. Phys. 19, 507.
- Aston, J.G. 1951 Disc. Faraday Soc. 10, 73.
- Aston, J.G., Fink, H.L. & Schumann, S.C. 1943 J. Amer. Chem.  
Soc. 65, 341.
- Bearden, J.A. & Watts, H.M. 1951 Phys. Rev. 81, 73.
- Bloch, F. 1946 Phys. Rev. 70, 460.
- Bloch, F., Hansen, W.W. & Packard, M.E. 1946 Phys. Rev. 69, 127.
- Bloembergen, N. 1948 Nuclear Magnetic Relaxation. The Hague:  
Martinus Nijhoff.
- Bloembergen, N., Purcell, F.M. & Pound, R.V. 1948 Phys. Rev. 73, 679.
- Bruce, C.R. 1953 Phys. Rev. 89, 896.
- Coulson, C.A., Daudel, R. & Robertson, J.M. 1951 Proc. Roy. Soc.  
A, 207, 306.
- Dewar, J. 1905 Chem News & J. Ind. Sci. 91, 216.
- Doulin, D.R. & Huffman, H.M. 1946 J. Amer. Chem. Soc. 68, 173.
- Dunitz, J.D. & Schomaker, V. 1952 J. Chem. Phys. 20, 1703.
- Eades, R.G. 1952 Thesis, University of St. Andrews.
- Evershed, S. 1920 Dict. App. Phys vol. II.

REFERENCES

- French, F. A. & Rasmussen, R. S. 1946 J. Chem Phys. 14, 389.
- Gorter, C. J. 1936 Physica 3, 995.
- Gorter, C. J. & Broer, L. F. J. 1942 Physica 9 591.
- Green, S. L. 1948 Theory and Use of the Complex Variable.  
London: Pitman.
- Gutowsky, H. S. & Pake, G. E. 1950 J. Chem. Phys. 18, 162.
- Hansen, G. E. & Dennison, D. M. 1952 J. Chem. Phys. 20, 313.
- Hassel, O. & Viervoll, H. 1946 Tids. Kjemi Bergvesen  
Met. 6, No. 3, 31.
- Hoselitz, K. 1950, 1951 Private communication.
- Jessop-Saville 1950 Technical Publication: Permanent Magnets.
- Kilpatrick, J. E., Pitzer, K. S. & Spitzer, R. 1947 J. Amer. Chem.  
Soc. 69, 2483.
- Klemm, W. 1928 Z. Anorgan. Allgem Chem. 176, 1.
- Mathieson, A. McL., Robertson, J. M. & Sinclair, V. C. 1950 Acta.  
Cryst. 3, 245.
- Miller, F. A. & Inskeep, R. G. 1950 J. Chem. Phys. 18, 1519.
- Müller, A. 1928 Proc. Roy Soc. A, 120, 437.
- Müller, A. 1930 Proc. Roy. Soc. A, 127, 417.
- Müller, A. 1932 Proc. Roy. Soc. A, 138, 514.
- Pitzer, K. S. 1951 Disc. Faraday Soc. 10, 66.
- Plesset, E. H., Harnwell, G. P. & Seidl, F. G. P. 1942 Rev. Sci.  
Inst. 13, 351.
- Post, B., Schwartz, R. S. & Fankuchen, I. 1951 J. Amer. Chem. Soc.  
73, 5113.
- Purcell, E. M., Torrey, H. C. & Pound R. V. 1946 Phys. Rev. 69, 37.

REFERENCES

- Roberts, A. 1947 Rev. Sci. Inst. 18, 845.
- Rose, M. E. 1938 Phys. Rev. 53, 715.
- Rushworth, F. A. 1952 J. Chem. Phys. 20, 920.
- Sinclair, V. C., Robertson, J. M. & Mathieson, A. McL. 1950 Acta.  
Cryst. 3, 251.
- Timmermans, J. 1950 Physico-Chemical Constants of Pure Organic  
Compounds. Amsterdam: Elsevier.
- Van Vleck, J. H. 1948 Phys. Rev. 74, 1168.
- Williamson, D. T. N. 1949 Wireless World 55, No. 8, 282.